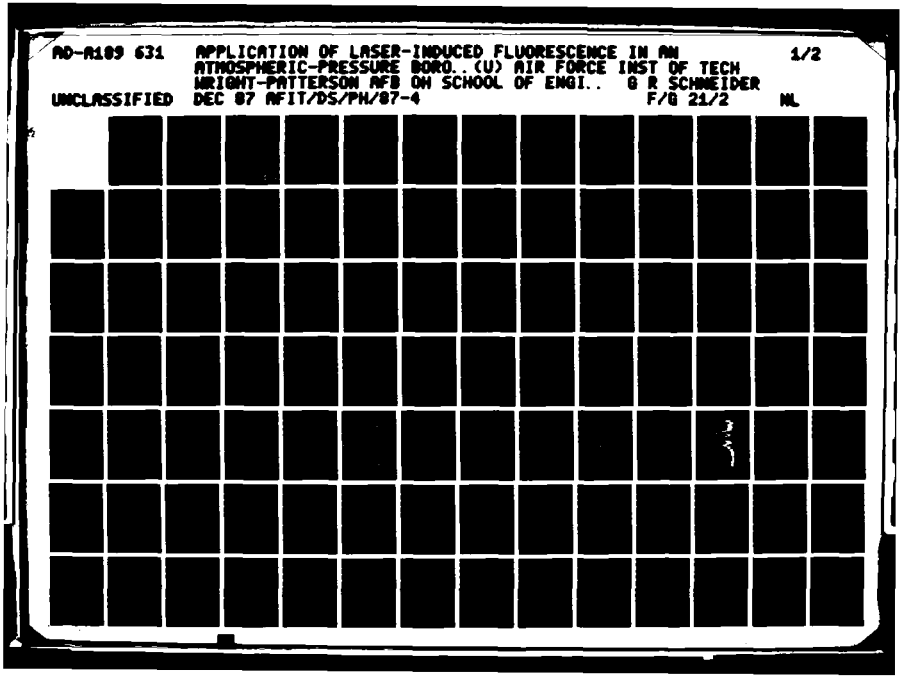
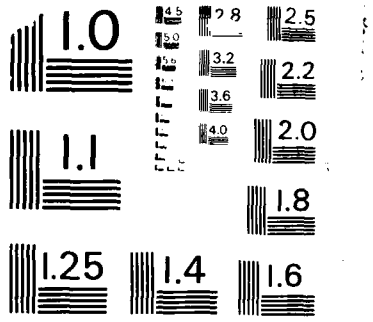
AD-A189 631 APPLICATION OF LASER-INDUCED FLUORESCENCE IN AN ATMOSPHERIC-PRESSURE BORO..(U) AIR FORCE INST OF TECH WRIGHT-PATTERSON AFB OH SCHOOL OF ENGI.. G R SCHNEIDER 1/2

UNCLASSIFIED DEC 87 AFIT/DS/PH/87-4 F/G 21/2 NL

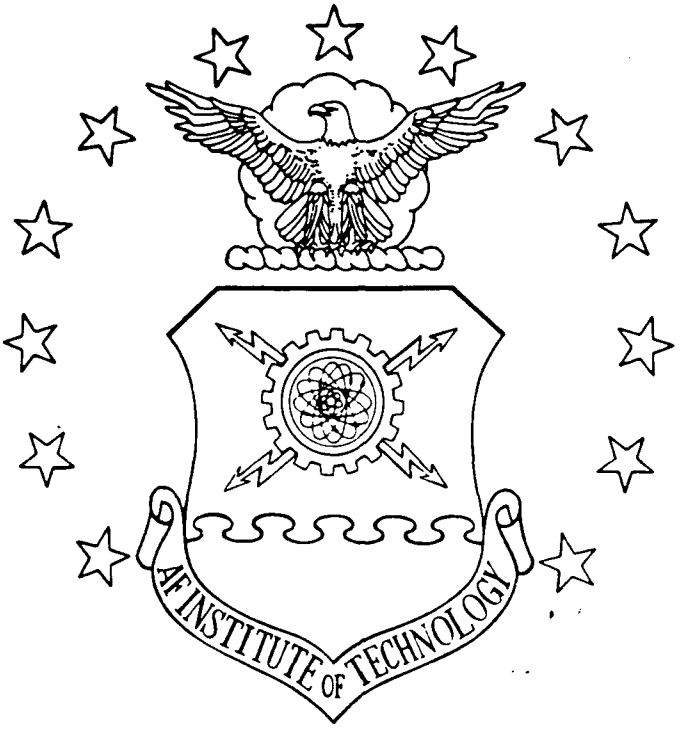




MICROCOPY RESOLUTION TEST CHART
NATIONAL BUREAU OF STANDARDS - 1963

DTIC FILE COPY

AD-A189 631



APPLICATION OF LASER-INDUCED FLUORESCENCE IN AN ATMOSPHERIC-PRESSURE BORON-SEEDED FLAME

DISSERTATION

Greg R. Schneider
Major, USAF

AFIT/DS/PH/87-4

DTIC
ELECTE
MAR 0 3 1988
S D
C4H

DEPARTMENT OF THE AIR FORCE
AIR UNIVERSITY
AIR FORCE INSTITUTE OF TECHNOLOGY

Wright-Patterson Air Force Base, Ohio

DISTRIBUTION STATEMENT A
Approved for public release;
Distribution Unlimited

88 3 01 135

AFIT/DS/PH/87-4

APPLICATION OF LASER-INDUCED FLUORESCENCE IN AN ATMOSPHERIC-PRESSURE BORON-SEEDED FLAME

DISSERTATION

Greg R. Schneider
Major, USAF

AFIT/DS/PH/87-4

Approved for public release; distribution unlimited

DTIC
ELECTE
MAR 0 3 1988
S
H

AFIT/DS/PH/87-4

APPLICATION OF LASER-INDUCED FLUORESCENCE IN AN ATMOSPHERIC-PRESSURE BORON-SEEDED FLAME

DISSERTATION

Presented to the Faculty of the School of Engineering

of the Air Force Institute of Technology

Air University

In Partial Fulfillment of the

Requirements for the Degree of

Doctor of Philosophy

Greg R. Schneider, B.S., M.S.

Major, USAF

December 1987

Approved for public release; distribution unlimited

AFIT/DS/PH/87-4

APPLICATION OF LASER-INDUCED FLUORESCENCE IN AN ATMOSPHERIC-PRESSURE BORON-SEEDED FLAME

Greg R. Schneider, B.S., M.S.

Major, USAF

Approved:

Won B. Roh, Chairman — 8 Dec 1987

Ernest J. Dorko — 3 Dec 1987

Alan Garscadden — 8 Dec. 1987

Alan V. Lair — 8 Dec 1987

F. Donald Stull — 8 Dec 1987

Accepted

J. S. Przemieniecki — 8 Dec. 1987

J. S. Przemieniecki
Dean, School of Engineering

Acknowledgements

Numerous people played important roles in this effort. I am deeply indebted to my principal advisor, Professor Won B. Roh, who patiently and expertly guided me through the program. I thank the other members of my Research Advisory Committee, Professors Ernie Dorko, and Alan Lair, and Dr. Don Stull, of the Aero Propulsion Laboratory. I wish to especially acknowledge the financial support of Dr. Stull and Dr. Julian Tishkoff, AFOSR/NA, which enabled the purchase of the dye laser and necessary supplies. Invaluable technical assistance with the maintainence of the experiment was provided by Mssrs. Bill Evans, Laboratory Supervisor, Rick Patton, and Walt Pemberton. I am also grateful for the assistance and encouragement of Drs. Alan Garscadden, Peter Bletzinger, Biswa Ganguly, Mssrs. Sigmund Kizirnis, Phillip Herren, Jr. and Don Linder, and Capt. Peter Haaland of the Power Division of the Aero Propulsion Laboratory. Dr. Kent Eisentraut of the Materials Laboratory provided valuable equipment and chemical analysis support. The friendship and cooperation of my fellow PhD candidates, Mr. George Baker, Capts. Jerry Bowman, Jeff Cavins, Wayne Chepren, Tim Kearns, and Laurie Wells, were a continuing source of strength.

Most of all, I am grateful to my wife Kathy, and my children, Rose, Sandy, and Michael. Their constant love and patience in the face of numerous frustrations made this effort possible. Their sacrifice for this project was every bit as great as mine. It is to them that I dedicate this work.

DTIC
COPY
INSPECTED
1

ion For

A-1

Table Of Contents

Acknowledgements iii

List of Figures vi

List of Tables viii

Abstract ix

I. Introduction 1

II. Description, Theory and Considerations of Laser-Induced Fluorescence 11

- Laser-Induced Fluorescence: A Description 11
- Theory of Laser-Induced Fluorescence 14
- LIF Considerations for BO and BO_2 19

III. Experimental Plan and Equipment 23

- Objectives 23
- Approach 23
- Equipment Description 28
  - Burner and Gas Supply Subsystem 28
  - Excitation Subsystem: The Lasers 31
  - Detection Subsystem 33

IV. Emission Spectroscopy Results 39

- Results for BO_2 39
- Results for BO 42
- Other Species 43

V. Laser-Induced Fluorescence Results and Discussion 44

- Flame Conditions 44
- LIF of BO_2 45
  - Excitation Scans 47
  - Fluorescence Scan 50
- Fluorescence Profile in the Flame 55
- Scattering in the Inner Cone 60
- LIF of BO 70
- Discussion of Results 70

VI. Conclusions and Recommendations 72

- Summary 72
- Recommendations for Future Work 73
- Alternative Techniques 74

Appendix A: Transition Probabilities for BO and BO_2 78

Table of Contents (continued)

Appendix B: Outline of NASA Chemical Equilibrium Code 78

Appendix C: Emission Spectra 80

Appendix D: Compiled Band Spectrum of BO_2 92

Appendix E: Laser-Induced Fluorescence Survey Spectra 112

Bibliography 132

Vita 137

List of Figures

Figure		Page
1.	Generic Laser-Induced Fluorescence Scheme	13
2.	Energy Change Processes	15
3.	Schematic Diagram of Experimental Apparatus	29
4.	Detection Signal Timing Schematic	36
5.	Boron Oxide Fluctuation Bands	40
6.	Emission from 00^00-00^00 Bandhead Region of A-X System of BO_2	41
7.	Non-Resonant Laser-Induced Fluorescence Signal from BO_2	46
8.	Excitation Scans at Different Laser Wavelengths	48
9.	Excitation Scan, Laser Wavelength at 5456.4 Å	49
10.	Excitation Scans of 00^00-00^00 R_2 Transition of BO_2	51
11.	Excitation Scan, Laser Wavelength at 5471.0 Å	52
12.	Composite Fluorescence Scan	54
13.	Fluorescence Signal vs Position in Flame, Total Flame	58
14.	Fluorescence Signal vs Position in Flame, Above Inner Cone	59
15.	Fluorescence Scan at Flame Base	65
16.	Raman Scattering Diagram	67
17.	Fluorescence Scans Showing Possible Raman Scattering	68
18.	Flame Emission, 5900-6100 Å	81
19.	Flame Emission, 5700-5900 Å	82
20.	Flame Emission, 5520-5720 Å	83
21.	Flame Emission, 5380-5580 Å	84
22.	Flame Emission, 5200-5400 Å	85
23.	Flame Emission, 5100-5300 Å	86

List of Figures (continued)

24. Flame Emission, 4800-5000 Å 87

25. Flame Emission, 4600-4800 Å 88

26. Flame Emission, 4400-4600 Å 89

27. Flame Emission, 4200-4400 Å 90

28. Flame Emission, 4000-4200 Å 91

29. Induced Fluorescence, 6330-6470 Å 113

30. Induced Fluorescence, 6210-6350 Å 114

31. Induced Fluorescence, 6080-6220 Å 115

32. Induced Fluorescence, 5940-6080 Å 116

33. Induced Fluorescence, 5820-5960 Å 117

34. Induced Fluorescence, 5720-5860 Å 118

35. Induced Fluorescence, 5610-5750 Å 119

36. Induced Fluorescence, 5480-5620 Å 120

37. Induced Fluorescence, 5350-5490 Å 121

38. Induced Fluorescence, 5230-5370 Å 122

39. Induced Fluorescence, 5120-5240 Å 123

40. Induced Fluorescence, 4990-5130 Å 124

41. Induced Fluorescence, 4860-5000 Å 125

42. Induced Fluorescence, 4750-4890 Å 126

43. Induced Fluorescence, 4635-4765 Å 127

44. Induced Fluorescence, 4515-4655 Å 128

45. Induced Fluorescence, 4395-4525 Å 129

46. Induced Fluorescence, 4275-4405 Å 130

47. Induced Fluorescence, 4140-4280 Å 131

List of Tables

Table		Page
I.	Comparison of Heating Values	1
II.	LIF Bands Observed	53
III.	Raman Transition Assignments	69
IV.	Transition Probabilities for the $A^2\Pi_u$ State of BO_2 . .	76
V.	Transition Probabilities for the $A^2\Pi_i$ State of BO . . .	77

Abstract

The purpose of this research was to demonstrate the feasibility of using laser-induced fluorescence (LIF) of boron oxide radicals in atmospheric-pressure flames. Such a demonstration would provide a useful tool with which to probe the detailed combustion chemistry of boron fuels. The radical species sought were BO_2 and BO, both having spectra in the visible region of the spectrum. These two species are believed to play critical roles in the boron combustion process.

A CH_4/air/O_2 flame was seeded with BCl_3 producing the green emission characteristic of boron flames. Unfortunately, it also created significant quantities of aerosols of solid boric acid from the reaction of the BCl_3 with the water vapor in the building air used in the flame. The burner was 1 cm in diameter and composed of approximately 60 capillary tubes. The burner could be remotely translated in two directions permitting investigation of different regions of the flame.

The flame was first probed using standard emission spectroscopy and exhibited only spectra from BO_2 and CH. The CH spectra dominated everything in its 0-0 band region, which also is the 0-0 band region of BO.

Next a tunable pulsed dye laser pumped by a Nd:YAG laser was used to produce a beam of photons tuned to absorption bands of either BO_2 or BO. A strong LIF signal was generated from the pumping of both the R_1 and R_2 branches of the $00^00\text{-}00^00$ transitions of the A-X system of BO_2. The effect was monitored by observing the $00^00\text{-}10^00$ transition. This is

the first known demonstration of LIF of BO_2 at atmospheric pressure. No LIF signal was observed from BO.

Certain regions of the flame exhibited strong Mie scattering due to the aerosols. These regions also showed preliminary evidence of resonant Raman scattering although a thorough examination of this effect was not made due to time limitations.

APPLICATION OF LASER-INDUCED FLUORESCENCE IN AN ATMOSPHERIC-PRESSURE BORON-SEEDED FLAME

I. Introduction

The combustion of boron in air has been a topic of periodic interest for over three decades. The interest is motivated by a continuing effort to achieve greater fuel performance for all kinds of combustion engines including aircraft, rockets and automobiles. Combustion researchers are looking beyond the derivatives of the well-known hydrocarbons, such as gasoline and kerosene, to completely different species such as aluminium, magnesium, and boron. The advantage being sought is a greater energy density in terms of calories per gram and/or calories per cubic centimeter. Theoretically, boron possesses advantages in both of these categories as shown in Table I.

TABLE I

Comparison of Heating Values (1:294)

Fuel	Gravimetric Heating Value, cal/g	Volumetric Heating Value, cal/cc
JP-5	10,150	8,230
Shelldyne-H	9,860	10,000
$(CH_2)_n$	10,400	9,600
Magnesium	5,910	10,300
Aluminium	7,420	20,000
Boron	13,800	32,200

Unfortunately, boron has not demonstrated its full potential in actual practice. The reason stems from the fundamental difference

between the burning processes for boron and the hydrocarbons. In hydrocarbon combustion, a volatile liquid fuel droplet vaporizes so that the actual oxidation, i.e., burning, occurs between gaseous species. Such gaseous reactions occur very rapidly which translates into compact combustion chambers and relatively small engines. However, because of the high melting and boiling temperatures of boron (approximately 2350 and 4150 °K, respectively (2)), boron oxidation reactions take place on the surface of the particle with no appreciable bulk melting or vaporization of the solid boron. Thus, the boron burning process is strongly dependent on the particle surface area and the diffusion rates of the gaseous oxidizer to the particle and the gaseous oxides away from the particle. In addition, for maximum heat output the reaction chain must continue until the final product is liquid B_2O_3. The resultant problems of long ignition times, incomplete combustion, and particle agglomeration dictate longer combustion chambers and larger engines with their obvious undesirable impact on the overall system. These difficulties, as well as interference from alternate chemical reaction channels which reduce the heat output, have prevented the dramatic performance gains sought and thus, precluded the large-scale development of boron fuels. However, the enormous potential of boron fuels justifies continued research into their combustion chemistry.

One of the first modern systematic studies of boron combustion was performed in the late 1950's by Talley (3). He used resistive heating of small boron rods in various atmospheres and measured the decrease in the rod's size to determine the combustion rate.

In the same time frame, Kaskan and Millikan used spectroscopy to analyze flames of trimethyl-borate (4). Their results showed that the

"fluctuation bands" of the boron flame, which extend from around 4500 Å to 6500 Å and were well known to chemists for many years from photometry experiments, are due to BO_2 not B_2O_3 as had previously been thought. This result prompted them to propose BO_2 as an important reaction intermediate. They also observed significant quantities of HBO_2 in their infrared spectra. The formation of HBO_2 is the principal alternative reaction channel in boron combustion and, being less exothermic than the B_2O_3 channel, causes a reduction of approximately 25% in the heat released (1:295).

Later, in the 1960's and early 1970's, Macek and Semple used photography to measure the burning rates of single boron particles dropped into a flame (5). Results of this work indicated a two-stage combustion process consisting of a slow ignition phase followed by a rapid burning phase. They concluded that because boron, like aluminium, oxidizes on the surface very readily, the first stage of combustion involved the removal of the oxide coating of B_2O_3. The second stage was the burning of the "clean" boron particle. By varying the gas mixture, they were able to show that the presence of water vapor could significantly lower the required ignition temperature. In seeking better experimental control, Macek replaced the flame with a focused laser beam (6,7). This permitted a more precise initiation point in time and space for the burning process. However, the primary diagnostic tool continued to be photography and the results were still only burning times. All of Macek's tests were done with crystalline boron particles.

Similar work by Mohan and Williams showed an apparent difference in burning rates for crystalline and amorphous particles (8). Whereas the crystalline boron went through the relatively long two-stage process

described above, the amorphous particles burned much more rapidly, almost explosively. The difference in burning characteristics is attributed to the belief that amorphous particles are really agglomerates of much smaller, submicron particles. The amorphous structure being highly non-uniform has a much greater surface area than the crystal so that it absorbs more laser radiation and oxidizes much more rapidly.

McLain and Evans used emission spectroscopy of simulated rocket flames burning Hybaline B-3 (CNB_2Be) in a hydrogen-oxygen gas mix to identify major combustion species such as BO_2, OH, CO_2, H_2O and HBO_2 (9). They demonstrated a qualitative correlation between observed intensities of spectral lines and theoretically predicted species concentrations. They did not see B_2O_3 in the infrared nor BO in the visible. In addition, they chemically analyzed the condensed combustion products of the flame and tentatively determined that a considerable amount of hydrogen had been trapped in the solid either as water or as a stable intermediate compound. The presence of hydrogen in the combustion products would reduce the specific impulse and the heat of reaction of the fuel (9:48).

Morrison and Schellar performed similar spectroscopic measurements on boron/JP-4 slurries (10). They were not able to observe the ultraviolet region, but their results in the visible and infrared were similar to those of McLain and Evans (9) with one notable exception. Morrison and Schellar claim to see a BO peak around 3400 Å, but only in the hottest part of the flame. If true, this peak would correspond to the (v',v")=(5,0) transistion of the A-X system of BO. Of further interest is the unlabeled peak near 4600 Å, which might be the (v',v")=(0,1) band of the A-X system of BO. Their diagram is unclear as to whether this

peak goes away in the lower temperature regions of the flame (10:96). It is surprising that this paper is the only one found in the course of this effort that indicates the presence of BO in a pure boron-seeded flame by other than theoretical equilibrium calculations. Gaydon does claim that BO is seen in flames of certain boron compounds such as diborane, B_2H_6, and pentaborane, B_5H_9 (11:315).

Schadow (12) and Ormand (13) performed engineering studies of boron cloud combustion. Schadow used boron powder entrained in $H_2/O_2/N_2$ or $CO/O_2/N_2$ gas flows in a large area combustion tunnel. Ormand used a smaller, constant area tube in which he entrained a boron dust cloud in air. Ormand achieved steady-state burning under fairly stringent conditions. Little spectroscopic or reaction rate data came from these studies, but some information on gross combustion control was obtained.

King and Macek analyzed the condensed exhaust products from rocket motor firings using boron-containing propellants (14). The condensed products were then burned in a controlled laboratory flame to examine possible afterburning requirements. The results showed that the products behave much as the original boron except the ignition times for the products were significantly shorter. This data harkens back to that of Mohan and Williams (8) indicating that the condensed products were agglomerates possessing large surface areas. (Komar has recently updated the old photographic techniques of Macek by using a two-dimensional CCD array to record the progress of particle combustion (15). The result is, in effect, a high-speed digital movie of the burning process. This technique will allow much more accurate determination of ignition times as well as the changeover to clean particle burning.)

Miller examined the conversion of HBO_2 to B_2O_3 (16). Using mass spectrometry of an expanding flow from a $H_2/O_2/N_2$ flame seeded with BCl_3, he showed that HBO_2 and its higher order compounds were the dominant reaction products. This is not unexpected with H_2O being the primary combustion product. While B_2O_3 was present, it was clear that once HBO_2 or its derivatives formed, the process of dehydration to B_2O_3 required many steps. Thus, it appears that the best course to avoid the loss of performance caused by HBO_2 may be to prevent its formation rather than trying to convert it to B_2O_3.

King wrote an extensive review paper on boron combustion wherein he described both theoretical models and experiments (1). His paper and a subsequent one by Glassman highlighted the lack of understanding of the actual reaction chains (1:302, 17:69-71). Glassman contends that boron oxidation starts with the formation of BO. The BO is then further oxidized via two channels. In the presence of H_2O, a series of fast reactions would dominate:

$$M + BO + OH \longrightarrow HBO_2 + M + 142.8 \text{ kcal/mole} \quad (1)$$

$$HBO_2 + BO \longrightarrow HBO + BO_2 - 50.3 \text{ kcal/mole} \quad (2)$$

$$BO_2 + BO \longrightarrow B_2O_3 + 130.0 \text{ kcal/mole} \quad (3)$$

$$M + HBO \longrightarrow BO + H + M - 73.0 \text{ kcal/mole} \quad (4)$$

The H radical then reacts with O_2 or H_2O to generate more OH. While the overall reaction set would be fast, the endothermic reactions

of Eqs. (2) and (4) would be slow relative to the other two reactions. If H_2O is not available, a much slower channel must be invoked:

$$BO + O_2 \longrightarrow BO_2 + O + 4.1 \text{ kcal/mole} \quad (5)$$

$$BO + BO_2 \longrightarrow B_2O_3 + 130.0 \text{ kcal/mole} \quad (6)$$

(The exothermicities shown above are calculated from the JANAF Thermochemical Tables (2) from the gaseous species' heats of formation at 2300 °K, i.e., near the melting point of boron.)

Of these reactions, only the reaction rate for Eq (5) has been measured. The most recent measurement by Oldenborg and Baughman shows a rate of approximately 2.5×10^{-12} cm^3/molecule-sec at 2000 °K (18:4). Incidentally, Oldenborg and Baughman present evidence that this reaction actually proceeds through another radical intermediate, BO_3 (18:4). Rate constants are not available for the other reactions. What is not evident in the equations above is the fact that HBO_2 is a relatively stable species such that the first reaction chain usually stops after Eq (1). Further, to obtain maximum benefit from the formation of the B_2O_3, it must be allowed to condense to the liquid state thereby releasing another 86.4 kcal/mole in the second reaction chain. Thus, the heat released by Eq (1) is only about 65% of that of the second reaction chain. Herein lies one of the reasons boron combustion performance has not met expectations. Unfortunately, the requirement to eliminate water vapor so as to avoid the formation of HBO_2 is extremely difficult to realize.

Either of these reaction chains requires significant concentrations of BO and BO_2 as intermediates. Glassman's primary justification for

these processes is by analogy with carbon oxidation. His hypothesis is supported at least qualitatively by the earlier experiments of Macek and Semple and their observations that water vapor lowered the required ignition temperature (5).

King has developed a model of boron combustion that encompasses both the ignition and clean burning phases and permits parametric analysis of the effects of pressure, temperature, particle size, and gas composition (1). The model can illustrate where the combustion is controlled by diffusion of reactants or by the kinetic rates of the reactions. As discussed above, there are two phases of the combustion process. During the ignition phase, the particle is heated by the surrounding gas and the oxide coating of the particle is gradually removed by melting and/or reaction with the water vapor in the gas, if any. Competing with the oxide coating removal is the reaction of the inner boron particle with the available oxygen to form more oxide. (There is disagreement over whether the oxygen diffuses to the boron through the oxide layer or the boron diffuses to the surface (17:63-67)). In order to maintain combustion during this phase, the temperature of the particle must be high enough so that the oxide vapor pressure at the surface is greater than that in the ambient gas. The diffusion of the gaseous oxide away from the surface tends to equalize the pressures and thus smother the reaction. King's model predicts that for an oxygen mole fraction of 20%, one atmosphere pressure, and no water vapor, the minimum temperature to avoid extinguishment is about 500°K for 10 micron particles and 1100°K for 5 micron particles. This trend of increasing temperature required with decreasing particle size arises from the fact that the smaller the particle, the faster the diffusion, such that the small particles are

actually kinetics rate limited. The model also illustrates that the presence of water vapor dramatically lowers the temperature required to maintain combustion, while the presence of B_2O_3 gas raises it. These effects are expected from the previous discussions. At higher pressures, diffusion of the oxide away from the surface is retarded and more oxide is produced such that the minimum temperature increases and the process becomes diffusion limited.

Continued heating of the particle will eventually cause the oxide layer to evaporate away sufficiently fast that the reactions begin taking place at the surface of the "clean" boron. For the small particles, 10 microns and less, the combustion is kinetics-driven also. As pressure increases such that more oxidant is available, the particle burn-time decreases eventually leveling out at pressures above 4 atmospheres. For larger particles, the burn time initially decreases with pressure but it reaches a minimum and then increases due to increased diffusion resistence.

Faeth has recently summarized the state of boron combustion (19). Among his recommendations for further investigation was work on the B-O-H chemistry. The crux of such an investigation is the development of diagnostics to measure the concentrations of relevant species. Some would argue that "simple" binary reactions should be studied first. Such an approach is certainly worthwhile, however, numerous such studies already exist (20,21,22,23,24). In most of these experiments, an atomic beam of boron is generated by heating solid boron in a crucible. The atomic beam then intersects a flow of the other reactant, such as O_2, H_2O, SO_2, N_2O, etc. and the resulting fluorescence is examined. Alternatively, Llewellyn, et al, reacted BCl_3 with O_2 that had been

passed through a microwave discharge to create BO and which was then combined with O_2 to create BO_2 (20). It is interesting to note that there appear to be no such studies of BO or BO_2 reacting with either H_2 or H.

An alternative or supplementary approach for analyzing the B-O-H chemistry is to examine boron reactions within the flame itself. Much progress over the last decade or so has been made in developing diagnostics, particularly non-intrusive, yet in-situ optical techniques, to examine hydrocarbon flames. These studies are now progressing beyond the small, well-controlled laboratory flames to full-sized combustion chambers and engines. However, it appears that very little of this capability has been applied to boron combustion. This study will begin to fill this void by applying one of these techniques, laser-induced fluorescence, to an atmospheric-pressure boron-seeded flame.

The next chapter discusses the theoretical background of laser-induced fluorescence as well as some of the practical considerations of applying this diagnostic to BO and BO_2 in an atmospheric-pressure flame. Chapter III details the experimental equipment, approach, and procedures employed. The next section discusses the results of applying standard emission spectroscopy to identify important species and possible transitions to be used later. The results obtained using laser-induced fluorescence are presented in Chapter V. Finally, Chapter VI contains a brief summary of results and conclusions along with some recommendations for follow-on efforts.

II. Description, Theory and Considerations of Laser-Induced Fluorescence

Laser-Induced Fluorescence: A Description

As discussed in the Overview above, BO and BO_2 are important reaction intermediates in the combustion of boron. To date, analysis of boron-seeded flames has been limited to survey emission spectroscopy and photographic records of boron particle burn times. The actual flame chemistry is still poorly defined. However, recent demonstrations of such laser spectroscopic techniques as laser-induced fluorescence (LIF) both in atmospheric-pressure hydrocarbon flames and on BO and BO_2 in low-pressure reactive flows have set the stage for unlocking the secrets of the boron flame.

With the advent of tunable dye lasers, a whole host of diagnostic techniques have been devised to perform in-situ measurements of such flame characteristics as species number density, temperature, velocity, flow field visualization, and more. This area is continually expanding with new ideas and refinements of existing methods. Schreiber, et al (25) and Crosley (26) have compiled excellent reviews of the primary methods in use while Harvey (27) discusses some of the newest innovations.

One of the earliest techniques to be applied was LIF. Conceptually straight-forward, LIF involves using a laser to excite a specific transition in an atom or molecule and then observing the resulting fluorescence as the species relaxes back to its ground state or some other lower energy state. The strength of the fluorescence signal can be related to

the laser pump power to yield a measurement of the number density of the particular species of interest. A generic energy level schematic of this process is shown in Figure 1.

There are basically two modes of operation: resonant LIF and non-resonant LIF. In resonant LIF, the transition observed is the same as the transition pumped. In order to avoid scattered light from the laser, this mode requires either a gatable detector that is turned on just after the pump beam passes through the sample, or a fast digitizer to record the temporal decay of the fluorescence signal, which is usually longer than the laser pulsewidth. With the digitized output, one can discard that portion of the signal due to the laser beam and only analyze the portion due to the fluorescence. In non-resonant LIF, the transition observed is one other than the pump transition, but, usually, still having the same upper state. Laser scatter is not a problem in this mode since the desired signal is in a different spectral region.

LIF possesses many advantages over standard absorption or emission spectroscopy. First, the narrow linewidths available with current dye lasers permit selective excitation of specific transitions thus making the technique species specific and, in fact, energy state specific. Second, the ability to focus the laser beam very tightly provides excellent spatial resolution. Third, pulsed or mode-locked lasers with pulsewidths of close to ten nanoseconds or picoseconds respectively, hold the potential for tremendous temporal resolution. However, in most cases, the signal must be integrated over a number of shots to achieve reasonable signal-to-noise ratios. Fourth, since the resulting fluorescence is emitted isotropically the detection system can be positioned out of the laser beam path. (Most systems have the spectrometer perpendicular

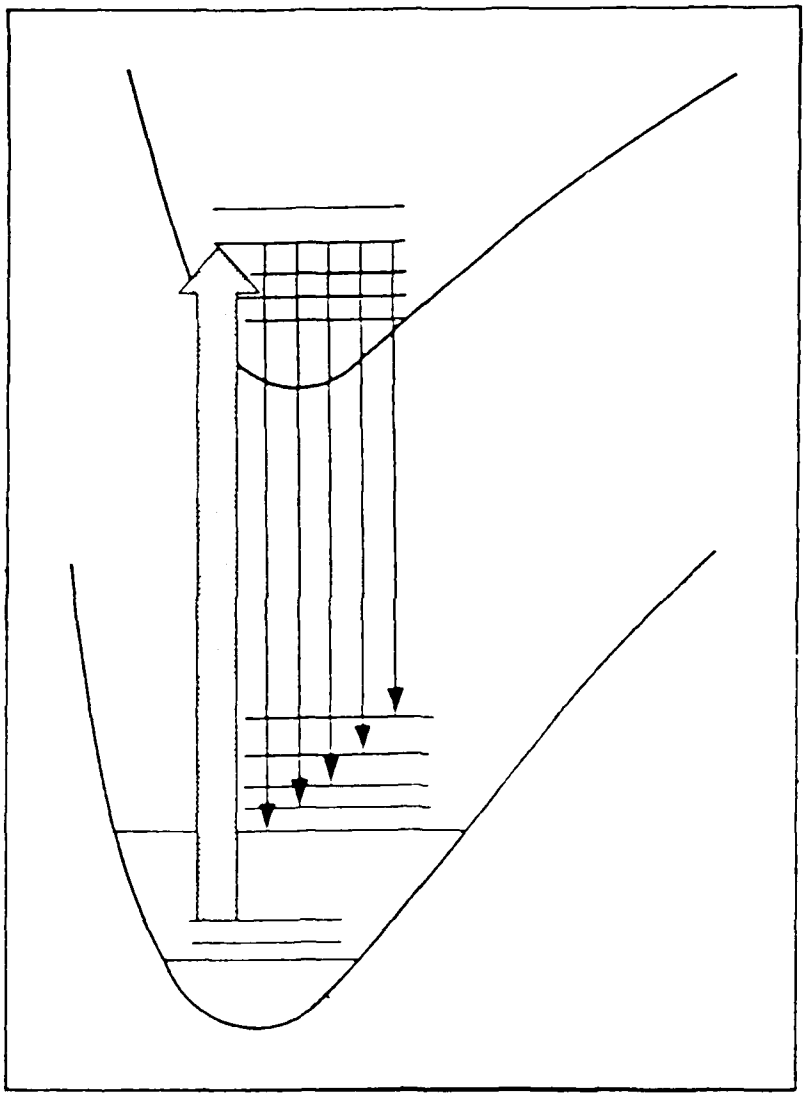


Figure 1. Ceneric Laser-Induced Fluorescence Scheme (29:550)

to the beam path.) Thus, unlike methods such as laser absorption, where one looks for a small change in a large signal, LIF produces a signal against a constant or nonexistent background depending on if the chosen transition for observation is already emitting in the flame. All of these advantages have contributed to demonstrated sensitivities in the parts-per-million range. This high sensitivity is ideal for minority species detection.

Unfortunately, the technique encounters limitations in high pressure environments where the collision frequency among the flame constituents approaches the spontaneous emission rate. Such conditions result in the loss of a significant number of excited states by the collisional transfer of their energy to other states of the same species or to other species altogether. This collisional quenching seriously degrades and complicates the fluorescence signal. Nevertheless, LIF has been demonstrated in atmospheric pressure flames for a variety of species (26:12).

Theory of Laser-Induced Fluorescence

Daily has discussed the theory of LIF in a review article (29). Consider a simple two-level system where N_1 is the number density of atoms or molecules in the lower level and N_2 is that in the excited level. Figure 2 illustrates the five processes occurring in LIF: absorption of the pump laser beam represented by the Einstein coefficient B_{12}, spontaneous emission of light, i.e., the desired fluorescence signal, represented by the Einstein coefficient A_{21}, collisional quenching, Q_{21}, which includes redistribution of energy within the same atom or molecule, collisional excitation represented by Q_{12}, and stimulated emission represented by the Einstein coefficient B_{21}. Following Daily's

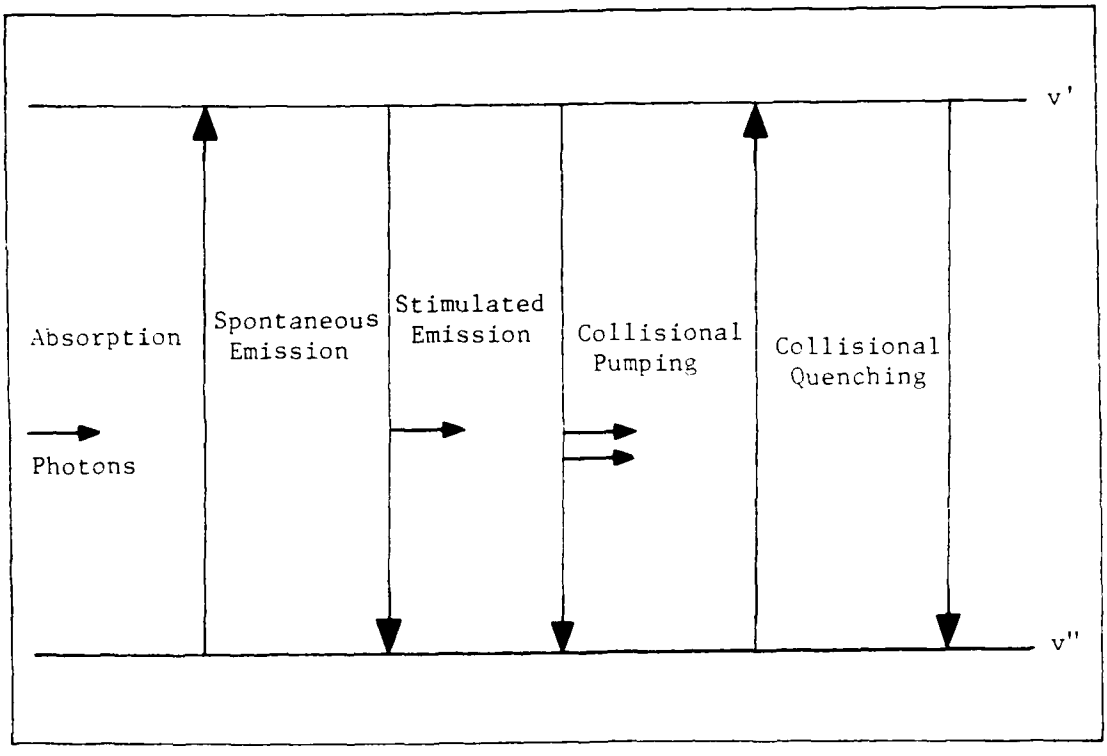


Figure 2. Energy Change Processes

derivation (29:63-65), one can write the rate equation for the change in the number density in the excited state as:

$$dN_2/dt = (Q_{12} + B_{12}\rho_\nu)N_1 - (Q_{21} + A_{21} + B_{21}\rho_\nu)N_2 \quad (7)$$

where ρ_ν is the spectral energy density of the laser beam. In addition, for this idealized two-level system the total number (N_T) of atoms or molecules is:

$$N_T = N_1 + N_2 \quad (8)$$

These equations can be solved in steady state making use of detailed balance such that $g_1B_{12} = g_2B_{21}$ (where g_1 and g_2 are the degeneracies of the respective levels):

$$N_2 = (Q_{12} + B_{12}\rho_\nu)N_T/(Q_{12} + Q_{21} + A_{21} + (B_{12} + B_{21})\rho_\nu) \quad (9)$$

Since N_1 is usually much greater than N_2 and since collisional excitation is usually much less than quenching Eq (9) can be simplified to:

$$N_2 = (B_{12}\rho_\nu/(Q_{21} + A_{21} + (B_{12} + B_{21})\rho_\nu))N_T \quad (10)$$

A saturation energy density ρ_ν^s can be defined at which the transition rates of the stimulated processes (absorption and stimulated emission) are equal to the sum of the rates for the other processes:

$$\rho_\nu^s = (Q_{12} + Q_{21} + A_{21})/(B_{12} + B_{21}) \tag{11}$$

This leads to a simple expression:

$$N_2 = N_T \quad /((1 + (g_1/g_2))(\rho_\nu + \rho_\nu^s)) \tag{12}$$

In the case of low pump power, Eq (12) reduces to:

$$N_2 = N_T \quad /((1 + (g_1/g_2))\rho_\nu^s) \tag{13}$$

The fluorescence yield, Y, represents the fraction of the total number of excited states that actually emit the desired photons and can be defined as:

$$Y = A_{21}/(Q_{21} + A_{21}) \tag{14}$$

With this definition, Eqs (11) and (13) can be combined to yield:

$$N_2 = (B_{12}/A_{21})Y\rho_\nu N_T \tag{15}$$

The fluorescence power detected will be:

$$P_F = h\nu A_{21} \Omega_c V_c N_2/(4\pi) \tag{16}$$

where V_c is the focal volume from which the fluorescence is collected, Ω_c is the solid angle of the collection optics, and ν is the frequency of the observed transition.

Upon substitution of Eq (15) into Eq (16), an expression is obtained that relates the number density of the particular species to the fluorescence power:

$$P_F = h\nu B_{12}\Omega_c V_c Y \rho_\nu N_T/(4\pi) \tag{17}$$

For the case of high pump powers an interesting situation arises. If the laser power is great enough, i.e., $\rho_\nu >> \rho_\nu^s$, the $B_{ij}\rho_\nu$ terms dominate in Eq (7) such that its steady state solution becomes:

$$N_2 = (B_{12}/B_{21})N_1 \tag{18}$$

or:

$$N_2 = (g_2/g_1)N_1 \tag{19}$$

This result means that the number densities in the two states will have a known ratio if the system is in a state of complete saturation. This effect is called saturated LIF. This condition leads to a simplification of Eq (12):

$$N_2 = N_T/(1 + g_1/g_2) \tag{20}$$

The potential advantage of using saturated LIF is that the effects of quenching are essentially removed by the large pumping rates. Since quenching rates are very hard to obtain, the elimination of this unknown

would greatly simplify the data analysis. Daily states that while the theory is straight-forward for atomic species, it becomes complicated for molecules because of the much greater number and density of energy levels to which the pump energy can be lost (29:65-71). Thus, for molecules, much greater laser powers are required for saturation to take place. This need might still be met however, by pulsed dye lasers. Bonczyk discusses such considerations as uniform beam intensity, rotational-vibrational state equilibration rates and other possible interferences that affect saturated LIF measurements (30).

LIF Considerations for BO_2 and BO

The first requirement for applying LIF is that the spectrum of the desired species be known. The spectrum of BO_2 was seen for many years though it was thought to be that of B_2O_3. Indeed, Dean and Thompson, among others, performed flame photometric tests on boron and boron compounds as photometry grew in popularity in the 1950's (38). As already noted, the discovery by Kaskan and Millikan that the green emission was from BO_2 actually resulted from flame studies of trimethyl borate (4). Johns then obtained a high resolution absorption spectrum of BO_2 using flash photolysis of BCl3 and O_2 (39). Snowden obtained a high resolution emission spectrum of BO_2 by passing the vapor from a heated mixture of KBF_4 and B_2O_3 through a microwave discharge (40). His results confirmed and extended those of Johns.

Russell, et.al., used an argon ion laser to explore several vibronic transitions that are resonant with the 5145 A and 4880 A laser lines (41). Fried and Mathews took the next step using a pulsed tunable dye laser to examine many transitions in the $A^2\Pi_u$-$X^2\Pi_g$ system (42). These

two efforts created BO_2 in low pressure reactions similar to Mulliken, but they stand as the first real demonstrations of LIF of BO_2. Their results primarily yielded additional transitions not seen by Johns as well as various spectroscopic parameters. Huie, et al., used LIF to measure the lifetime of some of the low lying excited states of BO_2 (43). In 1980, Clyne and Heaven demonstrated LIF of BO as well as BO_2, though still only at a total pressure of a few torr (44). Recently, Hodgson used LIF under similar conditions to more thoroughly examine the lifetimes of various BO_2 states (45). Oldenborg has devised an elegant experiment wherein he photolyzes BCl_3 to produce an instantaneous source of gaseous boron atoms (18). He then allows the boron atoms to react with a few torr of O_2 in an inert buffer gas of tens of torr using LIF to monitor the concentration of the boron atoms as well as the BO and BO_2 molecules. This technique allows the measurement of the reaction rates for some of the processes discussed above and provides a temporal profile of the species concentrations.

The spectrum of BO was analyzed as far back as 1925 by Mulliken (31) and 1932 by Jenkins and McKellar (32). The spectra for these studies came from mixing active N_2 with BCl_3 at very low pressure. The O_2 was not intentionally supplied and probably came from leaky vacuum systems. Various bands have been rotationally analyzed (33,34,35) and Franck-Condon factors have been calculated with a Morse potential (36) and using the RKR method (37). Thus, the BO spectrum is reasonably well in hand.

Thus, the groundwork is laid for the proposed study. Clearly, because BO_2 is easily seen in boron-containing flames, LIF of it should be possible. However, BO emission is rarely seen in a flame as noted

above. Therefore, the possibility of observing BO in LIF in an atmospheric-pressure flame remains questionable. The results of Clyne and Heaven are not definitive with regard to this matter. In their quenching rate measurements of BO by N_2, they saw no significant effect and thus bounded the rate at less than 2×10^{-11} cm^3 $molecule^{-1}sec^{-1}$ (44:306). Still, their range of pressure variation was only 0.3-1.15 torr, whereas the proposed tests will be performed at 760 torr. It is hard to believe that their quoted quenching rate will remain linear over almost three orders of magnitude. Such an extrapolation leads to a quenching rate of 4×10^8 sec^{-1} at 760 torr. The quenching rate of BO_2 by O_2 has been measured to be $1\text{-}2 \times 10^{-10}$ $cm^3 molecule^{-1}sec^{-1}$ or about $3\text{-}6 \times 10^9$ sec^{-1} at 760 torr, which is a factor of ten larger than the BO quenching rate (45:1446,1448). One must be careful in comparing the two quenching rates noting that the results are for different excited molecules as well as different quenching molecules. Thus, the collisional interaction physics for the BO_2 quenching is likely to be very different from that for BO. However, if one accepts the proposed reaction channels of Glassman (17) and, even King (1), BO is a precursor of BO_2. So, if BO_2 is present, as it surely is, then BO must also be present to some degree.

Before proceeding further, a rough calculation using Eq (17) should indicate if sufficient signal will be available to make the investigation worthwhile. Consider BO_2 and take as values a pump wavelength of 5470 Å, a lifetime of about 100 nsec, which yields an A coefficient of 10^7 sec^{-1}, which can be related to the B coefficient by:

$$B_{12} = A_{21} \lambda^3/(8\pi h) \quad \text{for } g_1 = g_2 \tag{21}$$

The apparatus parameters, to be discussed in more detail in the next chapter, are a collection lens radius of 3.75 cm and set a distance from the flame of about 34 cm, laser beam radius of 0.2 cm, projected slit width of 0.013 cm, laser bandwidth of about 0.2 cm^{-1} or 6 GHz, laser energy of about 5 mJ with a pulsewidth of 10 nsec for a laser power of $5x10^5$ W. Daily estimates that for heavily quenched molecules Y is near 10^{-5} (29:71).

Further Daily relates the laser power to its spectral energy density by:

$$\rho_\nu = P_L/(A_b c \delta\nu_s) \tag{22}$$

where P_L is the laser power, A_b is the cross-sectional area of the laser beam, and $\delta\nu_s$ is the laser bandwidth in sec^{-1} (29:71). Now assuming the BO_2 density is one part per million (10^{13} cm^{-3} at atmospheric pressure), then Eq (17) yields a fluorescence power of about 1 mw, which corresponds to about $3.5x10^{15}$ photons/sec. For reasonable values of optical efficiency of the spectrometer/detector of 30% and detector quantum efficiency of about 10%, and an integration time of ten molecular lifetimes or 1 microsecond, the number of counts expected per pulse is $1x10^8$. This signal should be observable. The greatest unknown in this calculation is the quenching rate. Before absolute quantitative results are obtained with LIF, more quenching rate measurements are required.

III. Experimental Plan and Equipment

Objectives

Three principal objectives were sought during this effort. The first was to apply emission spectroscopy in the visible spectrum to a small, controlled laboratory flame seeded with boron trichloride, BCl_3. Particular emphasis was placed on identifying the emission of BO_2 and BO. The second objective was to demonstrate LIF or other laser spectroscopic techniques on boron compounds, principally BO_2 and BO, in an atmospheric-pressure flame. Finally, an attempt was made to construct two-dimensional relative fluorescence map of BO_2 in the flame as a function of flame parameters using LIF or other techniques.

Approach

The project proceeded through three phases. The first phase consisted of examining the emission spectrum from a $CH_4/air/O_2$ flame seeded with BCl_3. The purpose of this phase was to allow familiarization with the flame control and data collection systems. More importantly, this phase identified the spectral bands or lines used for later LIF measurements. The use of BCl_3 rather than solid boron particles at this point was driven by the desire for a uniform distribution of the boron in the flame. BCl_3 is a gas at room temperature and atmospheric pressure and therefore mixed relatively easily with the fuel-oxidizer gases.

With the emission spectrum was characterized, the demonstration of LIF in a BCl_3-seeded flamewas performed. The BCl_3 was still used for uniform mixing. Based on the spectroscopic observations of Phase I and

those of other researchers discussed in Chapters I and II above, some possible LIF transitions were examined.

The strongest bands normally observed from BO_2 are at 5456 Å and 5470 Å, which comprise the $v'\text{-}v''=00^00\text{-}00^00$ transition in the $A^2\Pi_u\text{-}X^2\Pi_g$ system. (Note that transitions will be labeled with the upper state, v', listed first and the lower state, v", listed second as in common spectroscopic practice.) The splitting of the transition into two sub-bands results from the spin-orbit coupling of the electrons. The advantage of pumping this transition would be that the lower state is in fact the molecule's ground state, which would have the maximum population available for excitation. However, because it is the strongest band in the emission spectra, observation of the induced fluorescence from this same transition, i.e., resonant LIF, may involve looking for a small perturbation on a large background of chemiluminescence from the flame. Therefore, observation of the transition $00^00\text{-}10^00$ at 5813 Å or 5790 Å, i.e., non-resonant LIF, may be helpful since these are less intense chemiluminescent bands and the scatter from the laser beam would also be avoided. Llewellyn, et al., used a similar scheme to monitor the BO_2 production from BO in a fast-flow reactor (20:506). Exciting the 5470 Å or 5456 Å bands might be accomplished using the 5320 Å frequency-doubled output of a Nd:YAG laser to pump a Fluorescein 548 dye. Unfortunately the desired wavelength is on the very short wavelength end of the tuning curve of the dye such that the output power might be very low. Another scheme would be to pump a Coumarin 500 dye with a tripled-frequency Nd:YAG pulse at 3550 Å. However, generating the 3550 Å radiation was very difficult with the available equipment and the Coumarin dyes are fairly short-lived requiring frequent, time-consuming dye changes.

Inversely, one could pump the 5790 Å or 5813 Å band of the 00^00-10^00 transition already mentioned above. This transition's inherently weaker emission intensity may permit resonant detection of the same transition. If not, observation of the 6170 Å or 6202 Å lines in the 00^00-20^00 transition may be necessary. The distinct advantage of the 5790 Å and 5813 Å bands is the ability to excite them using stable Rhodamine dyes pumped with the easily obtained 5320 Å doubled-frequency Nd:YAG pulse.

LIF of BO should prove more difficult. While the $A^2\Pi_i$-$X^2\Sigma_+$ system of BO runs from 3100 Å to 8500 Å, the strongest transitions are in the 4000-5000 Å range. For example, the v'-v"=0-0 transition is at 4250 Å. Exciting this transition would require a tripled-frequency Nd:YAG pulse pumping a Stilbene 420 dye, which is even shorter-lived than the Coumarins. Moving out to longer wavelengths, the 0-1 band is near 4600 Å and the 0-2 band is around 5000 Å. Either of these would still require the tripled Nd:YAG pulse (though Coumarin dyes would be used). Finally, the 0-3 band is around 5500 Å, which would allow use of the Rhodamine dyes and the doubled Nd:YAG. Coincidentally, the 0-3 transition has the highest Franck-Condon factor of any of those in the A-X system (44:1049). This is obviously a plus, in addition to the fact that observation of the fluorescence could be made at the shorter wavelengths noted above, thus avoiding the pump beam scattering background. The big question is how many BO molecules are in the v"=3 vibrational level of the ground electronic state and available for pumping. A simple Boltzmann analysis assuming the vibrational states are in equilibrium with the flame temperature of about 2000°K predicts that only about 2% of the population is in the v"=3 level. However, because the vibrational states may not be in

equilibrium, there is a possibility that the v"=3 level will be more populated. The other advantage of the 0-3 band of BO is that it lies in a window in the BO_2 spectrum so that spectral overlap is more easily avoided.

If shorter wavelength transitions must be used, an interesting possibility arises. The 1-1 transition of BO has band heads at 4339.6, 4342, 4363.4 and 4365.9 Å. The 00^02-00^00 transition of BO_2 has assigned band heads at 4340.5, 4314.2 and 4349 Å. Thus, if one excites at 4340 Å and observes at the other bandheads, one may be able to simultaneously observe BO and BO_2 using a single laser. Clyne and Heaven did observe BO_2 using the 4340 Å excitation, but not BO (44). The reason is that in their experimental arrangement they used different gas mixtures and pressures to produce either BO or BO_2. They never detected both species together (44:301). Llewellyn, et al., did observe both species in the same flow, but used different excitation wavelengths for each molecule (20). It must also be noted that use of the 4340 Å wavelength for excitation could generate significant interference from the spectrum of CH and thereby preclude this scheme (46,47). While the experimental difficulties of such a simultaneous observation would be great and questions about the relative quenching rates, etc. would exist, the possibility of monitoring both species at the same point in space and time might be worth the effort.

With the demonstration of LIF, Phase III was initiated to produce a two-dimensional map of fluorescence intensity in the flame by precision translation of the flame vertically and horizontally. Thus, the excitation and observation volumes were fixed in the laboratory reference frame and the flame moved so that different regions of it were sampled. From

the theory developed in Chapter II, one can roughly equate the fluorescence profile to a species number density profile. Clearly any detailed quantitative analysis of such measurements must somehow account for differences in excitation and quenching rates. Such a map may yield some insight into the reaction channels of boron combustion. Further, if a similar map could also be made of the local flame temperature, two of the three critical quantities needed for a combustion model would be in hand. (The other quantity necessary for a complete model is the velocity of the molecules.)

Unfortunately, temperature measurements by optical means in our laboratory pose significant experimental difficulties. On the one hand, one might suppose that the rotational states of a molecule would equilibrate rapidly such that if one could measure the relative intensity of several rotational lines, one might be able to back out the temperature via Boltzmann statistics. However, Crosley has shown that the rotational and vibrational state population distributions may be considerably non-Boltzmann even at high pressure with many collisions (48). The primary reason for this is that the quenching rate and rate of energy transfer between states of the same molecule are often very state-specific. Thus, unless detailed information is known about these rates for the states involved, significant errors can result from such a calculation. The only quenching rates that exist for BO and BO_2 are from Huie, et al., (43), Clyne and Heaven (44), and Hodgson (45) and these only cover a few states and a few quenching species.

To somewhat offset the lack of detailed temperature measurements, predictions of adiabatic flame temperatures were made. Using the chemical equilibrium code developed by Gordon and McBride, calculations

yielding flame temperature and overall species concentrations were made based on known experimental parameters such as fuel (CH_4), oxidizer (air and O_2), and seedant (BCl_3) flow rates (49). A brief description of the code can be found in Appendix B. Correlation of the predicted relative concentrations and the observed fluorescence intensities might provide insight as to where in the flame equilibrium conditions were approached. Of course, such correlations must be viewed critically because of the associated inherent assumptions about equal quenching rates and other loss and energy-branching processes.

Equipment Description

Figure 3 is a schematic showing the experimental layout and electronic connections.

Burner and Gas Supply Subsystem. The burner was supplied by Mr. S. Kizirnis of the Aero Propulsion Laboratory. It consisted of a central bundle of sixty-one 1 mm diameter stainless steel capillary tubes brazed together to form a core approximately 1 cm in diameter. Surrounding the core is a brass annulus approximately 6.3 cm in diameter with approximately 120 2 mm holes in the top surface. The premixed flame reactants flow through the core bundle and support the flame. Though rarely used, a shroud flow of non-reacting gas such Ar or N_2 through the outer annulus could be used to isolate the flame from the laboratory air and its associated turbulence.

A cylindrical chamber 4.5 cm in diameter by 2 cm high which threaded into the base of the burner served to premix the gases. The CH_4 and the air/O_2 were brought in through two tubes positioned tangentially to the chamber and in opposing directions. This provided a swirling of

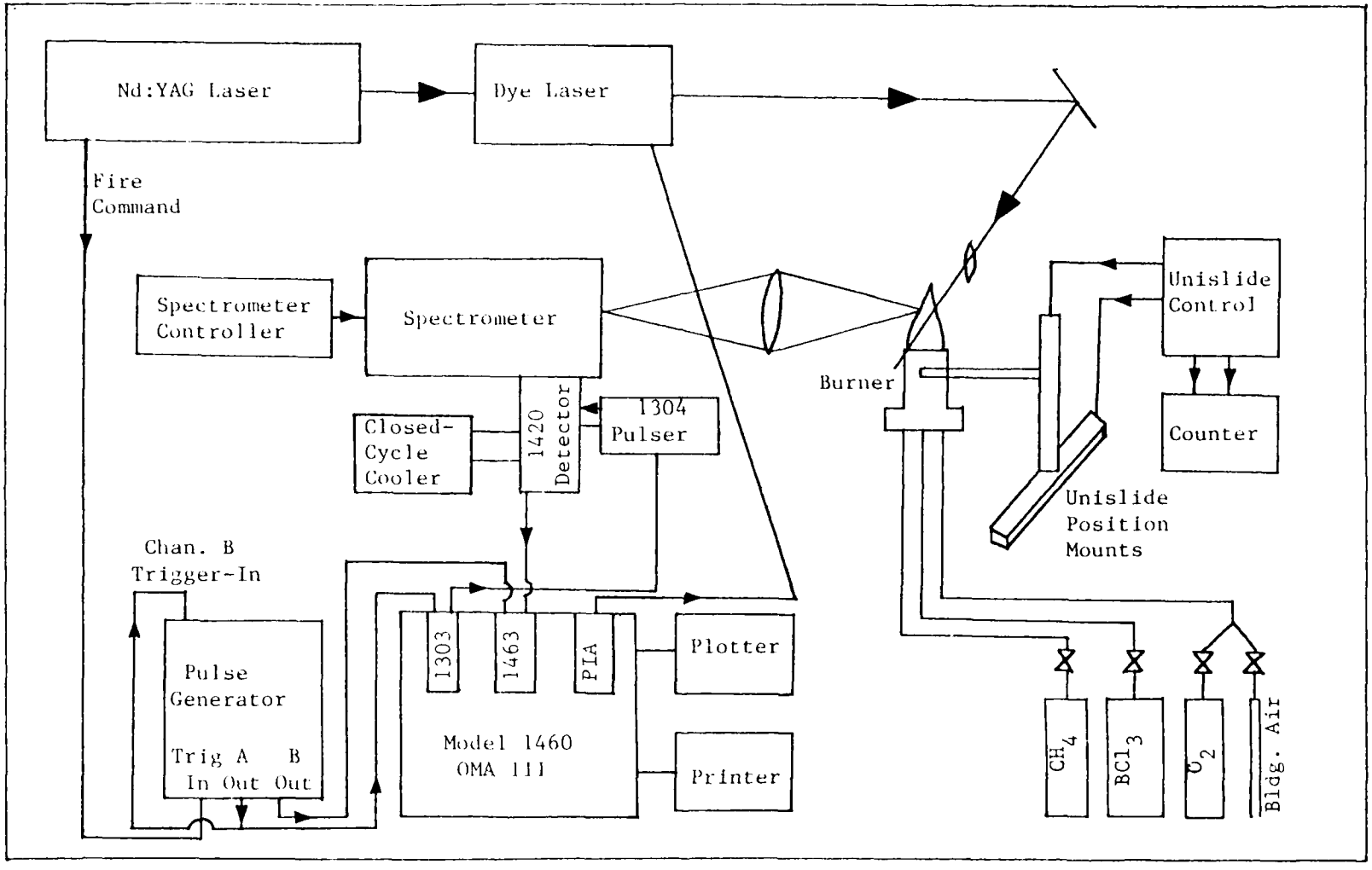


Figure 3. Schematic Diagram of Experimental Apparatus

the gases necessary for good mixing. The BCl_3 entered through a tube directed radially into the chamber.

Methane (CH_4), Matheson CP-grade, was the fuel. The oxidizers were air, obtained from the building supply, and oxygen (O_2), Matheson Zero Gas-grade. Methane-oxygen flames have high temperatures, over 2000°K, which are desirable for boron combustion, but their resulting high flame speeds make them difficult to control. The air was used to reduce the flame speed so that the flame would remain on top of the burner and not propagate back into the mixing chamber and feed lines. This increase in control required a sacrifice in the flame temperature. The BCl_3 was purchased from Matheson also and came as a liquid under pressure in a size-3L gas cylinder. No special processing was done on the BCl_3. Its vapor pressure at room temperature, which is approximately 4 psig, was used to flow the gas through the system. The gases were controlled through Matheson rotameters so that input species concentrations were known.

The flame had a narrow regime in which it was stable, i.e., well-formed and not fluctuating or bouncing due to its own turbulence. Typically, the methane and air were first ignited and their flow rates adjusted to produce a stable blue flame with no yellow coloring apparent. Yellow emission in these flames indicates soot formation from incomplete combustion of carbon. The height of the flame was adjusted via the gas flow to be approximately five to seven centimeters tall. Next, the oxygen was added with its flow determined by the formation of an inner flame cone approximately one-half to one-third the height of the overall flame. The addition of oxygen was fairly sensitive and required care to prevent the inner cone from propagating back down the capillary bundle.

A particularly annoying problem with this arrangement was the formation of a white crystalline powder from the reaction of the BCl_3 with the other gases. The powder would clog the BCL_3 rotameter necessitating the installation of a helium purge system to try to clear the BCl_3 line prior to opening the BCl_3 source. Further, this powder would clog the input ends of the burner capillaries after 20 to 30 minutes of operation depending on the BCl_3 flowrate. This occurred even when the flame was present. Fortunately, the powder was soluble in water and could easily be removed by simple soaking or by use of a heated ultrasonic cleaner filled with distilled water. The identification of the powder and its impact on the experimental results are discussed in Chapter V.

The burner and mixing chamber assembly was cantilevered from a motorized Unislide Model B2500 translation stage oriented vertically. This stage was itself mounted on a second identical stage oriented to travel parallel to the laser beam path. This arrangement permitted precision movement (resolution of 5 microns) of the cross section of the flame facing the detection system. Movement of the sample volume along the third direction (perpendicular to the laser and along the detection optics path) was achieved by translation of the laser beam with turning mirrors. The translation stages were controlled with a Unislide Model 8202M1 Stepping Motor Controller and monitored with a Hewlett-Packard Model 5280A Reversible Counter.

Excitation Subsystem: The Lasers. A Quantel Model YG481 Nd:YAG Laser was used to pump a Lambda Physik Model FL3002E Dye Laser which provided the excitation for the LIF. The Nd:YAG laser was Q-switched with a pulse width of approximately 10 nsec and a maximum repetition rate

of 10 Hz, though it was usually operated at 5 Hz. The Nd:YAG laser beam, in the infrared at a wavelength of 1.064 microns, was frequency-doubled to yield a beam at approximately 5320 Å. Because of pumping constraints in the dye laser, the maximum pulse energy used in the frequency-doubled Nd:YAG laser beam was limited to about 120 mJ, which was obtained with flashlamp voltages of approximately 1.62 kV. This was well below the flashlamps' maximum operating voltage of 1.8 kV. The Nd:YAG laser system generated a considerable amount of electrical noise from both the flashlamps and the Q-switch driver circuit that created significant problems for the detection electronics.

The dye laser was operated with Fluorescein 548 dye from Exciton, Inc. Lasing was achieved over a range from 5450 Å to 5650 Å with pulse energies ranging from 1 to 10 mJ. The laser linewidth at 5460 A is specified in the operations manual as approximately 0.05 Å without the use of an intracavity etalon. This could not be verified because the detection system resolution was only about 1.1 Å. However, using 50 micron slits on the spectrometer, the Rayleigh scattering peak of the laser in air showed a width of less than 2 Å in full-width-at-half-maximum (FWHM). An optogalvanic measurement of the linewidth using an argon hollow cathode lamp failed because of noise interference from the Nd:YAG laser system. The dye laser is quite easy to use having its own programmable microprocessor control, communications capability with other devices, and simple alignment and dye cell exchange procedures.

This dye laser was designed primarily for use with excimer pump lasers whose wavelengths are well into the ultraviolet. An unfortunate characteristic of this system that seems to result from using a frequency-doubled Nd:YAG laser pump is the appearance of a broad secondary

fluorescence peak approximately 100 Å to the red side of the laser line. This peak is only significant when working in the wings of the dye tuning curve where it could cause additional complication of the LIF spectrum. No method currently exists to easily eliminate this peak. The user must simply avoid working in the dye wings or where this peak may excite unwanted transitions.

The beam was slightly focussed by an f/3 lens to produce a roughly circular cross section with a diameter of about 4 mm at the flame. At 5 mJ pulse energies, this yields a power density of nearly 4 MW/cm^2.

Detection Subsystem. The detection system centered around an optical multichannel analyzer (PAR Model 1460 OMA III). The OMA III is an extremely powerful data collection and analysis system based on its own microprocessor. The operating system software provides a variety of data acquisition modes via different permutations of triggering, scan rates, integration times, background subtraction and source compensation. The software also supplies almost all the necessary calculation and data display options one could use including data storage on floppy disks, plotting on its own CRT and an external plotter, hard copy printout, curve area calculations, and communication facilities with other computers or computer-controllable devices. With its capacity to be programmed in BASIC so that all of these capabilities could be employed with a relatively simple code, the OMA III was used to control all data acquisition and analysis and dye laser control. In the latter case, the OMA's PIA port was used to send TTL pulses to the dye laser's control port allowing software control of the scanning of the laser.

For the emission spectroscopy, the spectral dispersion was performed by a 0.5 m spectrometer (Jarrell-Ash Model 82-020) with a grating

having 1180 lines/mm. A silicon photodiode detector (PAR Model 1454) having an intensified linear array of 512 diodes detected the optical signals. Resolution of this arrangement was approximately 1.6 Å for 25 micron slits. The flame emission was collected with an F/2 lens, which was considerably faster than the spectrometer. The system was spectrally calibrated using Jarrell-Ash Hollow Cathode Lamps with atomic lines in the region of interest. The data acquisition consisted of establishing a stable flame without the BCl_3 positioned so that the region just above the inner flame cone was focussed on the center of the slits. This emission was accumulated for a set period and then stored as background. Next, the BCl_3 was introduced into the flame and this emission was accumulated for the same period. The first file was then subtracted from the second by the OMA yielding the net emission due to the addition of the BCl_3. The slit width and integration periods varied depending on the strength of the emission in different spectral regions. The goal was to use the narrowest slits possible to obtain the best resolution while still retaining a good signal-to-noise ratio.

The LIF experiments used the same collection lens which directed the fluorescence photons into a 0.64 m spectrometer (Instruments SA, Inc. Model HR-640) with a 1200 g/mm grating. A PAR Model 1420R-512-G Solid State Detector replaced the Model 1454. This configuration had an improved resolution with 25 micron slits of about 1.1 Å. This Model 1420 detector also had 512 diodes but used a microchannel plate to intensify the signal. By switching the bias voltage between the photocathode and the microchannel plate, the detector could be gated. Gating was controlled by the OMA III via a pulse amplifier (PAR Model 1303) driving a second pulse amplifier (PAR Model 1304). The former has programmable

delays and gate widths set by the operator through the OMA III software and puts out a TTL-level gate pulse. The 1304 maintains the bias between the photocathode and the microchannel plate at +200 V keeping the gate closed and the detector "off" until it receives the gate pulse from the 1303 whereupon the bias is driven to 0 V for the duration of the pulse. The advantage of gating the detector for this experiment is that it reduces the amount of flame chemiluminescence that acts as a background signal and must be eliminated by later signal processing. Of course even when the gate is closed, the detector still collects "dark" counts from thermal electrons in the detector. However, the "dark" count is reduced significantly by cooling the detector to approximately -30°C with its own thermoelectric cooler aided by a closed-cycle cooler flowing a distilled water/ethylene glycol mixture through the detector's cooling channels.

A pulse generator (Hewlett-Packard Model 8010A) served to synchronize the excitation and detection systems by providing the necessary trigger pulses to control the gate pulse generation and the scanning of the diode array. Figure 4 is a timing diagram for the data acquisition process. Channel A of the 8010A was operated in the double-pulse mode and triggered by the fire command pulse from the Nd:YAG laser control module. In the double-pulse mode, Channel A provided two pulses for each trigger pulse it received. The time between these pulses could be adjusted over a wide range. This capability was used to allow pseudo-real time background subtraction by causing two identical, complete data acquisition sequences to occur for each laser pulse. The sequences were temporally spaced so that in one sequence the detector integrated during and for a short time after the laser pulse. This data would contain background ("dark" counts and flame chemiluminescence) plus the desired

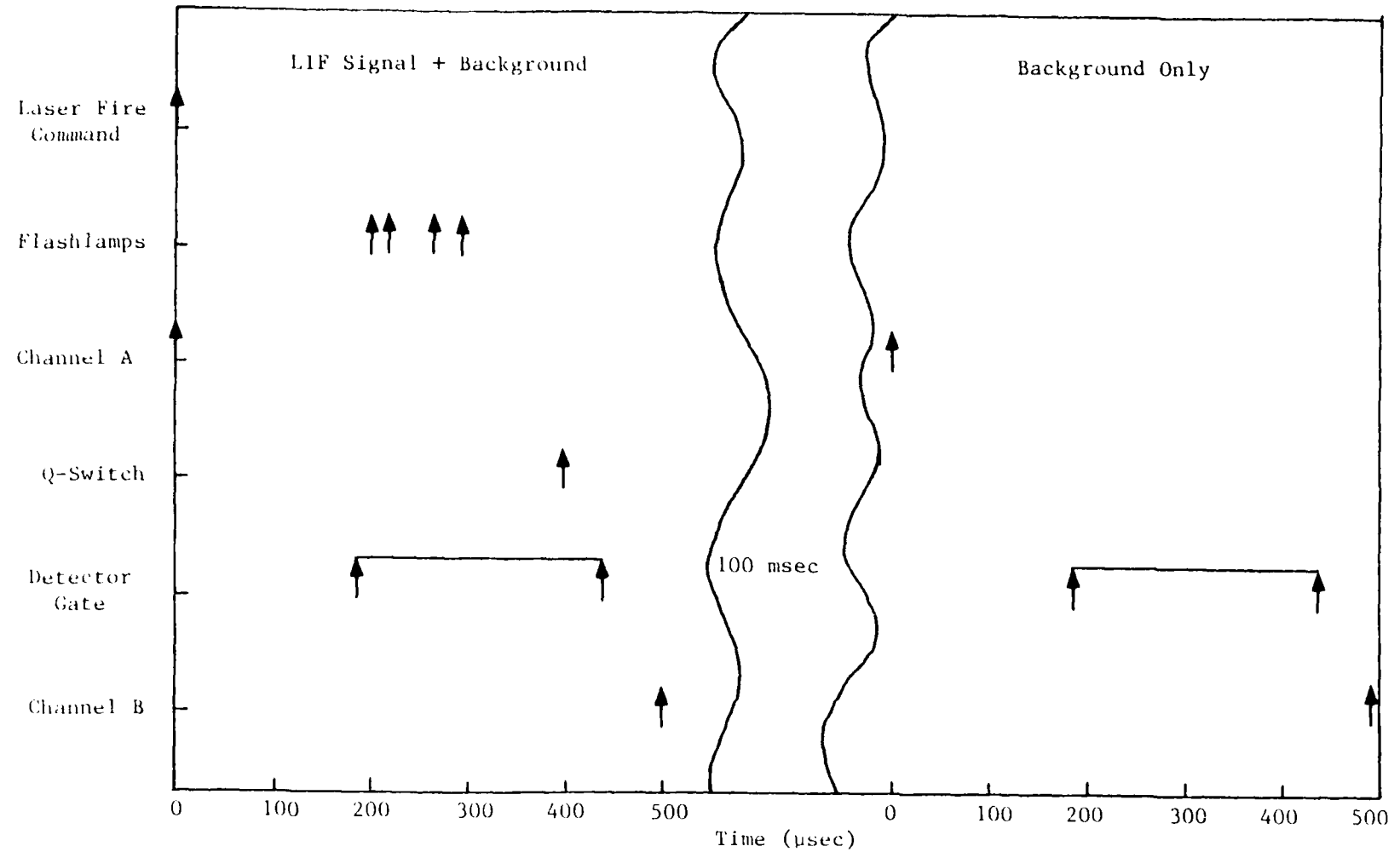


Figure 4. Detection Signal Timing Schematic

LIF signal. The second sequence was triggered halfway between laser shots and contained only the background. The OMA would automatically subtract these two sets of data leaving only the LIF signal. The laser was operated at a 5 Hz repetition rate so the time between the signal and background sequences was set by spacing the Channel A pulses 100 msec apart. Since the "dark" count rate is dependent only on thermal effects on the detector, this rate is virtually constant over this time period and the midway spacing of the sequences effectively eliminated it. A subtle assumption is made in this scheme that the chemiluminescence is also constant over this time period. This is certainly not true for turbulent flames, but for the relatively stable flames used in this study, this assumption proved reasonable as will be shown in Chapter V.

The output pulse from Channel A was used to trigger the Model 1303 gate pulse generator in the OMA and to trigger Channel B of the 8010A. To avoid the electrical noise problems from the Nd:YAG laser during the signal data sequence, the 1303 initially delays the gate pulse until a few microseconds before the first flashlamp fires. Delay times were usually around 170 microseconds. The 1303 then generates a gate pulse that lasts until about 10 microseconds after the Q-switch fires permitting signal integration over the induced fluorescence pulse. The gate pulse width was typically set at 285 microseconds. In this way the gating system (1303, 1304 and detector) is at some elevated voltage that is unperturbed by the electrical noise.

Channel B was delayed by the 8010A so that its output pulse came well after the gating sequence was completed, usually 500 microseconds, insuring that all of the induced fluorescence signal was accumulated. This pulse triggered the OMA's Model 1463 Detector Controller to "read"

the signal on the diodes and store the data in memory.

As described above, this whole data acquisition sequence is repeated 100 msec later when Channel A outputs its second pulse, thus generating the background data for subtraction by the OMA. This arrangement insures a one-to-one correspondence between the signal and background data for proper subtraction. Finally, the OMA would accumulate and display a user-specified number of subtracted scan pairs. This processed data could be stored on floppy disk for later analysis.

IV. Emission Spectroscopy Results

The first phase of the experiment was simply to obtain emission spectra from the flame with particular interest on the identification of bands from BO_2 and BO. As noted in Chapter II, the absorption and emission spectra of both of these molecules are reasonably well known. The spectral region investigated extended from 6300 Å down to 4000 Å. In general, the results of this work compare well with previous efforts.

Results for BO_2

As expected BO_2 was easily observed. The general spectral pattern consisted of a set of nine large peaks, some over 100 A wide, each made up of a large number of heavily overlapped vibrational and rotational bands. These large peaks have been traditionally called the boron oxide fluctuation bands and, as mentioned in Chapter I, until 1960 were thought to come from B_2O_3. A good example of the fluctuation bands is displayed in Figure 5, which is extracted from Morrison and Scheller (10:96) and shows in low resolution their spectrum from a JP-4/boron powder slurry flame. The resolution of the present system was such that the rotational structure could not be resolved. However, discrete vibrational bandheads were identifiable as structure on the large peaks.

The large peaks varied in intensity with the strongest being centered around the $00^00\text{-}00^00$ bands of the A-X system near 5460 Å. Figure 6 shows this peak with some of the more prominent bands labelled. This plot along with those of the other regions are displayed in Appendix C. Some of the waves were less symmetric in shape than the one

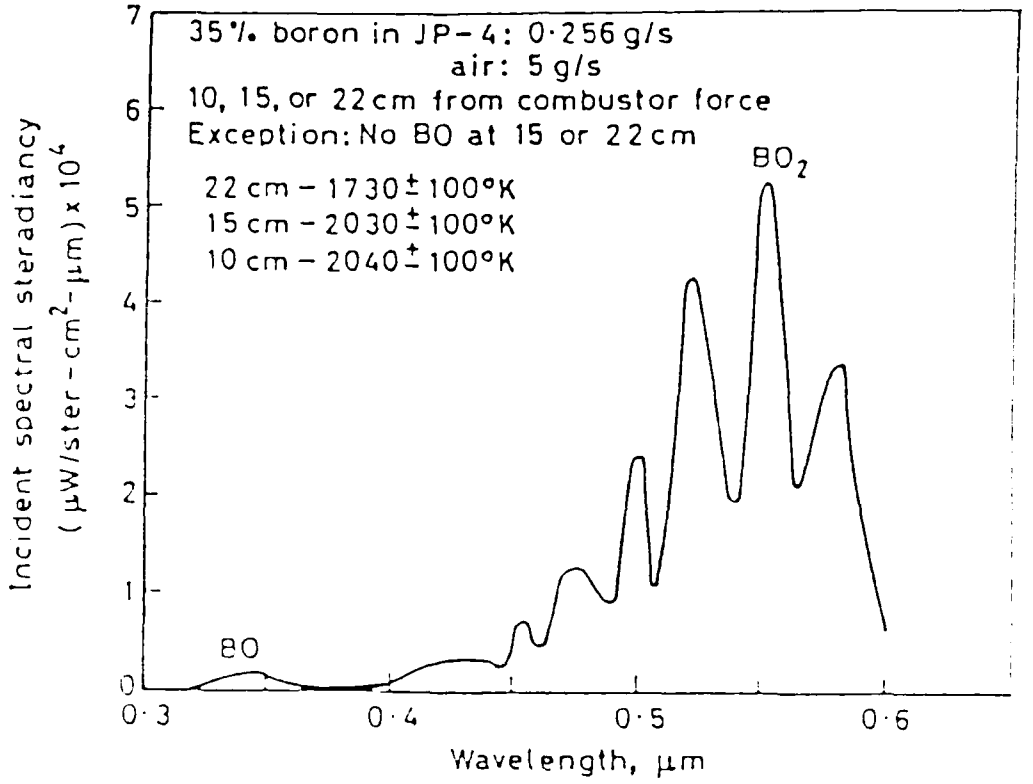


Figure 5. Boron Oxide Fluctuation Bands (10:96)

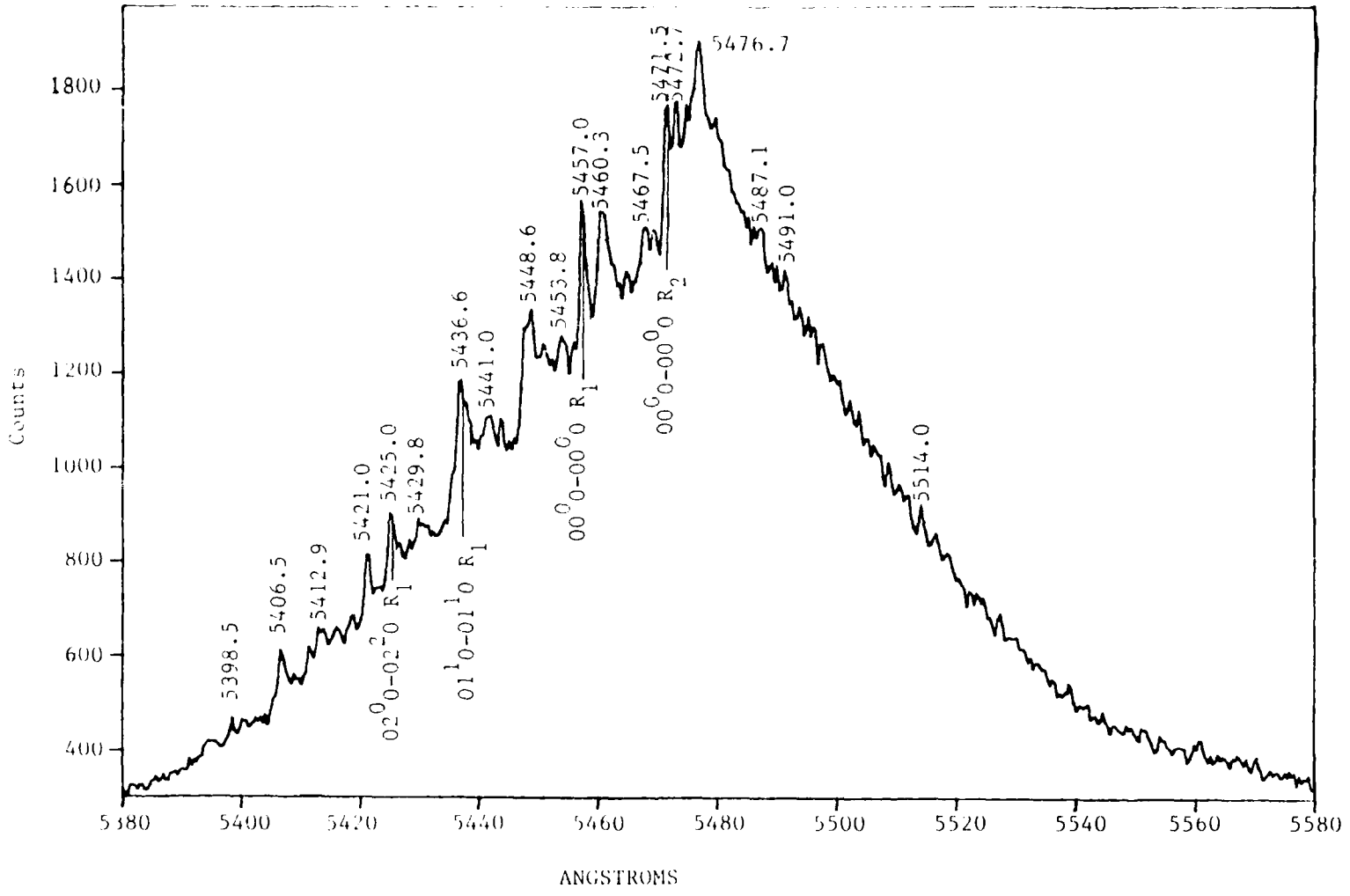


Figure 6. Emission From 00^0_0-00^0_0 Bandhead Region of A-X System of BO_2

in Figure 6. In particular, the wave centered on the $00^00\text{-}10^00$ band near 5800 Å rises abruptly at 5760 Å but, falls off to longer wavelengths much more slowly than the 5460 Å wave. No BO_2 emission was observed in the 4200-4400 Å region due to an overwhelming signal from CH. This was not totally unexpected since this is also the region of the 0-0 A-X band of CH (46:20). It was curious that the CH emission dominated this area even though the "background" flame emission was corrected for as described in Chapter III. This situation may have been the result of the BCl_3 reacting with the available O_2 more rapidly than the CH_4 such that the combustion of the latter was slowed leaving large quantities of CH to react higher in the flame via diffusion of outside air. In Appendix D a compilation of over 400 bandheads of the BO_2 spectrum seen in this work and those of Johns (39), Snowden (40), and Freid and Mathews (42) is presented.

Results for BO

No bands were observed in this work that could be confidently assigned to BO. It is possible that the BO bands were masked by the dominant BO_2 emission. The region around 4250 Å possessed the greatest likelihood of BO detection because it is here that the 0-0 band of the A-X transition of BO lies. Unfortunately, this area was completely dominated by emission from CH.

The implications of these results for the LIF experiments on BO were not good. If BO could not be seen in emission, then its concentration might be extremely low. This coupled with the potential quenching problem discussed above could preclude its observation in this configuration, even with LIF. It could also be that the BO is present, but, that

it is not electronically excited by the flame reactions. In the previous work by Clyne and Heaven (44:301) and Llewellyn, et.al., (20:504), they were forced to react nitrogen atoms from a microwave discharge in NO to yield excited oxygen atoms that would then react with BCl_3 to produce BO. The simple excitation of oxygen atoms in the discharge yielded much BO_2, but no BO. The exact role of the nitrogen atoms is still unclear. The need for such a chain reaction may indicate that the current flame conditions and reactants are not appropriate for the production of BO.

Other Species

A fortunate result of the choice of reactants was that with the exception of CH no other reactant or product species should have a spectrum in the region of interest. The data bears this out with only CH appearing in any significant quantity and then only in one spectral region, albeit, an important one. The C_2 Swan bands could be observed if the flame was allowed to get sooty, indicated by a yellow coloration. But, even then, their intensity was extremely small relative to that of the BO_2 bands.

V. Laser-Induced Fluorescence Results and Discussion

With the completion of the emission spectra, Phase II of the project began, i.e., the application of LIF to the flame. The results discussed in this chapter constitute the first known demonstration of LIF of BO_2 in an atmospheric-pressure flame.

Flame Conditions

Gas input flow rates were adjusted as discussed in Chapter III to produce a stable flame. These flow rates were recorded so that subsequent runs were all at the same conditions or small variations thereof. The nominal flow rates were: CH_4--9.55×10^{-3} moles/min, Air--2.34×10^{-2} moles/min, O_2--5.27×10^{-3} moles/min, and BCl_3--6.6×10^{-4} moles/min. Using these values as inputs to the NASA chemical equilibrium code written by Gordon and McBride (49), calculated results for the adiabatic flame temperature and the equilibrium concentrations of the flame products could be obtained. The adiabatic temperature assumes no heat is lost to the surrounding environment which of course in this case was not true. However, the code did provide some idea of the flame temperature particularly at the boundary of the inner cone. For the above gas mix, the predicted temperature was 2026 °K. The predicted equilibrium concentrations of BO and BO_2 were 3.6×10^{18} cm^{-3} and 7.2×10^{18} cm^{-3}, respectively. Changes in the air and/or BCl_3 flowrates resulted in the predicted adiabatic temperature varying between about 2000 °K and 2200 °K with little change in the BO and BO_2 concentrations within the resolution of the code. It is curious that the code predicts

a BO concentration only a factor of two less than that of BO_2, yet no BO emission is observed. No explanation for this result has been found other than those proposed in the previous chapter.

LIF of BO_2

Detection of LIF from BO_2 was readily achieved. In all cases non-resonant LIF was used between the first excited electronic state ($A^2\Pi_u$) and the ground electronic state ($X^2\Pi_g$). Figure 7 is an example of the data obtained. In this case, the pump band was the R_1 of the $00^00\text{-}00^00$ transition at 5456.8 Å. The strongest band observed is the R_1 of the $00^00\text{-}10^00$ transition. This was expected since the lower states of these two bands have the same parity and in the absence of collisions parity would be conserved. At low pressure, such as that used for previous LIF experiments on BO_2, only this band would be anticipated. However, at the relatively high pressure of the present experiment, one atmosphere, the spectra showed considerable collisional mixing resulting in the appearance of bands having upper states other than the one being pumped by the laser. Most notable of these bands is the R_2 of the $00^00\text{-}10^00$ transition at 5813 Å. Separated only by the spin-orbit coupling of approximately 103.3 cm^{-1}, this upper level is readily populated through collisions by the excited molecules. Also evident is a band centered around 5784 Å. This emission could be due to the comparable R_1 band of the $01^10\text{-}11^10$ transition or it may be due to the R_1 band of the $00^00\text{-}10^00$ transition from the $^{10}BO_2$ isotopic molecule. The small peak near 5767 Å is probably the R_2 band of the $00^00\text{-}02^00$ transition.

The overall shape of the curve is reminiscent of the emission spectra whereas LIF spectra usually exhibit much sharper peaks. Thus,

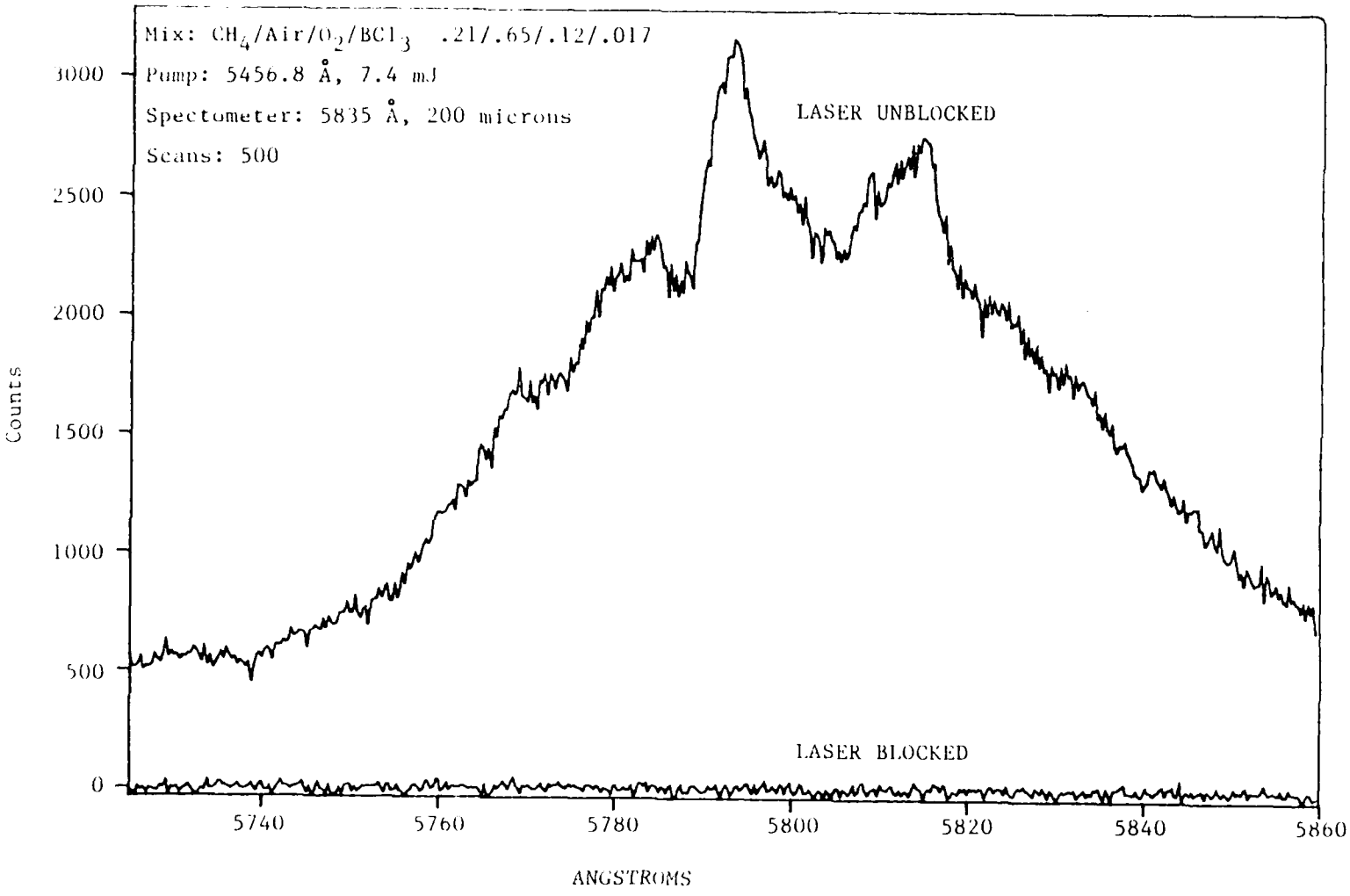


Figure 7. Non-Resonant Laser-Induced Fluorescence Signal from BO_2

one might suspect that a considerable amount of chemiluminescence is still being observed. However, also included in Figure 7 is the result from identical operation conditions, but with the laser blocked from reaching the flame. Some random noise is evident, but this curve clearly shows the effectiveness of the background subtraction scheme and the validity of the assumption about the constancy of the flame emission. It must be noted that the data in Figure 7 is not typical of that normally obtained. In an attempt to improve the signal-to-noise ratio, a BCl_3 concentration was used that was much higher than that normally used due to the burner clogging problem discussed in Chapter III. The other gas concentrations however, were close to those usually employed.

Excitation Scans. Excitation scans were performed in which the spectrometer was fixed so that the detector always viewed the same spectral region while the dye laser beam was tuned through one or more absorption bands. In both of the scans presented here, the spectrometer was tuned so that the detector array spanned the region from about 5720 Å to 5870 Å. The observation focal volume was positioned 3 cm above the burner, which was just above the tip of the inner cone, and 4 mm from flame-center along the laser beam path. In the first scan, the dye laser was tuned in 0.5 Å steps from 5455.4 Å to 5463.8 Å, thus tuning through the $00^00\text{-}00^00$ R_1 band at 5456.4 Å and the $01^10\text{-}01^10$ R_2 band at 5460.3 Å. The step size is larger than the rotational line spacing for BO_2 of approximately 0.3 Å in this spectral range. Figure 8 is a composite plot of a few of the steps in this scan. Note the distinct resonant behavior displayed by the 5790 and 5814 Å detection bands as the laser was tuned across the 5456.4 absorption band. Figure 9 is an enlargement of the data with the laser tuned to 5456.4 Å, i.e., near resonance with the

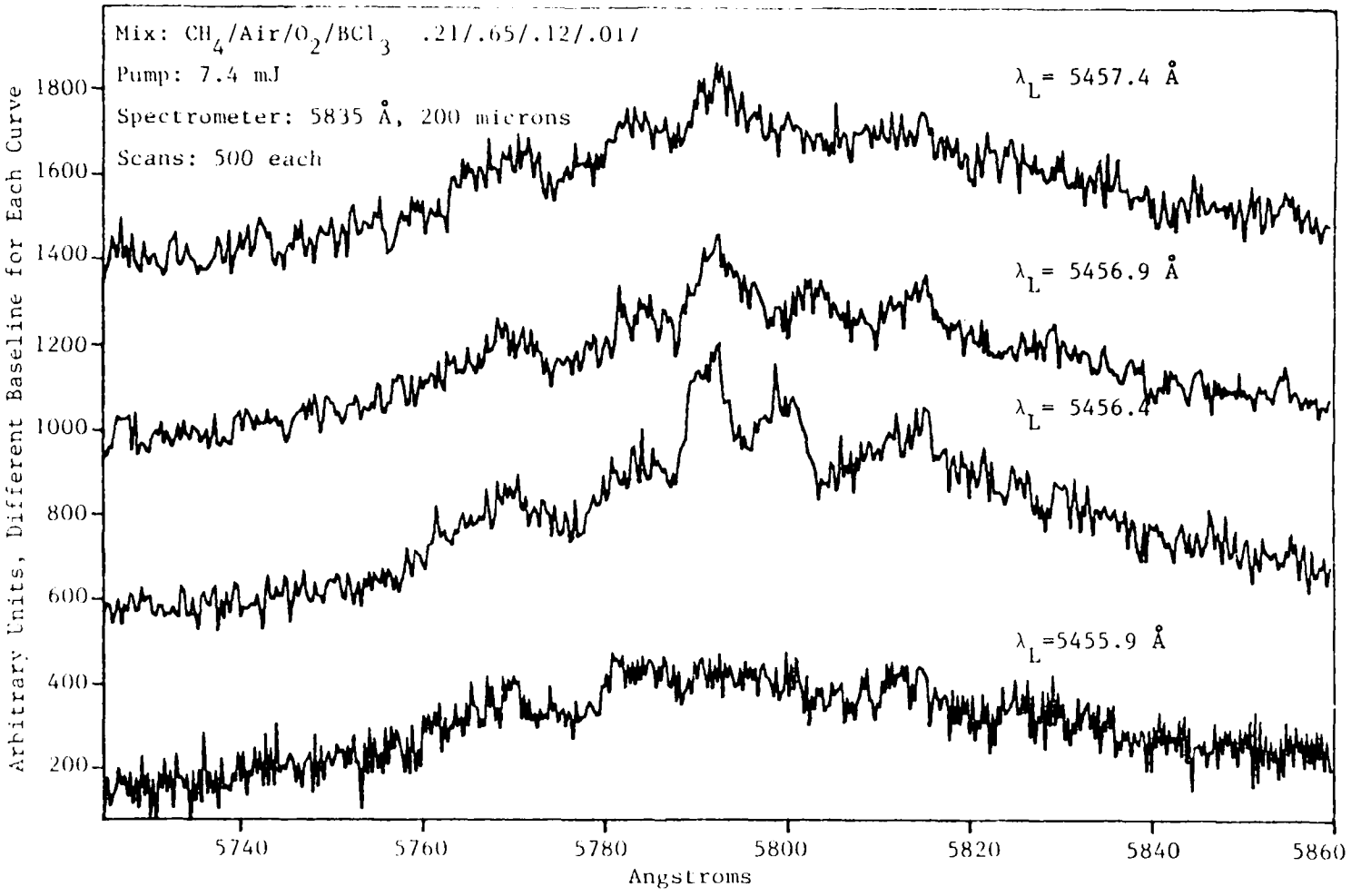


Figure 8. Excitation Scans at Different Laser Wavelengths

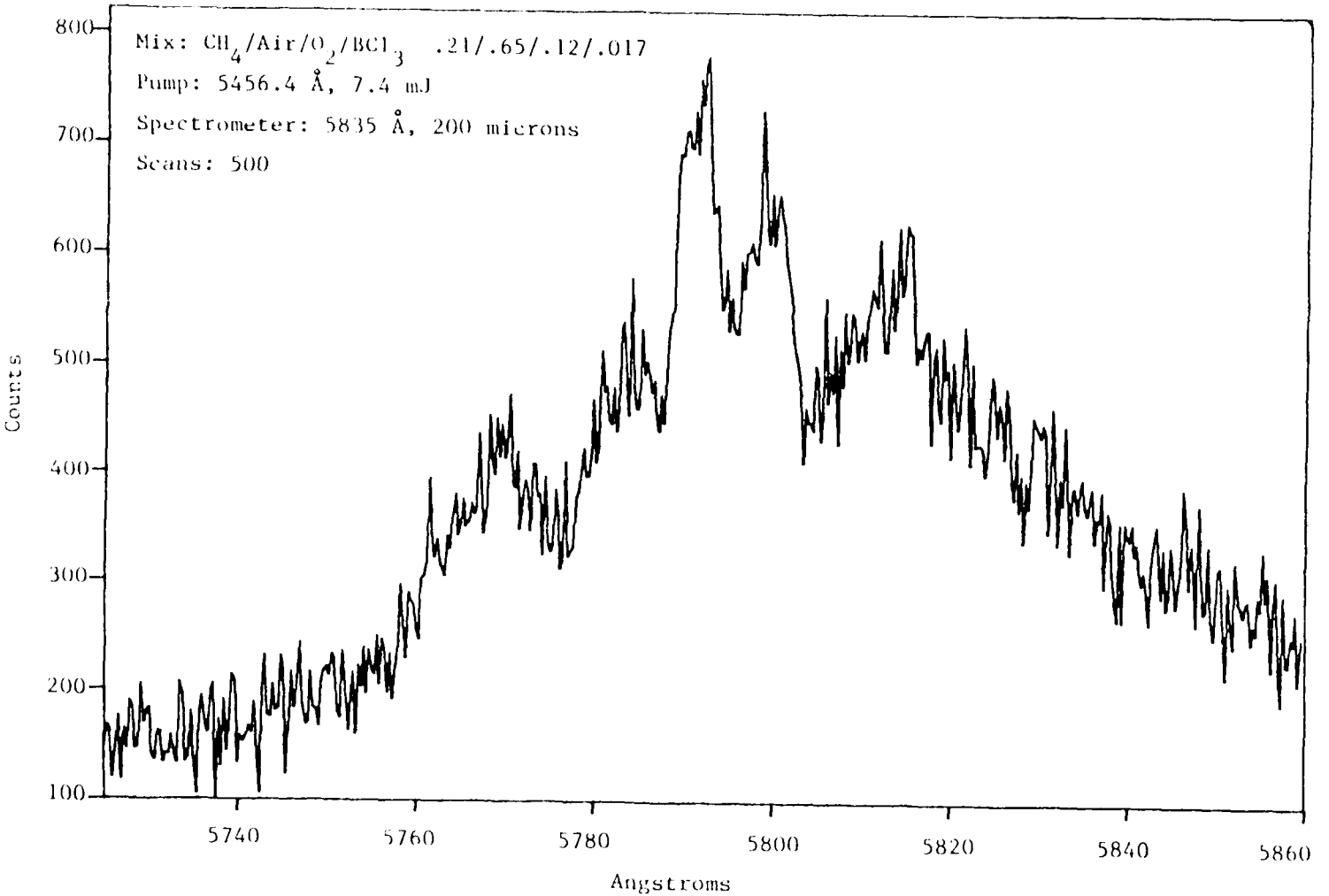


Figure 9. Excitation Scan, Laser Wavelength at 5456.4 Å

absorption band. Five bands are clearly discernible at 5790, 5814, 5800, 5784, and 5767 Å. Four of these were discussed above, the fifth at 5800 Å is the R_2 band of the $01^10\text{-}11^10$ transition. The appearance of this band further supports the assignment of the 5784 Å band as its spin-orbit coupled companion.

A second excitation scan was performed under the same conditions but with the laser scanning over the range from 5466 Å to 5474 Å, which covers the R_1 band of the $10^00\text{-}10^00$ transition at 5467.5 Å and the R_2 band of the $00^00\text{-}00^00$ transition at 5471 Å. Figure 10 is a composite plot of a portion of this scan. The spectra are similar to those obtained in the above scan with the exception of the bands near 5806 Å, 5830 Å and 5820 Å. The first of these is most likely due to the R_1 band of the $10^00\text{-}20^00$ transition, as expected from the 5467.5 Å pump band listed above. The 5830 Å band could be either (or a combination of both) the R_2 band of the $10^00\text{-}20^00$ transition or it might be the R_2 band of the $02^00\text{-}12^00$ transition. No assignment has been given for the 5820 Å band, but it seems to couple strongly to $00^00^2\Pi_{1/2}$ level of the $A^2\Sigma_u$ state since it is observed in this scan, but not in the previous scan. The sharp resonance behavior of the 5813 Å band is similar to that seen with the 5790 Å band in the previous scan. The inversion of intensities between the spin-orbit components of the $00^00\text{-}10^00$ transition at 5790 Å and 5813 Å is as expected. Figure 11 is an enlarged view of the spectra with the laser tuned very near to resonance with the 5470.8 Å pump band.

Fluorescence Scan. A fluorescence scan was performed wherein the dye laser frequency is fixed at an absorption resonance and the spectrometer is tuned over a wide spectral region. For this scan, the laser was tuned to 5471 Å to excite the R_2 band of the $00^00\text{-}00^00$ transition.

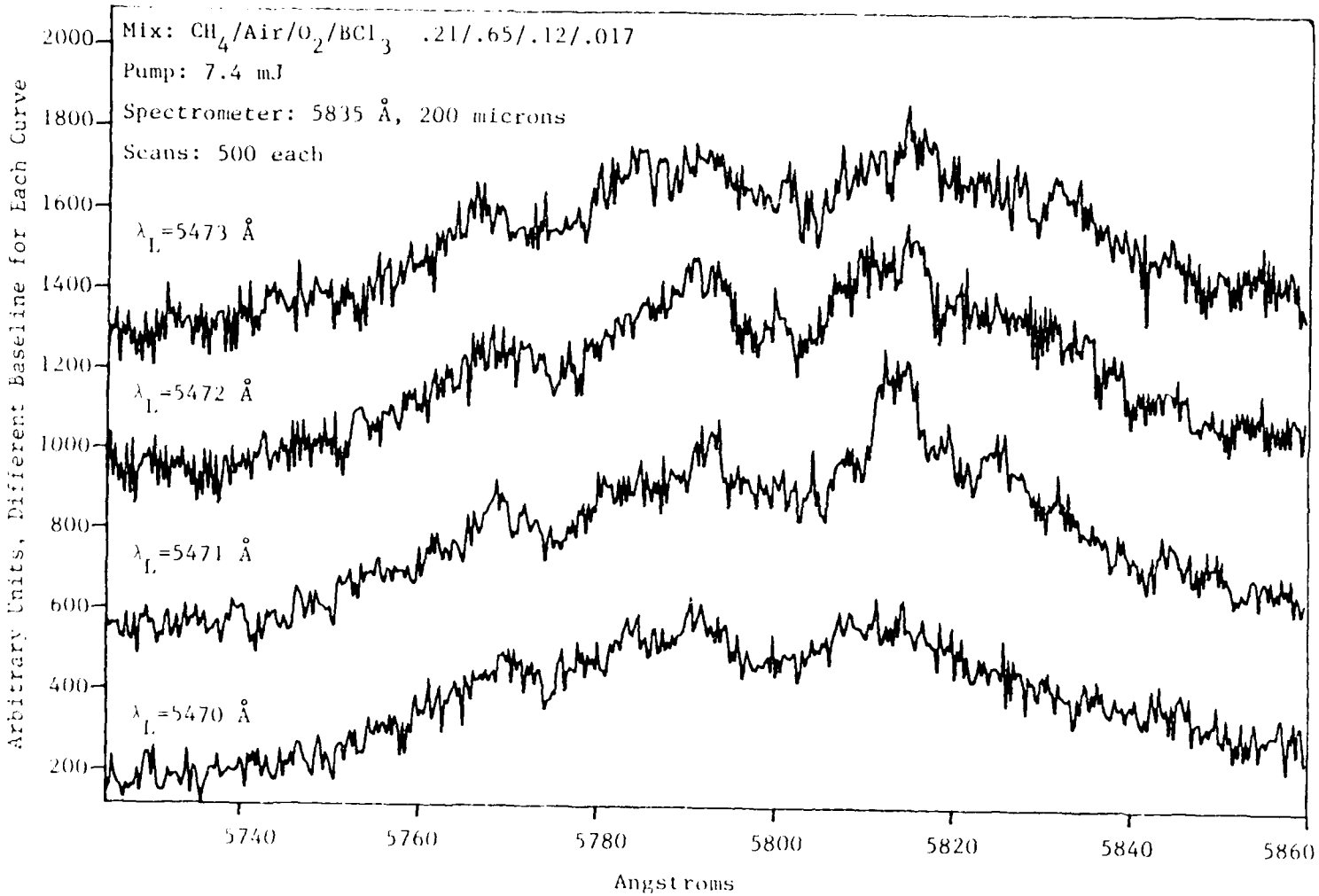


Figure 10. Excitation Scans of 00^00-00^00 R_2 Transition of BO_2

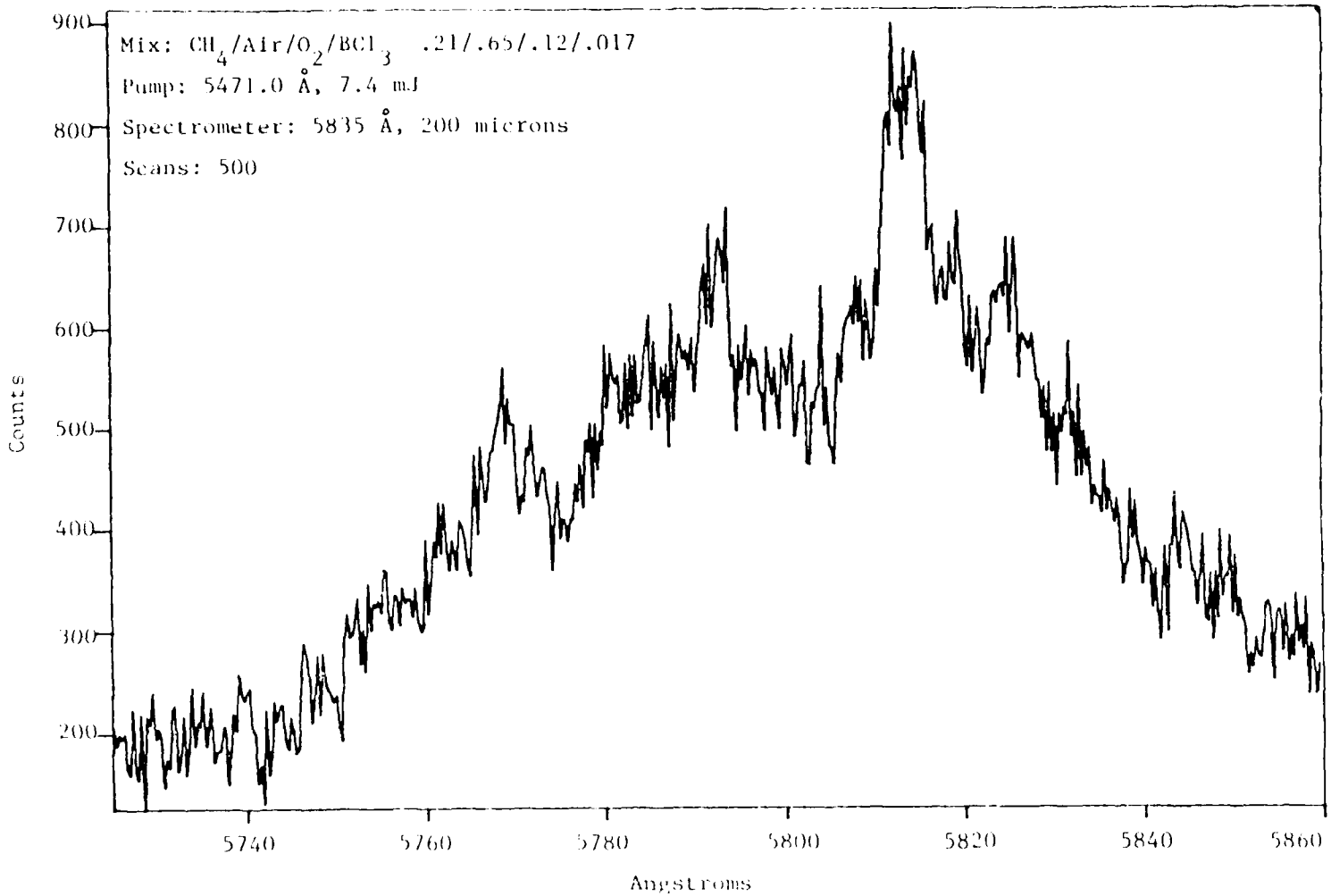


Figure 11. Excitation Scan, Laser Wavelength at 5471.0 Å

The spectrometer was scanned to permit observation from 6460 Å to 4140 Å in approximately 125 Å increments, which was a little less than the viewing range of the detector array and assured overlap with adjacent increments. Figure 12 is a composite plot of the fluorescence spectra produced. Table II lists the prominent bands observed in the fluorescence scan.

Table II

LIF Bands Observed

Wavelength (Å)	Band
6396	$00^00\text{-}00^02$ R_2
6376	$00^00\text{-}00^02$ R_1
6202	$00^00\text{-}20^00$ R_2
6171	$00^00\text{-}20^00$ R_1
5825	Not Assigned
5813	$00^00\text{-}10^00$ R_2
5806	$10^00\text{-}20^00$ R_1
5790	$00^00\text{-}10^00$ R_1
5784	$00^00\text{-}10^00$ R_1*
	or $01^10\text{-}11^10$ R_1
5767	$00^00\text{-}02^00$ R_2
5169	$10^00\text{-}00^00$ R_1

Appendix E contains the nineteen individual data plots which were combined to produce Figure 12. While a few isolated bands are observed elsewhere, clearly the richest region is around 5790 Å. Also evident is the secondary peak produced by the laser and discussed in Chapter 3.

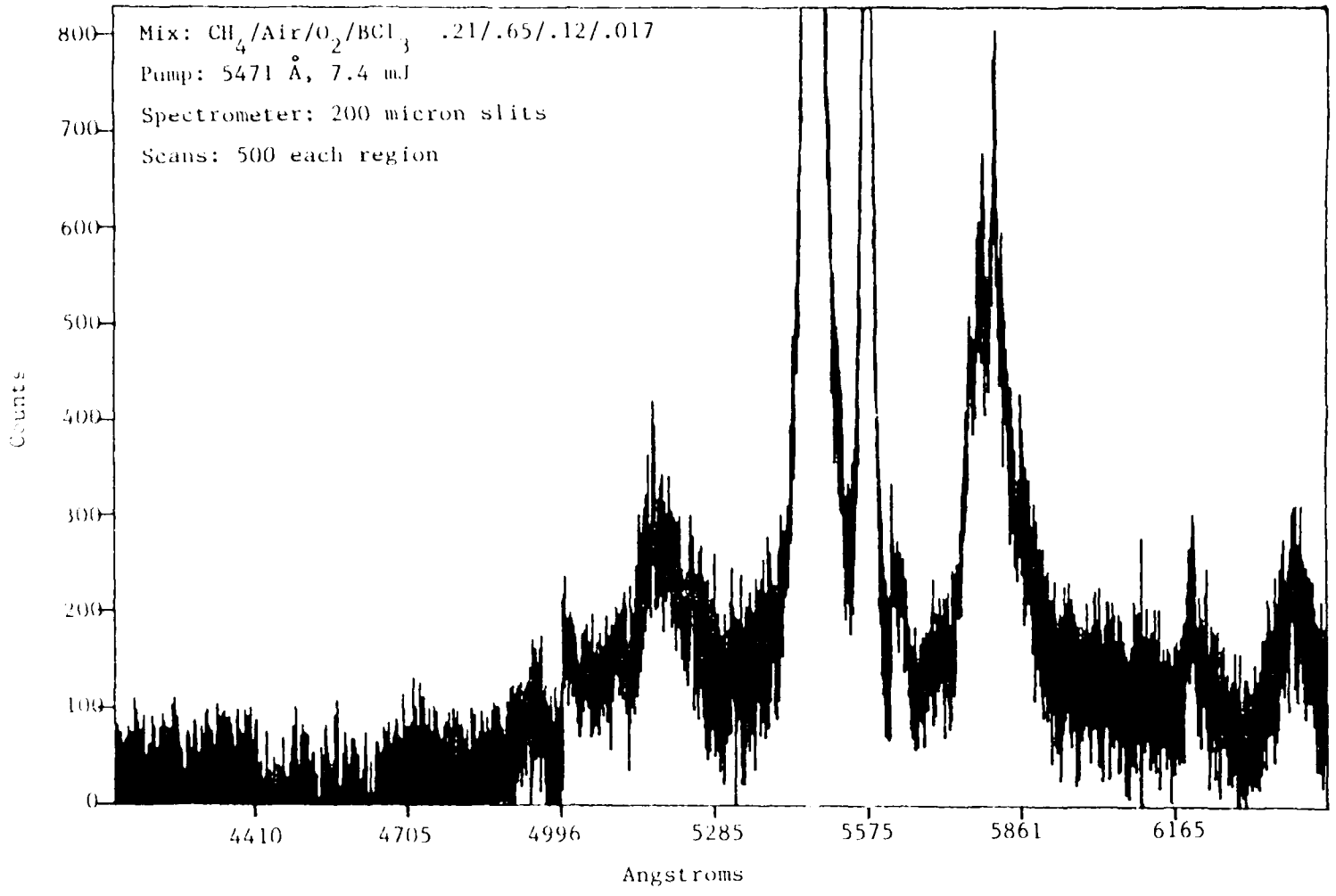


Figure 12. Composite Fluorescence Scan

Fortunately, it fell in a portion of the BO_2 spectrum having virtually no transitions and should have had little effect on the results except for stealing power from the excitation peak. The data has not been corrected for detector sensitivity, but the system response is specified as being flat over this region. Two small unexplained discontinuities appear at 5620 Å and at 5000 Å. These were breakpoints between settings of the spectrometer. They had no bearing on the data and should not be interpreted as actual spectral features. This scan was made with the spectrometer slits open to 200 microns, which yielded greater signal but lower resolution. With 100 micron slits, the 5456.8 Å spin-orbit coupled companion to the excitation band could be observed next to the laser line.

Fluorescence Profile in the Flame

Phase III of the effort was an attempt to map the relative fluorescence spatial profile of BO_2 in the flame. Recalling the theoretical development in Chapter II, the number density of the species of interest is proportional to the fluorescence signal obtained. The area under the spectral peaks of the desired species is a measure of the total signal and therefore, the number density. One major caveat must be placed on such assertions however. At the high pressure of the present experiment, there is a significant amount of quenching and redistribution of energy, neither of which can be accurately quantified at this time. Further, these processes change as the local flame parameters, most notably temperature, change. Thus, to say a relative fluorescence map is directly equivalent to a number density map requires the assumption that the quenching and energy redistribution processes do not change signifi-

cantly over the spatial region of interest. Such a claim cannot be made for the results shown here for the following reasons. First, since only a portion of the total induced fluorescence signal is recorded, changes in the redistribution of energy within the BO_2 are not fully included. Indeed, loss of energy to non-radiative states could not be included even if the entire spectrum were recorded. Second, since the entire flame was scanned, the local temperature in the detection volume changed by as much as a factor of four or more with the inner cone boundary being very much hotter than that of the outer cone. This change in temperature would translate into a change in the collison frequency, which under constant pressure varies as $T^{-(1/2)}$. Thus, the collision frequency at the inner cone would be less than that at the outer cone such that the quenching and redistribution rates would be less at the inner cone.

The laser was tuned to the 5471 Å absorption band and the spectrometer was tuned to the 5813 Å region for observation of the non-resonant LIF signal. The flame was then moved via the burner translation stages so that the observation focal volume was scanned both horizontally and vertically through the flame. The overall flame dimensions were approximately 1.5 cm across at the base and approximately 6.5 cm tall. The inner cone was approximately 1.1 cm across and 2.5 cm tall. The burner clogging problem discussed previously dictated that only about 16 runs of 500 shots each could be collected before serious flame instabilities were encountered. Further, with the spectrometer slits at 200 microns, the observation focal width was approximately 250 microns. Thus, to maintain as much consistency as possible in the data, the flame was scanned horizontally along the path of the laser beam in 1 mm steps, which usually permitted one horizontal scan across the total width of the

flame to be completed before the burner had to be cleaned. The focal volume was approximately 3 mm high determined by the dimension of the detector diodes. In an effort to keep the amount of data reasonable, the flame was scanned vertically in 1 cm increments from the base of the flame up to near the tip at 6 cm. The laser beam was positioned in the middle of the flame along the observation axis.

The raw data obtained was the same as seen previously, i.e., LIF spectra. Figure 7 shows that even though only a few resolved peaks were observed, the overall increase in the spectral curve is due to excitation by the laser. Thus, by using the OMA's analysis capability, the area under each spectral curve from pixel 70 to pixel 500 (corresponding approximately to 5727.2 Å to 5850.2 Å) was computed. The range was chosen somewhat arbitrarily to include more or less all of the LIF photons belonging to the 00^00-10^00 transition. Figure 13 is a 3-D plot the integrated signal as a series of curves corresponding to horizontal scans at the different heights. The x-axis of these plots corresponds to the lateral position of the detection volume in the flame in one millimeter steps with the zero point, or center of the flame, being in the center of the x-axis. The y-axis is the magnitude of the integrated signal in arbitrary units. The z-axis corresponds to the different heights above the flame at which horizontal scans were taken.

The most dramatic features of Figure 13 are the large peaks in the flame center at the lowest heights, i.e., just above the surface of the burner. These will be discussed in detail below. Figure 14 shows enlarged plots of the five curves taken at heights ranging from 2 to 6 cm above the burner surface. These plots do not exhibit the large central peaks of the lower curves. The notable feature in Figure 14 is that the

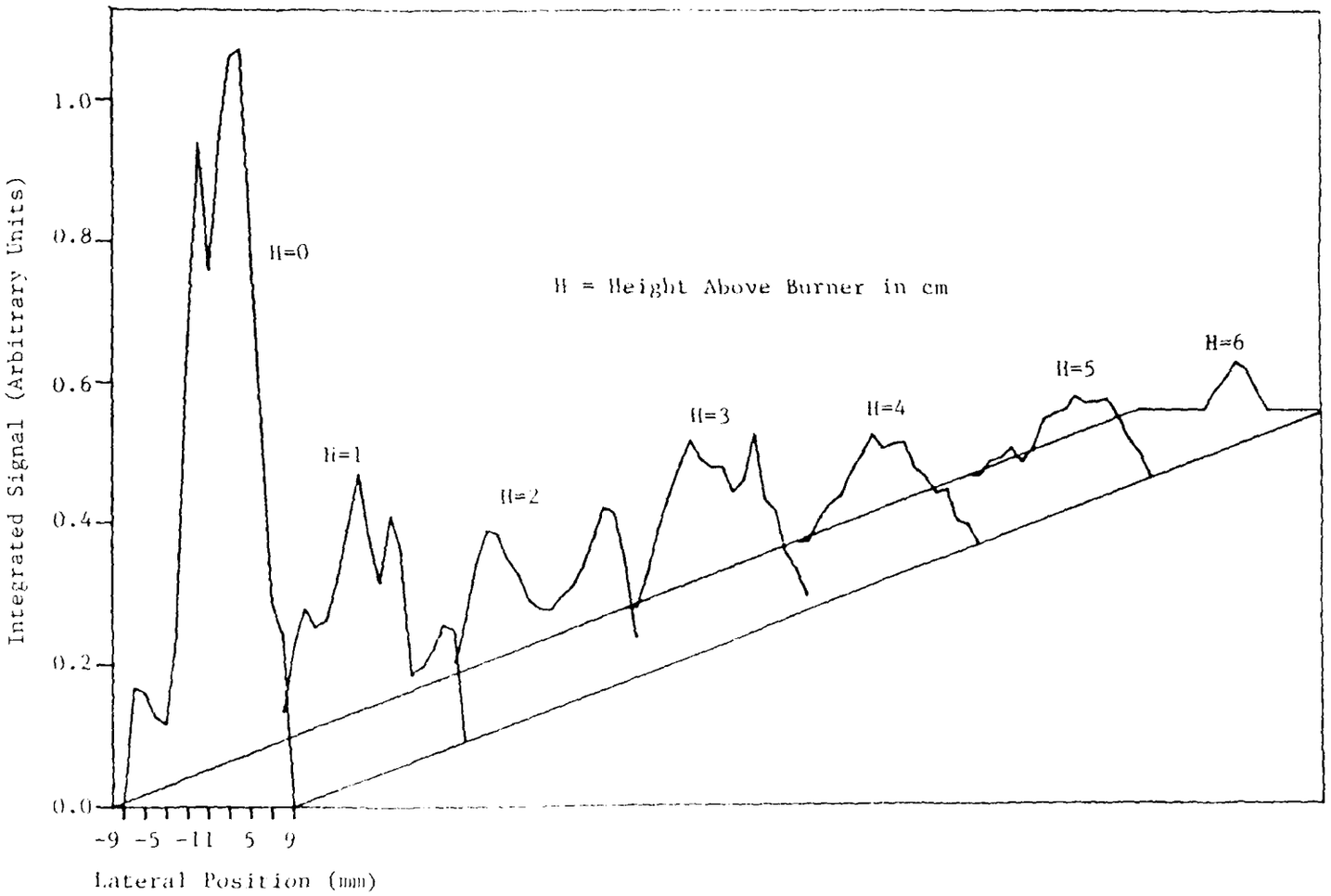


Figure 13. Fluorescence Signal vs Position in Flame, Total Flame

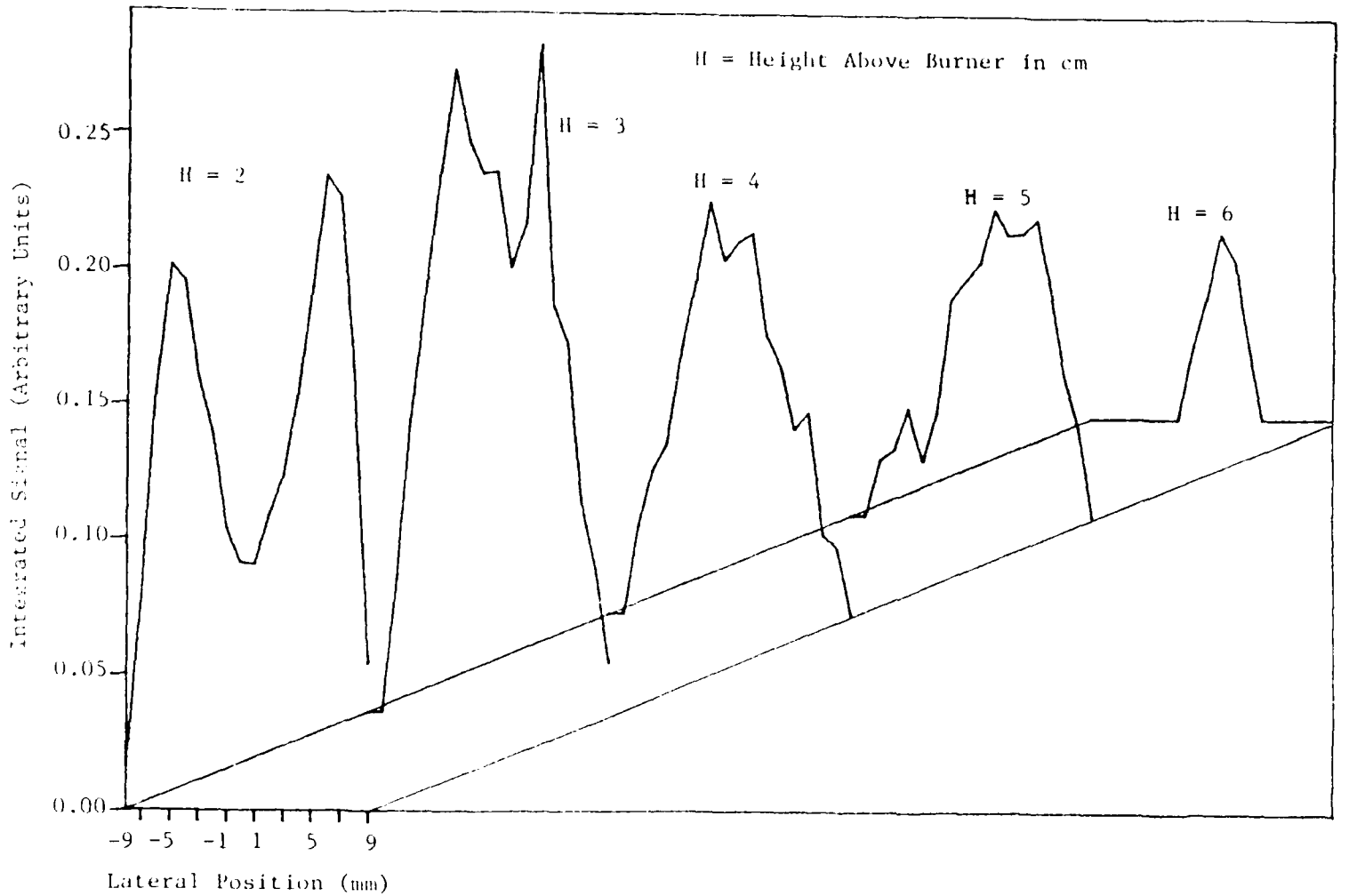


Figure 14. Fluorescence Signal vs Position in Flame, Above Inner Cone

BO_2 fluorescence is greater outside the inner cone. This fact is particularly evident in the scan 2 cm above the burner (the third trace from the left in Figure 13 and the first trace on the left in Figure 14). Higher in the flame as it converges, the signal peaks in the center.

This result is similar to the profile of OH commonly observed in hydrocarbon flames. It appears that much of the BO_2 is being formed at or near the boundary of the inner cone where the flame is the hottest. However, in view of the facts that the lifetime of the A state of BO_2 is only approximately 100 nsec (44) (which is much shorter than the gas transit time in the flame) and that BO_2 fluorescence is still observed far beyond the inner flame front, it might be concluded that BO_2 continues to form higher up in the flame.

Further, in view of the caveat discussion above, these relative fluorescence maps probably underestimate the relative concentration maps. Since the energy losses at the outer cone boundary would be more than those at the inner cone, a higher concentration of molecules would be needed at the outer cone to produce the same signal as that produced at the inner cone. Thus, a relative concentration map at H=2 cm would have higher peaks at the edges relative to the valley in the middle, whereas the profile at H=6 cm might actually be somewhat flatter with the outside edges increasing relative to the center peak Quantifying this amplification effect requires detailed understanding of the quenching and energy redistribution rates for the species involved.

Scattering in the Inner Cone

A surprising phenomenon was observed when the laser beam passed through the inner cone. A tremendous amount of radiation was emitted,

but only from within the inner cone. The "scattered" light was clearly visible to the naked eye. If the spectrometer was tuned to the laser wavelength, the resulting signal saturated the detector being many times stronger than Rayleigh scattering in ambient room air. While some of this light was emitted in all directions, it visually appeared to be stronger in the forward direction, i.e., the direction of propagation of the laser beam, than in the sideways or backward direction. Further, the boundary of the inner cone was a sharp boundary for the "scattered" light. As the burner was lowered so that the laser beam crossed the tip of the inner flame front, the "scattering" disappeared. In fact, if the flame was positioned so that the beam straddled the boundary, that portion of the beam inside the inner cone exhibited "scatter", that portion outside did not. The temperature of the inner flame front should be close to the adiabatic flame temperature of around 2000 °K.

The first hypothesis concerning this effect was that some aerosol was causing Mie scattering of the laser beam. Mie scattering tends to be directed more forward than backward and would explain the anisotropy of the emission. Clearly the aerosol must be coming from the pre-mixing of the flame gases and it must vaporize as it crosses the inner flame front else the effect would be observed higher in the flame. No scatter was observed in the flame if no BCl_3 was flowing, which indicated that the aerosol must come from some boron or chlorine-containing species. Further, if all the gases were flowing, but the flame was not ignited, a white smoke emanated from the burner and produced a similar scattering. (The white smoke is typical from the reaction of BCl_3 with water vapor in the air and makes detection of BCl_3 leaks easy.)

The likely aerosol was the white crystalline powder discussed in Chapter III that clogged the burner. A sample of the powder was taken to the Materials Laboratory for analysis. Its melting point was found to be approximately 170 °C. This value matched well with that for orthoboric acid, H_3BO_3. The boiling point of H_3BO_3 is not published but is probably well below the flame front temperature and such that crystal would vaporize at that boundary as observed. This acid is also very soluble in water, as was the powder. A small amount of the powder was further crushed, mixed with KBr and pressed into a small disk. The disk was inserted into a infrared spectrophotometer having a glowbar source of radiation. An infrared absorption spectrum of the powder closely matched that of H_3BO_3. The KBr is transparent in the spectral region of interest and served simply as a binder material to contain the sample.

An elemental analysis revealed that hydrogen made up approximately 2.83% of the mass of the material and boron made up approximately 22.2% of the mass. In H_3BO_3, hydrogen makes up 4.89% of the mass and boron makes up 17.48% of the mass. In metaboric acid, HBO_2, the respective values for hydrogen and boron are 2.3% and 24.67%. Thus, the elemental analysis indicated that there may have been some HBO_2 in the powder. The sample was observed to be hygroscopic. Since the sample had been sitting around for a couple of weeks before the analysis was performed, although it was sealed in a plastic vial, it surely absorbed water from the air, which would convert HBO_2 to H_3BO_3. Thus, it was concluded that the powder probably consisted of a mixture of H_3BO_3 and HBO_2. (Later research in the literature found that BCl_3 readily reacts with water to form HCl and H_3BO_3 but, it does not easily react with the other flame constituents (50:256). The air for the experiment was drawn from the

building supply which was known to contain a considerable amount of water vapor, which could not be easily removed. Future experiments should be done with bottled dry air and thus avoid this problem.)

Mie scattering applies for particles with charateristic dimensions of the the same order as the wavelength of the incident light. A crude calculation shows that there is more than sufficient time for clustering to the required size. Following a treatment by Garscadden (51), if one assumes particles of around 1000 Å dimension then for a typical solid density of 10^{21} cm^{-3}, approximately 10^6 molecules make up the cluster. The agglomeration rate would be something on the order of NQvS, where N is the number density of the clustering species, which may be 0.1% of the total gas density of roughly 10^{19} cm^{-3}, Q is the average collision cross-section of roughly (50 Å)^2, v is the molecular random velocity of around 10^5 cm/sec, and S is a sticking coefficient with a maximum value of 1. Using these values yields an agglomeration rate of about 10^8 sec^{-1} such that the time to produce the required size particle is $10^6/10^8$ or 10 msec. Assuming a uniform flow speed through the flame, which is adequate for this calculation, the volume flow is roughly 20 cm^3/sec with a burner area of 0.8 cm^2, so that the gas flow is about 25 cm/sec. The residence time for the inner cone having a height of approximately 2 cm, is 80 msec, which is clearly long enough for the clustering process. Further, it must be realized that the clustering would actually begin down in the mixing chamber so that cluster times could be several hundred milliseconds. Thus, the spatial and temporal requirements for the formation of the aerosols are easily met by the experimental design.

While Mie scattering seems to explain much of the observed effect, it does not explain the spectral output. Figure 15 shows a spectrum

obtained with the laser tuned to the 5471 Å as usual. Clearly, something more than simple LIF and/or Mie scattering was occurring. The overall rising signal level toward the shorter wavelengths, i.e., toward the laser pump wavelength, would be expected from the Mie scattering generating an enormous signal having a very long tail. Unlike Figure 7 where the background was essentially flat across the spectral region, the background or underlying broadband scatter changes significantly over the same wavelength range. Thus, a calculation of the area under these curves included a significant amount of background, which really was not a measure of the BO_2 concentration and only served to create artificially large values. Unfortunately, no simple way of eliminating the scatter was available since it was generated by the laser itself.

Expected LIF peaks at 5790 Å and 5813 Å are present, but their relative intensities are reversed for this pump configuration and none of the other peaks in the spectra are readily assigned to known bands of BO_2 or BO. The observed peaks displayed a very wide (nearly 25 Å full width) resonance behavior as the laser was tuned. (It must be noted that even when the laser was tuned far off resonance from the 5471 Å pump band, the scattering was still visible to the eye. The spectra of the scattered photons continued to display a rising intensity toward the laser wavelength, but the peaks shown in Figure 15 disappear.) In the case of the 5790 Å peak, the intensity increased then decreased as the laser was tuned through the absorption band at 5471 Å. Thus, this peak could simply result from LIF. In most cases, however, including the 5813 Å peak, in addition to an intensity variation, the frequency of the peaks shifted by nearly the same amount and in the same direction as the laser beam. Such behavior is indicative of Raman scattering.

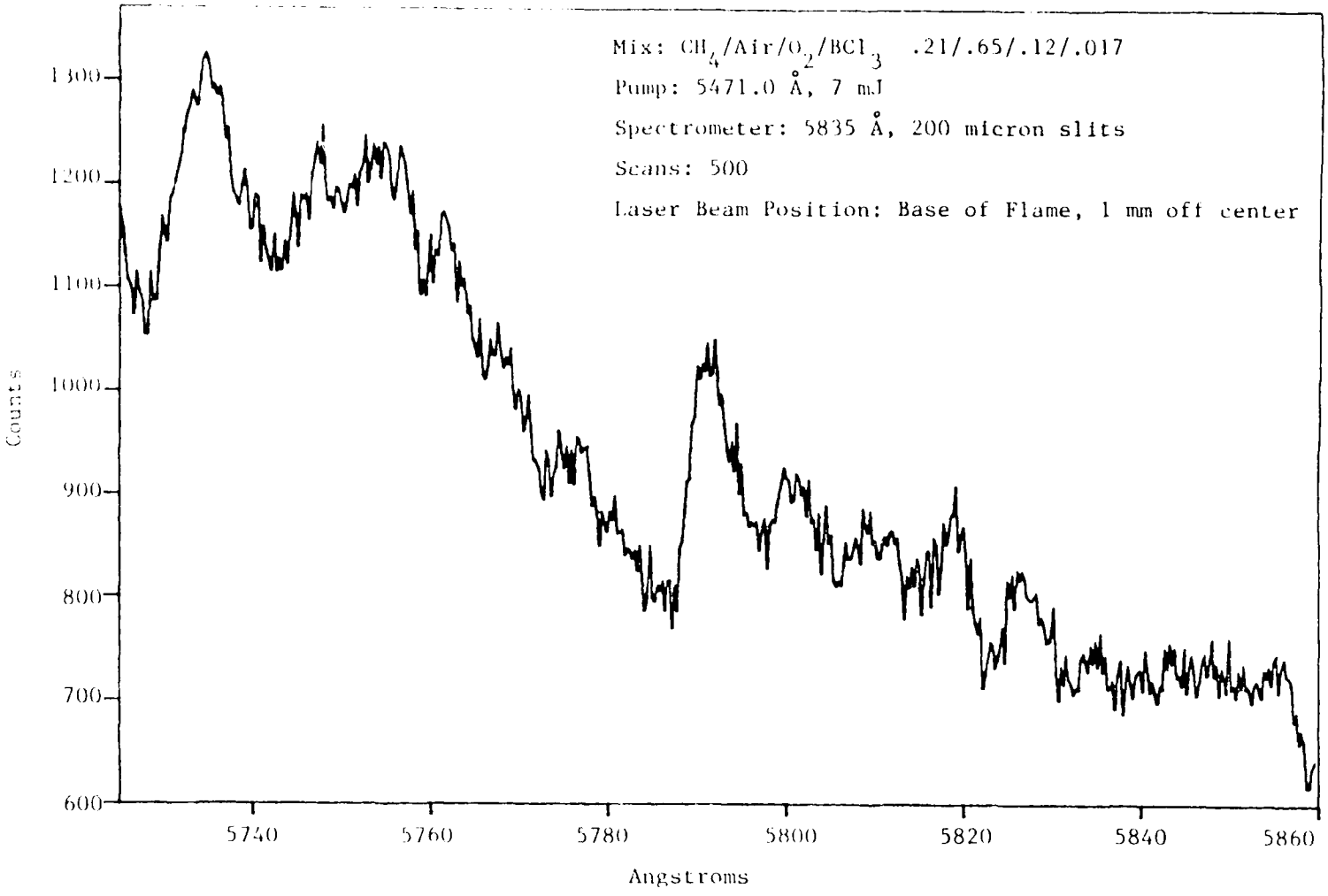


Figure 15. Fluorescence Scan at Flame Base

Raman scattering is a process in which photons are inelastically scattered by molecular vibrations. Raman scattering is similar to LIF in that a molecule is excited to some upper level and then relaxes to either a higher level than that from which it started or a lower level, if any. The photon emitted in the former case is called a Stokes photon, where in the latter case, it is called an Anti-Stokes photon. Figure 16 is a generic energy level diagram of the Raman scattering process. The difference in the energy of the pump and emitted photons is simply the energy difference between the initial and final states. The distinction between LIF and Raman is that in LIF, the upper level of the pump transition is a real eigenstate of the molecule, whereas in Raman, the upper state is not a real eigenstate and is called a virtual level. This fact usually means that the Raman signal is very small. However, as the exciting laser frequency is tuned close to a transition between two real eigenstates, a resonant enhancement of the Raman scattering process takes place which dramatically increases its signal strength. Because the upper level of a Raman transition is not fixed, being determined solely by the energy of the pump photon, but the final lower levels are fixed, since they must be real eigenstates of the molecule, as the pump photon frequency is changed, the frequency of the emitted photon will also change by the same amount. Thus, by following the spectral movement of a peak as the pump frequency is changed, one can determine if that peak comes from Raman or LIF.

Figure 17 shows three spectra taken under identical conditions but with the pump laser tuned to three different wavelengths. Note that the 5790 Å peak changes intensity, but not position. The peaks at 5795 Å, 5813 Å, and 5820 Å (with a 5465 Å pump wavelength) change intensity

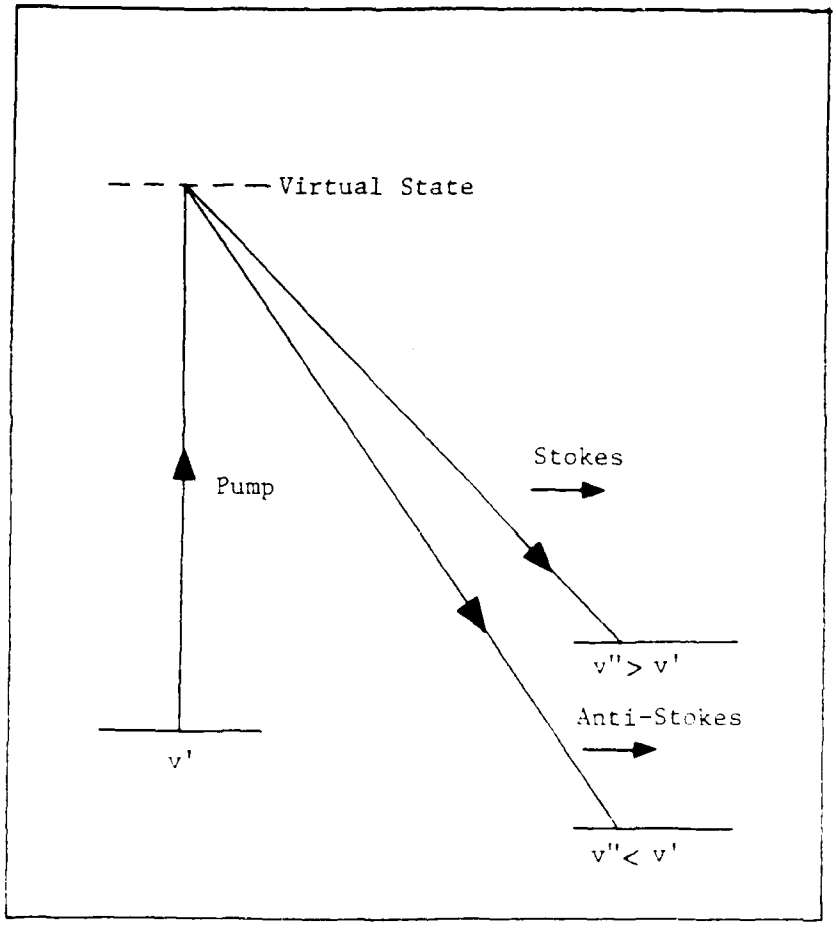


Figure 16. Raman Scattering Diagram

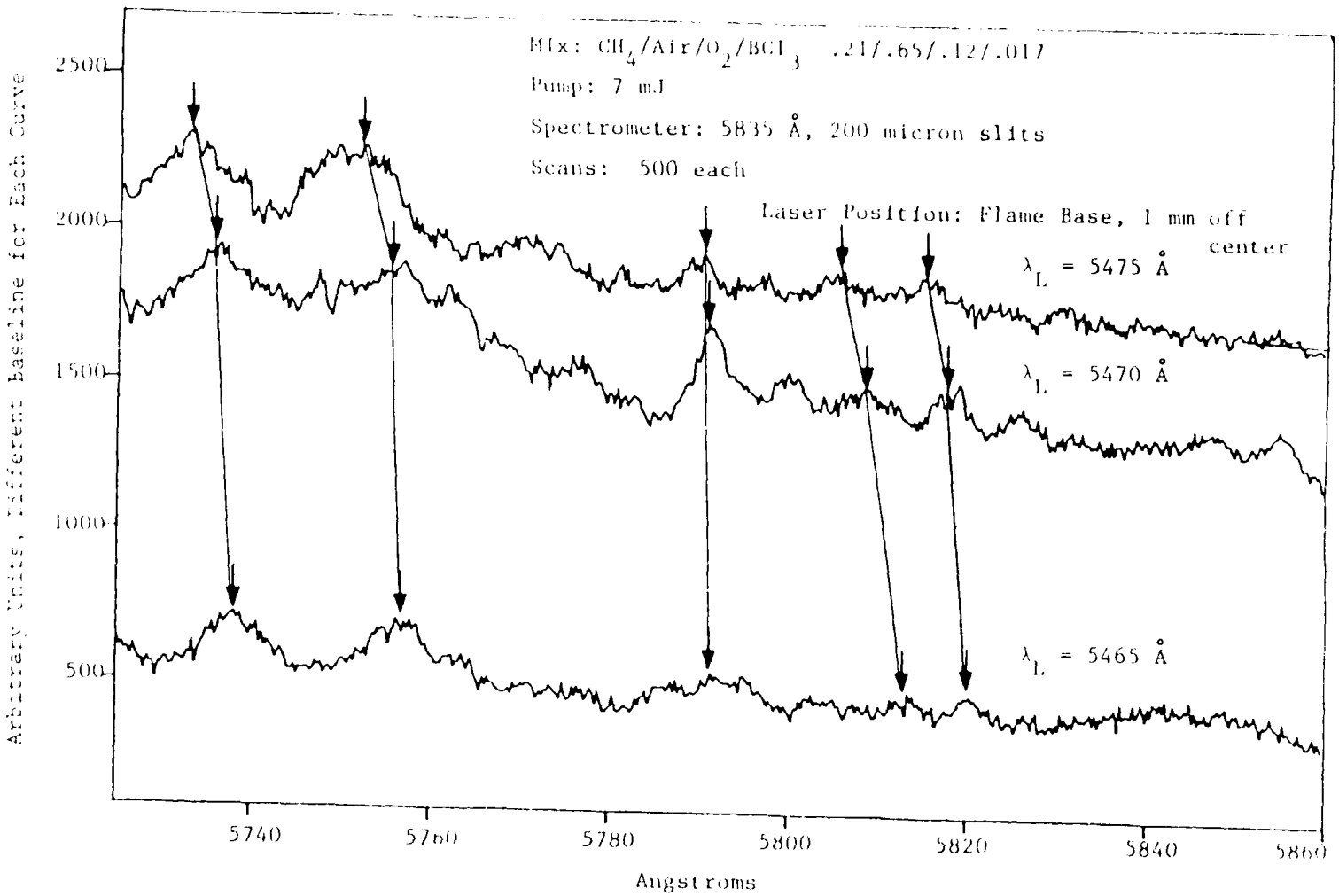


Figure 17. Fluorescence Scans Showing Possible Raman Scattering

somewhat, but more dramatically change position to 5805 Å, 5823 Å, and 5830 Å, respectively when the pump wavelength is 5475 Å. After reviewing the data collected over a pump wavelength range of 30 Å (5455-5485 Å), six Raman transitions were assigned. Table III lists the assigned transitions where the frequencies observed are the differences between the pump and emitted photons and the frequencies given are the difference between the initial and final vibrational states.

Table III

Raman Transition Assignments

Observed Freq (cm^{-1})	Given Freq	Difference Freq	Initial State	Final State	Molecule
809.8	810.0	0.2	00^00	02^00	BO_2
874	876	2.0	----	----	H_3BO_3
933.8	939.4	5.6	00^00	02^00	BO_2
1064.1	1064.0	0.1	01^10	11_{10}	BO2
1093.4	1093.1	0.3	02^00	12^00	BO_2
1116	1121.6	5.6	00^00	02_{20}	BO2

All BO_2 vibrational frequencies are from Fried and Mathews (42:366). The H_3BO_3 vibrational frequency is from Bell, et al., but they did not assign it to a specific state (52:211-213). Three other transitions were observed having frequencies of 826, 1016, and 1040 cm^{-1}, but could not be matched to published data for BO_2, BO, or H_3BO_3. To the best of our knowledge, no Raman spectra of HBO_2 has been observed.

It was concluded that the tremendous scattering observed in the inner cone was principally caused by Mie scattering from some aerosol

produced in the gas mixing chamber just upstream of the burner. The likely aerosol candidates are HBO_2 and H_3BO_3. Further, some LIF and resonant Raman scattering was detected as the laser was tuned through an absorption band. This problem caused anomalous results in the lower regions of the inner cone when a concentration profile was attempted.

LIF of BO

Attempts to use LIF on BO were unsuccessful. As discussed above, the electronic energy levels of BO were so far apart that excitation from the lowest electronic state, where the population was greatest, was not possible. Without tripling the frequency of the Nd:YAG laser pump beam, which was a dubious procedure with the available system, the dye laser simply could not produce photons of sufficient energy to pump the 0-0, 0-1, 0-2 transitions of the A-X system. Attempts were made to pump the 0-3 transition at 5551.5 Å with observation of each of the aforementioned bands. No identifiable signal was obtained. The focal volume of the detection system was positioned in various regions of the flame including just above the inner cone of the flame where the gases should have been the hottest and the BO most likely to exist.

The failure to observe LIF in BO could be due any and all of the considerations discussed in Chapters II and III. However, the result does not necessarily mean that BO is not significant in the combustion of pure, solid boron.

Discussion of Results

In general the results of this work show that LIF can be used for detection of at least BO_2 in atmospheric-pressure flames. The prospects

for obtaining accurate absolute number density measurements using this technique are reasonable. The spectra show a considerable amount of collisional redistribution of energy among the excited states. How this shifting of energy is affected by changes in temperature, gas mixture, flame configuration, etc., are questions that must be answered before reliable concentration measurements can be made.

As discussed in Chapter II, the quenching issue can sometimes be circumvented by using high pump powers so as to saturate the desired transition. For BO_2 under these conditions, the required power would be very high. Since the molecule exhibits rapid redistribution of energy to other states at this pressure virtually all of those transitions would have to be saturated before the effect of quenching is minimized. Thus, though very difficult, with the continual advances in high power dye lasers, saturated LIF of BO_2 at atmospheric pressure may be possible.

The lack of results for BO must be viewed as only a partial answer to the question of its detection by LIF in an atmospheric-pressure boron flame. First, the flame used here was actually a reaction of methane, oxygen, air and boron trichloride, not pure boron flame. As such, it was only a gross approximation of the combustion systems of interest. It was not assured that BO would be produced in a measurable amount in such a reaction. While BO has been generated from BCl_3 reacting with active N_2 and O_2, the conditions were quite stringent as discussed previously. Thus, the most one can say is that it is doubtful that BO is produced in significant quantities under these particular conditions.

VI. Conclusions and Recommendations

Summary

In support of on-going research into the prospects of using boron as a primary fuel for future aerospace systems, this project was formulated to demonstrate the feasibility of using laser-induced fluorescence (LIF) as an in-situ probe for particular radical species (BO_2 and BO) in boron-seeded atmospheric-pressure flames. First, a $CH_4/Air/O_2$ flame was seeded with BCl_3 and examined using standard emission spectroscopy. The resulting spectra agreed well with published results for BO_2. No BO emission was observed.

Second, LIF of BO_2 was demonstrated in the A-X electronic system by exciting either of the spin-orbit-coupled components of the $00^00\text{-}00^00$ transition with spectrally resolved detection in the region of the $00^00\text{-}10^00$ transition using an optical multichannel analyzer. This was the first known demonstration of LIF of BO_2 at a pressure above a few tens of torr. The LIF spectra showed a considerable amount of redistribution of energy among excited states resulting in emission from a number of different transitions and clouding the prospects for the use of saturated LIF under similar conditions. A two-dimensional profile of the relative BO_2 fluorescence in the flame was produced by translating the flame vertically and horizontally along the laser beam path. The integrated LIF signal can be used as a rough measure of the number density of the BO_2. The profile resembles that of OH in that the BO_2 seems most heavily concentrated outside the flame's inner cone. A significant amount of Mie scattering was observed in the inner conal region of the

flame. It is believed this results from aerosols of either HBO_2 or H_3BO_3, or both, which are produced in the gas mixing chamber. In addition to the Mie scattering, resonant Raman scattering from BO_2 and H_3BO_3 was also observed in the inner cone of the flame.

Third, BO was not observed using LIF. It is possible that significant quantities of BO are not produced in the reaction of the species used. As this was only a crude approximation of the combustion of solid boron, this result should not be interpreted as diminishing the potential importance of BO in an actual boron-fueled combustor.

Recommendations for Future Work

In the interest of completeness, a more thorough examination of the possible combinations of excitation-detection transitions should be undertaken. In particular, pumping of the 00^00-10^00 transition with observation of the 00^00-00^00 transition should be attempted. (Note that this combination is the inverse of the one principally used in this effort.) Continuing the present experiment using BCl_3 to explore the aerosol production or the source of the apparent Raman scattering would be of academic interest, but would add little to the boron combustion research base. As discussed above, dry air should be used so as minimize the aerosol scattering that complicated this study.

The next significant step is to seed an atmospheric-pressure flame with small solid boron particles and use LIF to probe for BO_2 and BO. The crude tests done here with relatively large pieces of boron indicate the presence of BO_2 from the green emission of the flame. The determination of the relative concentrations of BO and BO_2 under various flame conditions could lead to a greater understanding of the combustion

reaction chain. It is this understanding that is critical to the success of the boron combustion program. This project has demonstrated the feasibility of using LIF to obtain this knowledge.

Alternative Techniques

If the quenching issue is insoluble alternative techniques would have to be explored that are insensitive to the quenching rate. Two such techniques are described below.

Kizirnis, et al., recently demonstrated a technique called photothermal deflection spectroscopy (PTDS) on the hydroxyl radical (OH) where the heat generated by quenching of the laser-excited states of a species causes refractive index changes that deflect an intersecting low-power off-resonance probe laser beam (53). The deflection is measured by a position-sensitive detector and can be related to the species number density at least on a relative scale throughout a given flame. Such a method may be employed if quenching is the limiting factor of LIF.

A second possible technique is degenerate four-wave mixing (DFWM). This method first discussed by Yariv and Pepper (54) uses two strong counterpropagating pump beams crossed at a small angle by a weak probe beam all of the same wavelength. The result is a phase-conjugate beam counterpropagating along the probe beam path when the beams are tuned to an absorption resonance of the medium. This method has the advantage that the desired signal can be spatially resolved from background radiation such as the flame emission. Further, since the desired signal is always at the same wavelength as the pump and probe beams, no spectrometer is required. Bloom, et al., first used this technique on sodium in a heat-pipe (55). Pender and Hesselink demonstrated DFWM in flame using

sodium-seeding (56). And recently, Ewart and O'Leary de'ected OH in flame using this method (57). A significant potential advantage of DFWM over LIF is that it is a coherent process that occurs on time scales much shorter than fluorescence and, in most cases, quenching as well (56:266, 58:281).

Appendix A: Transition Probabilities for BO and BO_2

Table IV

Transition Probabilities for the $A^2\Pi_u$ State of BO_2 (46)

State	Lifetime (nsec)	A Coeff. (10^7 sec^{-1})	
$00^00\ ^2\Pi$	91 ± 4	1.1	
$10^00\ ^2\Pi_{1/2}$	94.8 ± 1.6	1.05	
$10^00\ ^2\Pi_{3/2}$	91.6 ± 3.8	1.09	
$11^10\ ^2\Sigma^+_{1/2}$	91.4 ± 3.6	1.09	
$11^10\ ^2\Sigma^+_{3/2}$	110 ± 2	0.91	
$11^10\ ^2\Delta_{3/2}$	102 ± 12	0.98	
$11^10\ ^2\Delta_{5/2}$	101 ± 2	0.99	
$20^00\ ^2\Pi_{3/2}$	98.5 ± 0.6	1.02	
$20^00\ ^2\Pi_{1/2}$	101.6 ± 1.4	0.98	
$20^00\ ^2\Pi_{3/2}$	103.8 ± 1.4	0.96	^{10}B
$02^20\ ^2\Pi_{3/2}$	89.3 ± 3.8	1.12	
$02^00\ ^2\Pi_{1/2}$	97.1 ± 4.2	1.03	
$02^00\ ^2\Pi_{3/2}$	103 ± 4	0.97	
$12^00\ ^2\Pi_{3/2}$	101.3 ± 2.8	0.99	
$12^00\ ^2\Pi_{1/2}$	124 ± 2	0.81	
$12^00\ ^2\Pi_{3/2}$	103 ± 0.8	0.97	^{10}B
$12^00\ ^2\Pi_{1/2}$	96.2 ± 2	1.04	^{10}B
$00^02\ ^2\Pi_{3/2}$	105 ± 6	0.95	
$00^02\ ^2\Pi_{1/2}$	121 ± 6	0.83	

Table V

Transition Probabilities for the $A^2\Pi_i$ State of BO (45)

State (v')	Lifetime (μsec)	A Coeff. (10^5 sec^{-1})
0	1.78 ± 0.14	5.62
4	1.94 ± 0.17	5.15
7	1.62 ± 0.02	6.17
9	1.86 ± 0.01	5.38
10	1.67 ± 0.13	5.99
11	1.66 ± 0.09	6.02
Average	1.7 ± 0.1	5.88

Appendix B: Outline of NASA Chemical Equilibrium Code

A computer code developed by NASA Lewis Research Center called CEC-71 has gained wide acceptance for the calculation of chemical equilibrium compositions, rocket performance, incident and reflected shocks, and Chapman-Jouguet detonations. This code is well documented in Reference (58). This appendix is a brief overview of the code as it relates to the present work.

The CEC-71 code was used in this effort to provide an estimate of the adiabatic flame temperature as well as some crude estimate of the equilibrium concentrations of BO and BO_2. For this purpose only the chemical equilibrium calculation capability of the code was exercised. The code determines the equilibrium concentrations and states by minimizing the Gibbs free energy through an iterative procedure employing a descent Newton-Raphson technique to correct initial estimates of the concentrations. A number of tests are performed as the calculation proceeds to determine whether species have condensed or are approaching a phase transition. The code can accomodate condensed species by assuming they are a minor fraction of the total number density of the gas.

The code is relatively easy to use. Required inputs are the initial gas composition and a pair of thermodynamic state parameters such as temperature, pressure, enthalpy, volume, internal energy, or entropy. For the cases used in this work, the inputs were pressure (one atmosphere) and enthalpy of each reactant. In fact, the code will calculate the enthalpy for the most of the gases for the user from its stored thermodynamic data bank. This data bank is based of the JANAF Thermo-

chemical Tables and contains required information for 600 different gaseous and condensed species.

From the input information the code examines all possible reaction products for concentrations above some specified lower bound, typically one part-per-million. It also calculates the adiabatic temperature, resultant enthalpy, density, and other thermodynamic values.

A typical case input to the code for this effort specified one atmosphere pressure and reactant input amounts of 0.0096 moles of CH_4, 0.00076 moles of BCl_3, 0.0054 moles of O_2 and 0.0281 moles of air. The enthalpies were calculated by the code itself for an incident temperature of 298 °K. The calculated adiabatic temperature was 2143 °K with equilibrium mole fractions of such pertinent reaction products as BO (10^{-5}), BO_2 ($2x10^{-5}$), HCl (0.043), B_2O_3 ($1.4x10^{-4}$), HBO_2 (0.014), CO (0.15), H_2 (0.15) and H_2O (0.18). Other obvious products such as Ar, N_2, etc., are also analyzed and output, but are not important for this discussion.

Appendix C: Emission Spectra

The following figures illustrate the background-corrected emission spectra observed from the BCl_3-seeded flame. Note that certain experimental parameters such as spectrometer slit width and detector integration time vary from curve to curve. Thus, direct comparison of signal strength between curves is difficult. Key spectral bandheads are noted.

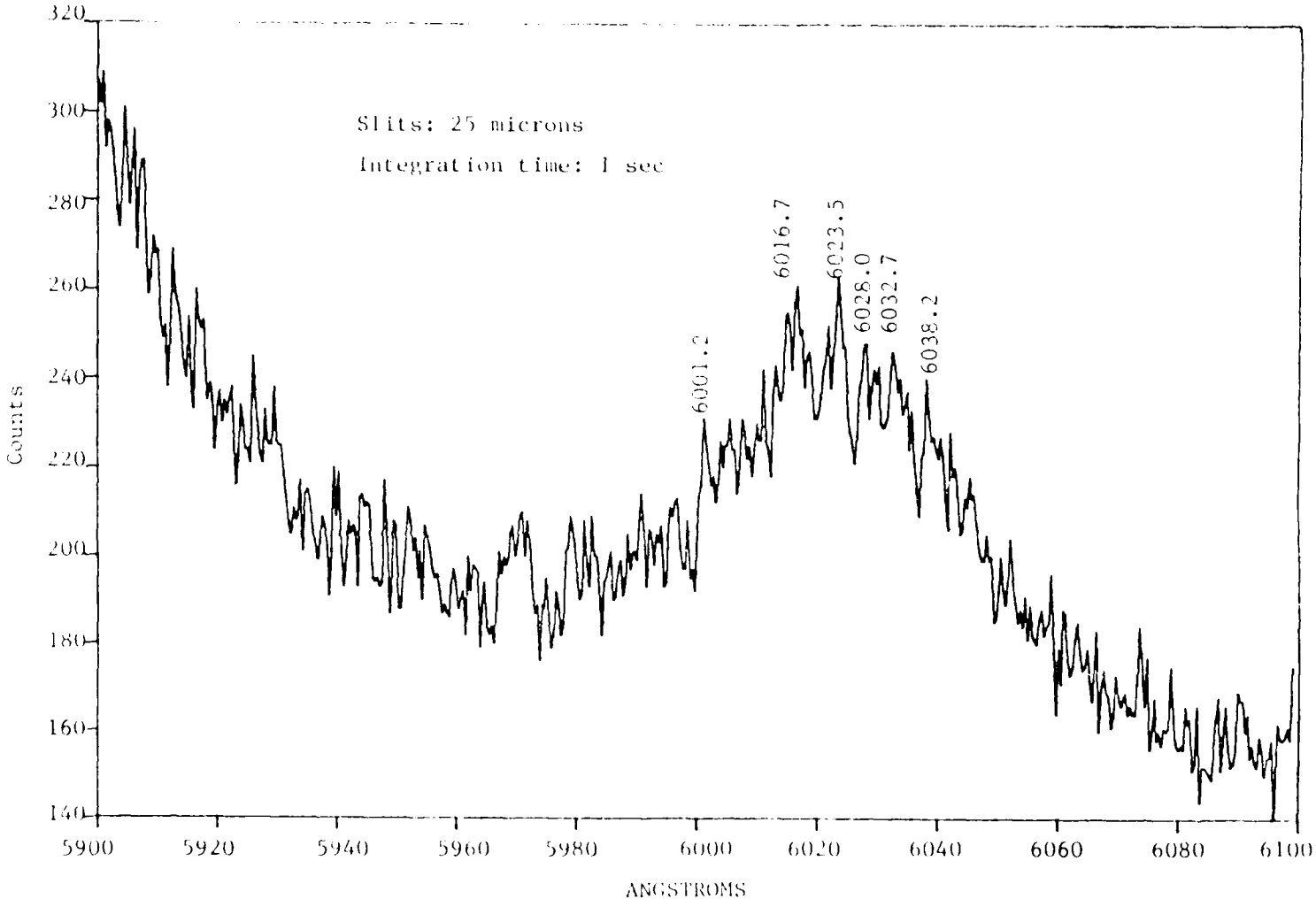


Figure 18. Flame Emission, 5900-6100 Å

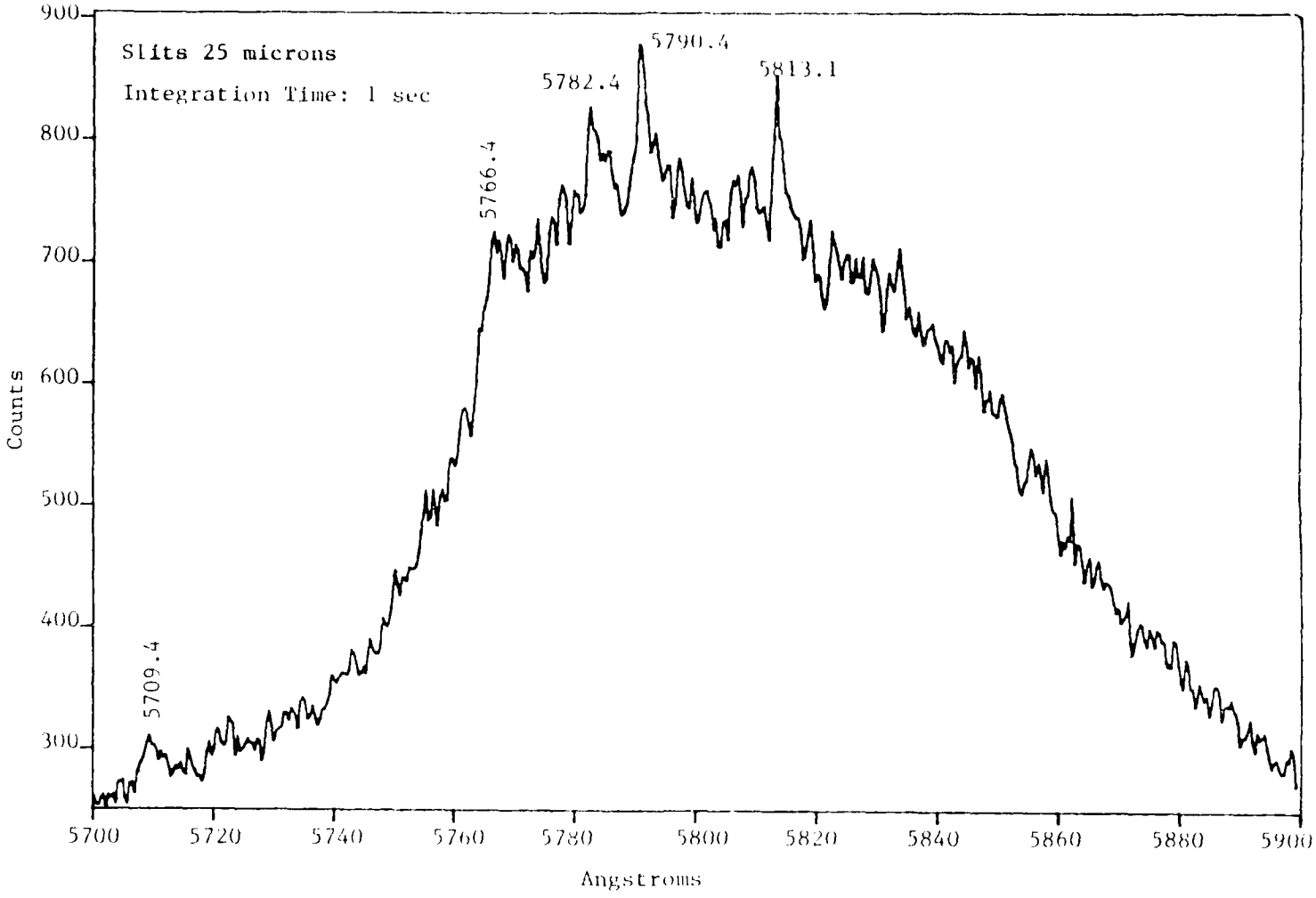


Figure 19. Flame Emission, 5700-5900 Å

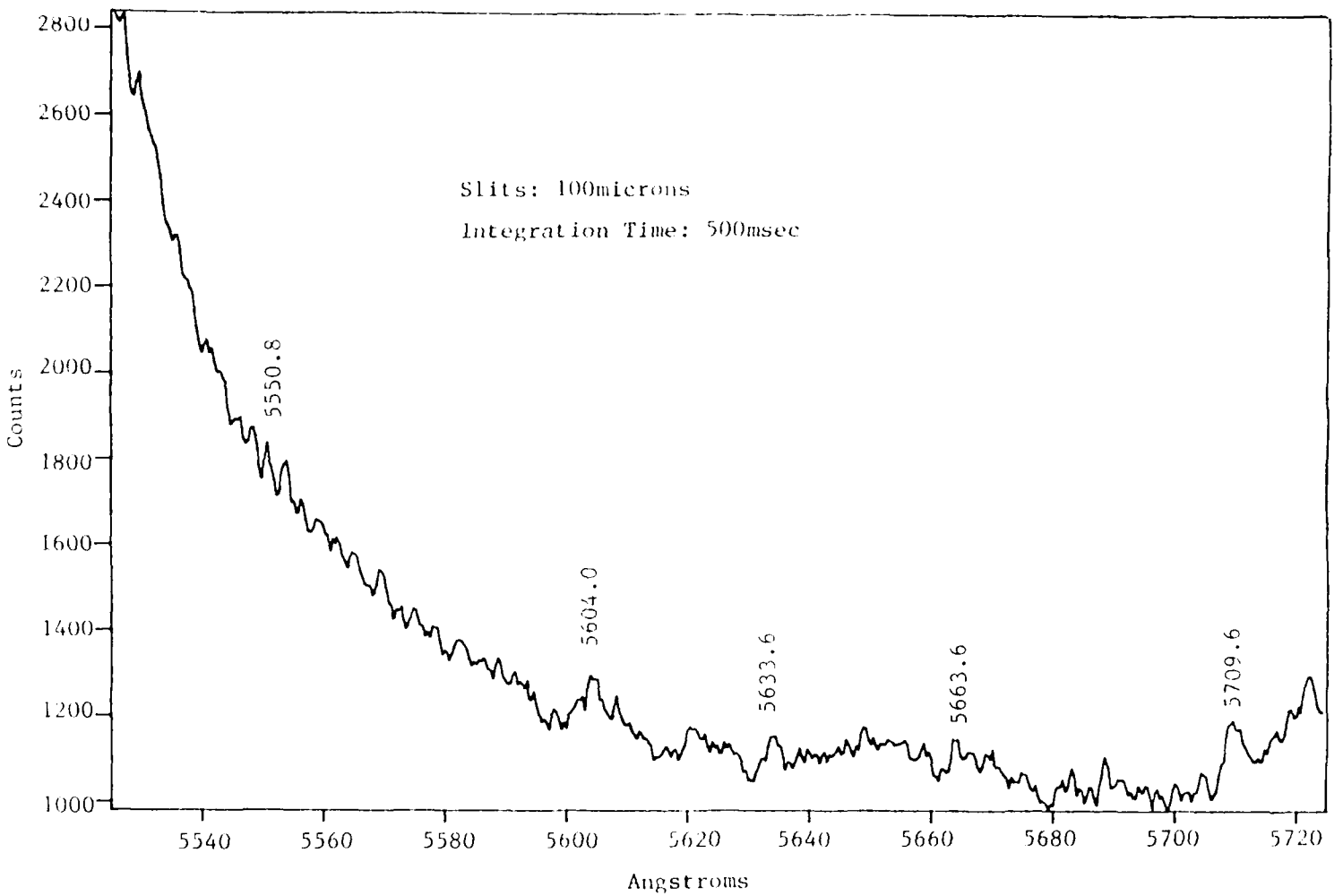


Figure 20. Flame Emission, 5520-5720 Å

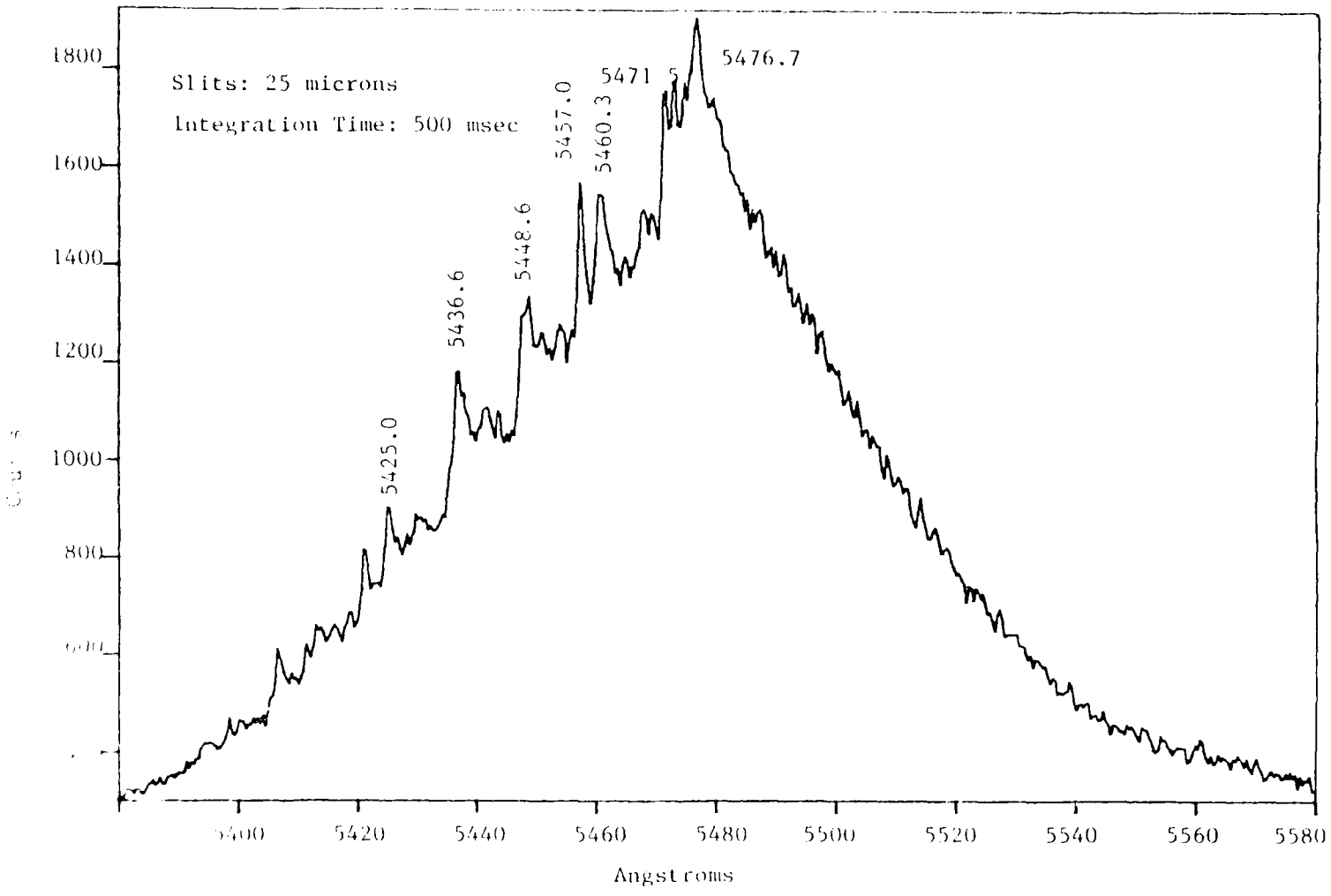
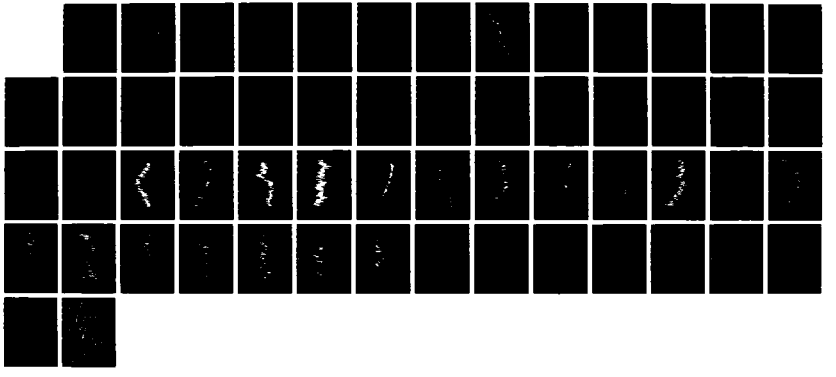
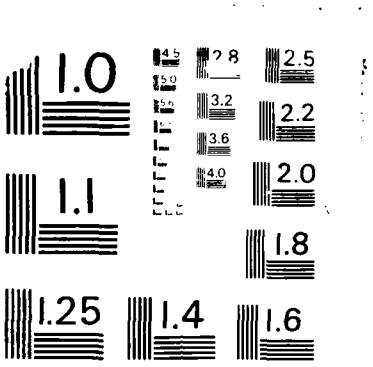


Figure 21. Flame Emission, 5380-5580 Å

AD-A189 631 APPLICATION OF LASER-INDUCED FLUORESCENCE IN AN ATMOSPHERIC-PRESSURE BORO..(U) AIR FORCE INST OF TECH WRIGHT-PATTERSON AFB OH SCHOOL OF ENGI.. G R SCHNEIDER 2/2

UNCLASSIFIED DEC 87 AFIT/DS/PH/87-4 F/G 21/2 NL





MICROCOPY RESOLUTION TEST CHART
NATIONAL BUREAU OF STANDARDS-1963

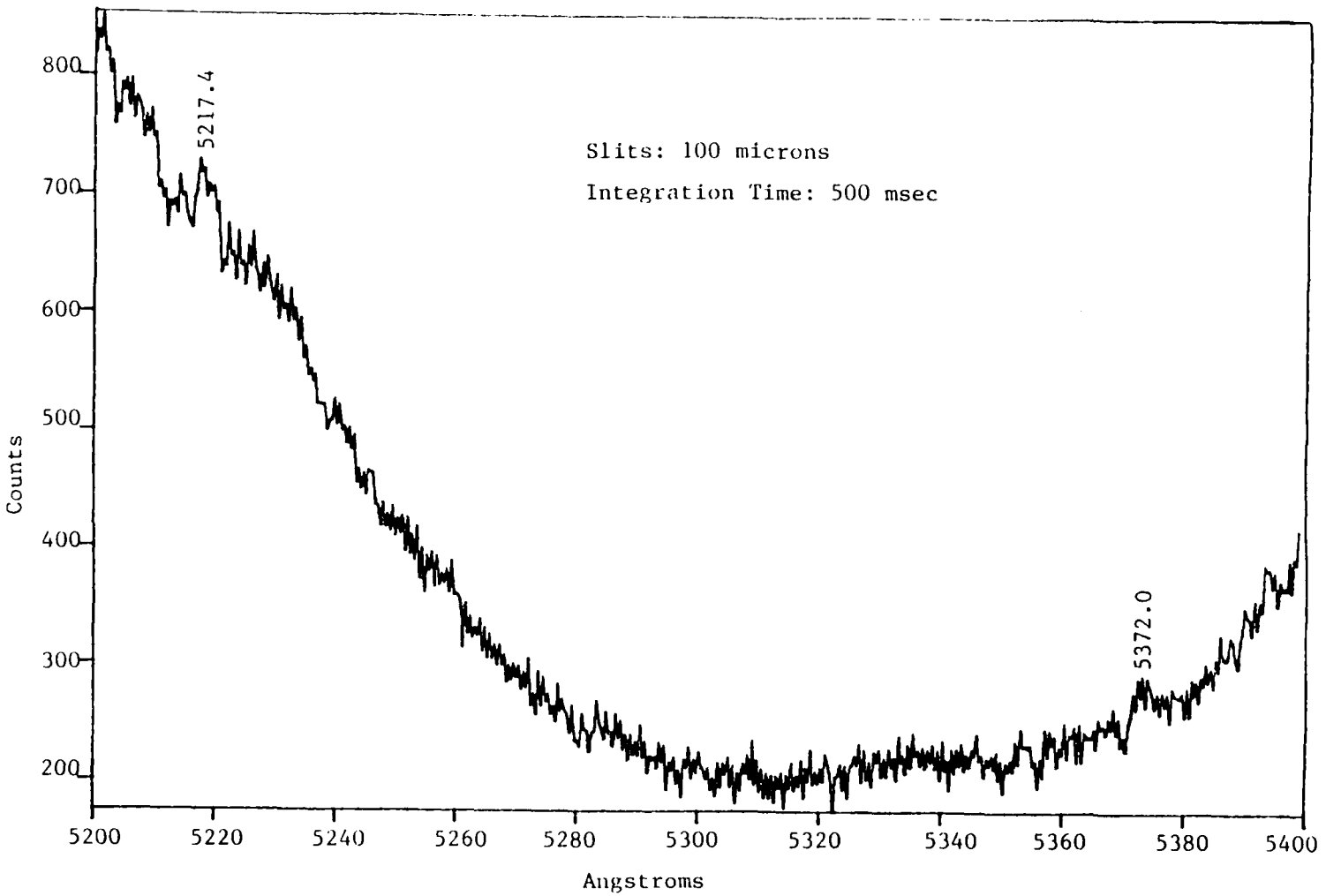


Figure 22. Flame Emission, 5200-5400 Å

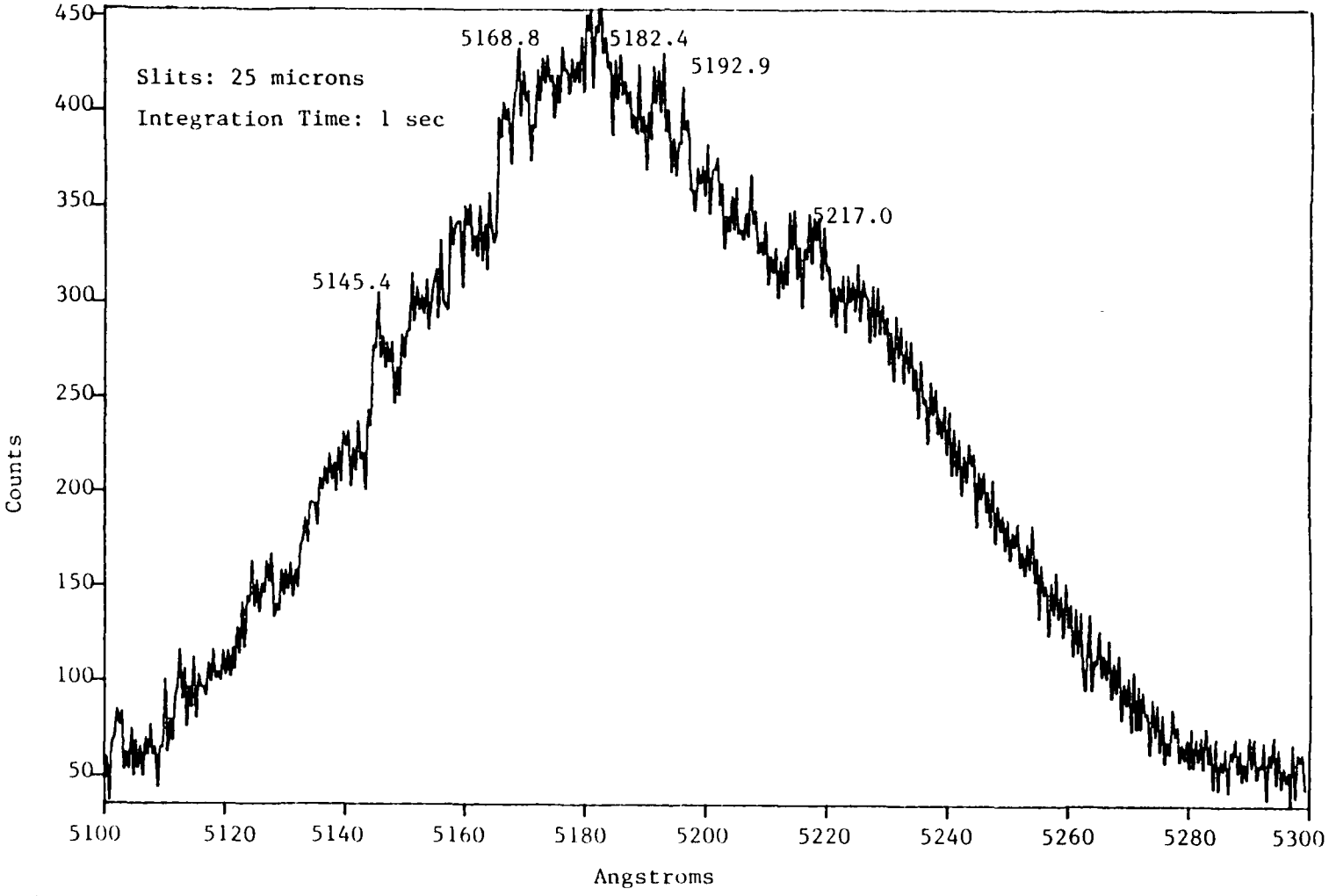


Figure 23. Flame Emission, 5100-5300 Å

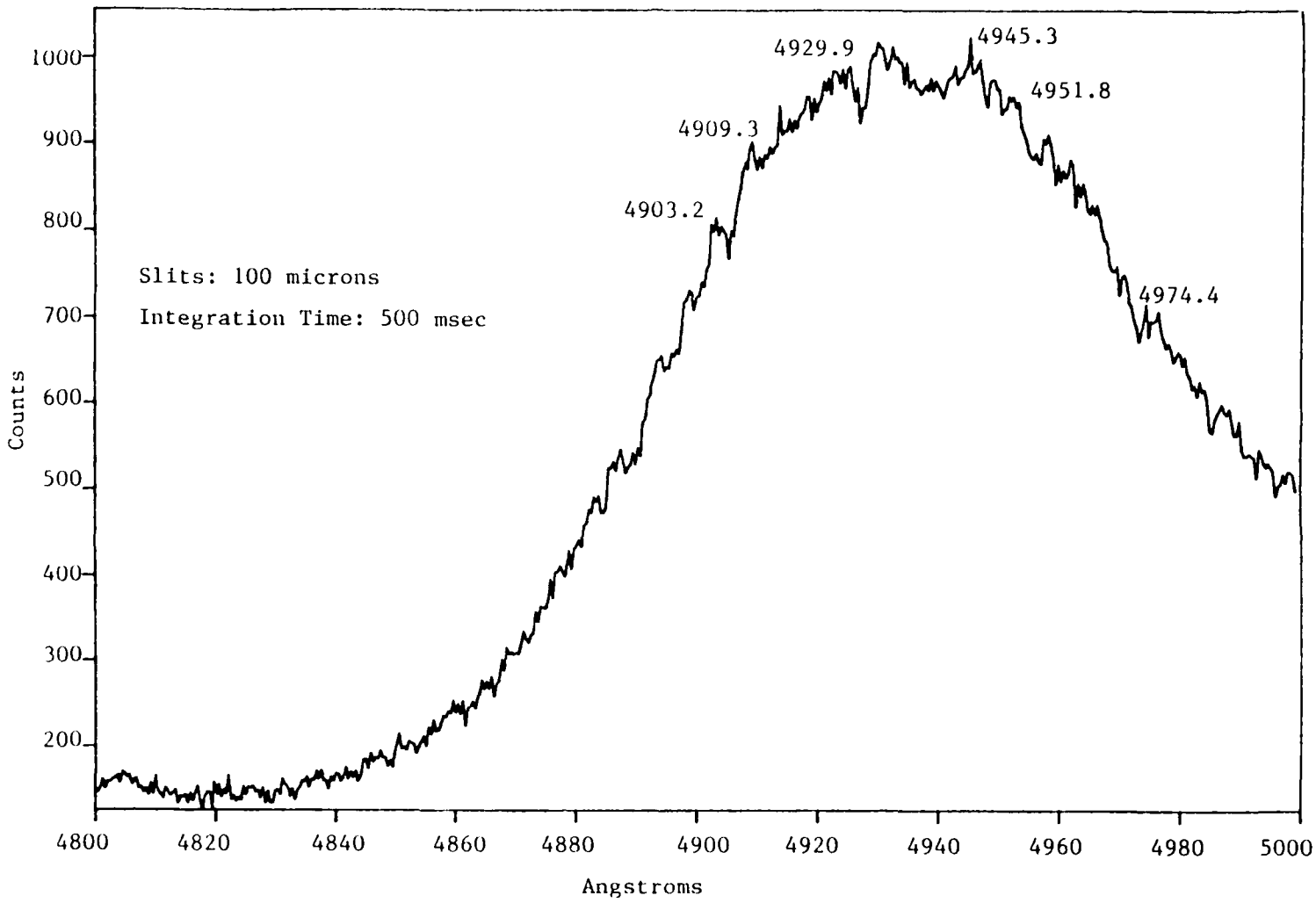


Figure 24. Flame Emission, 4800-5000 Å

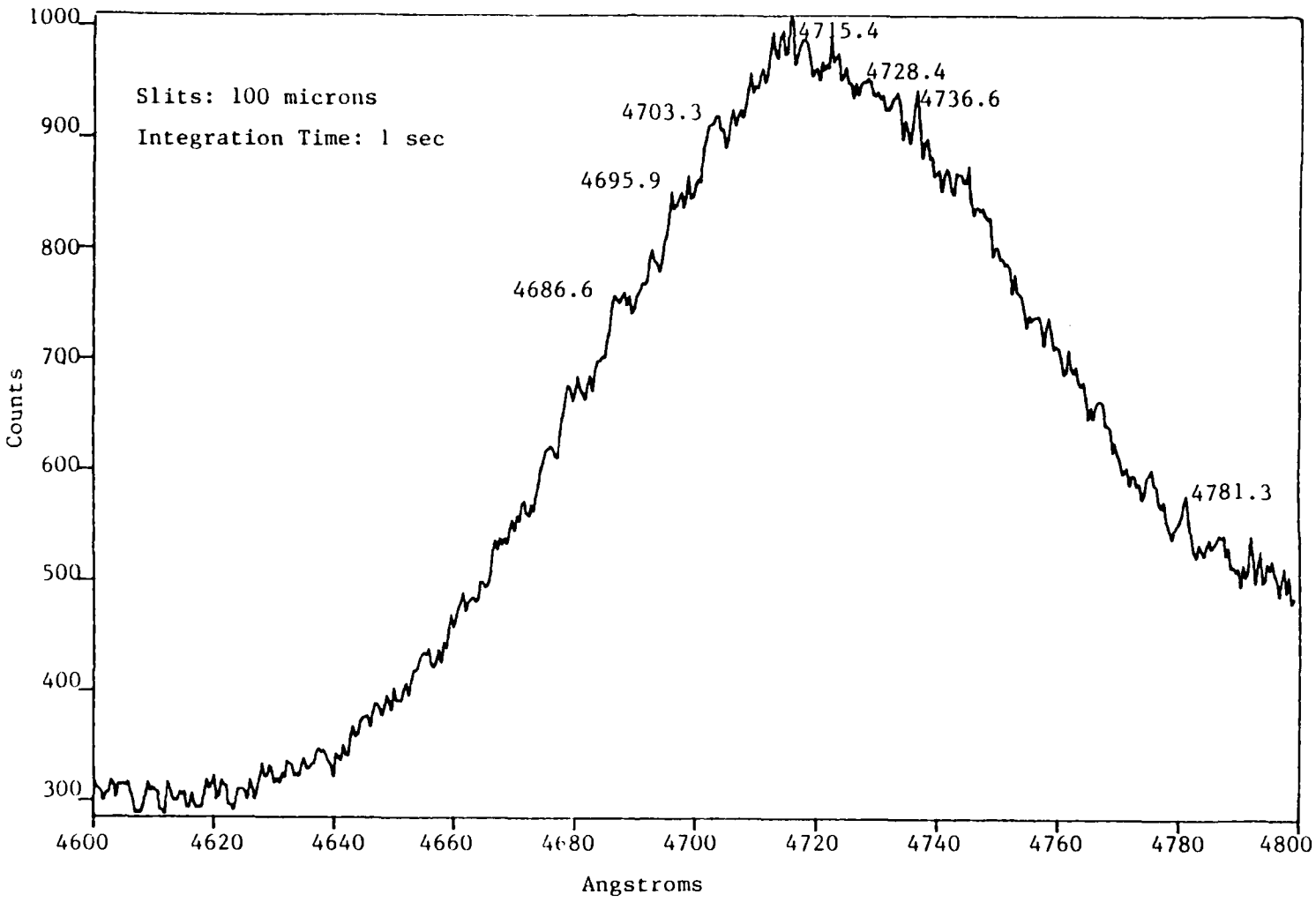


Figure 25. Flame Emission, 4600-4800 Å

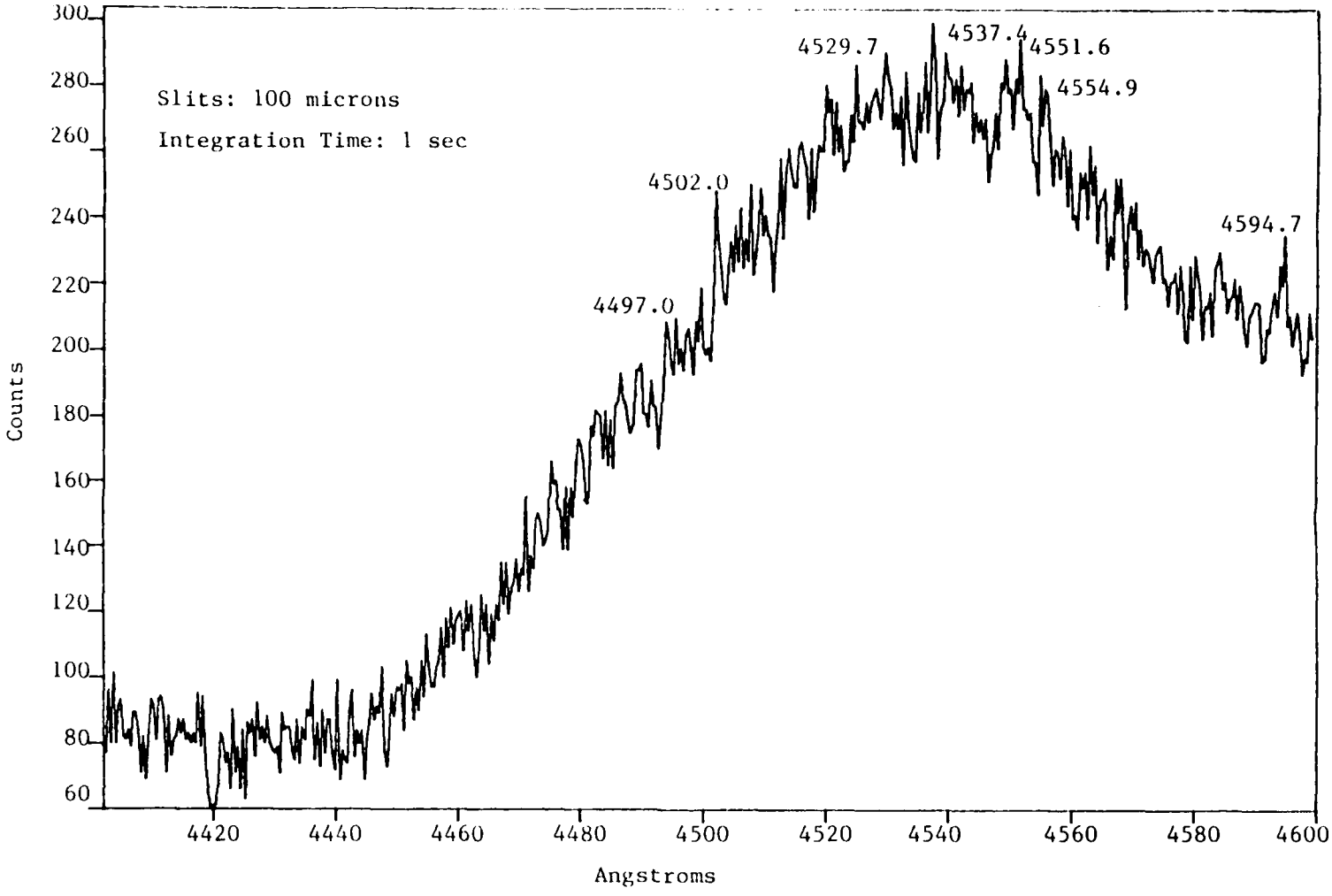


Figure 26. Flame Emission, 4400-4600 Å

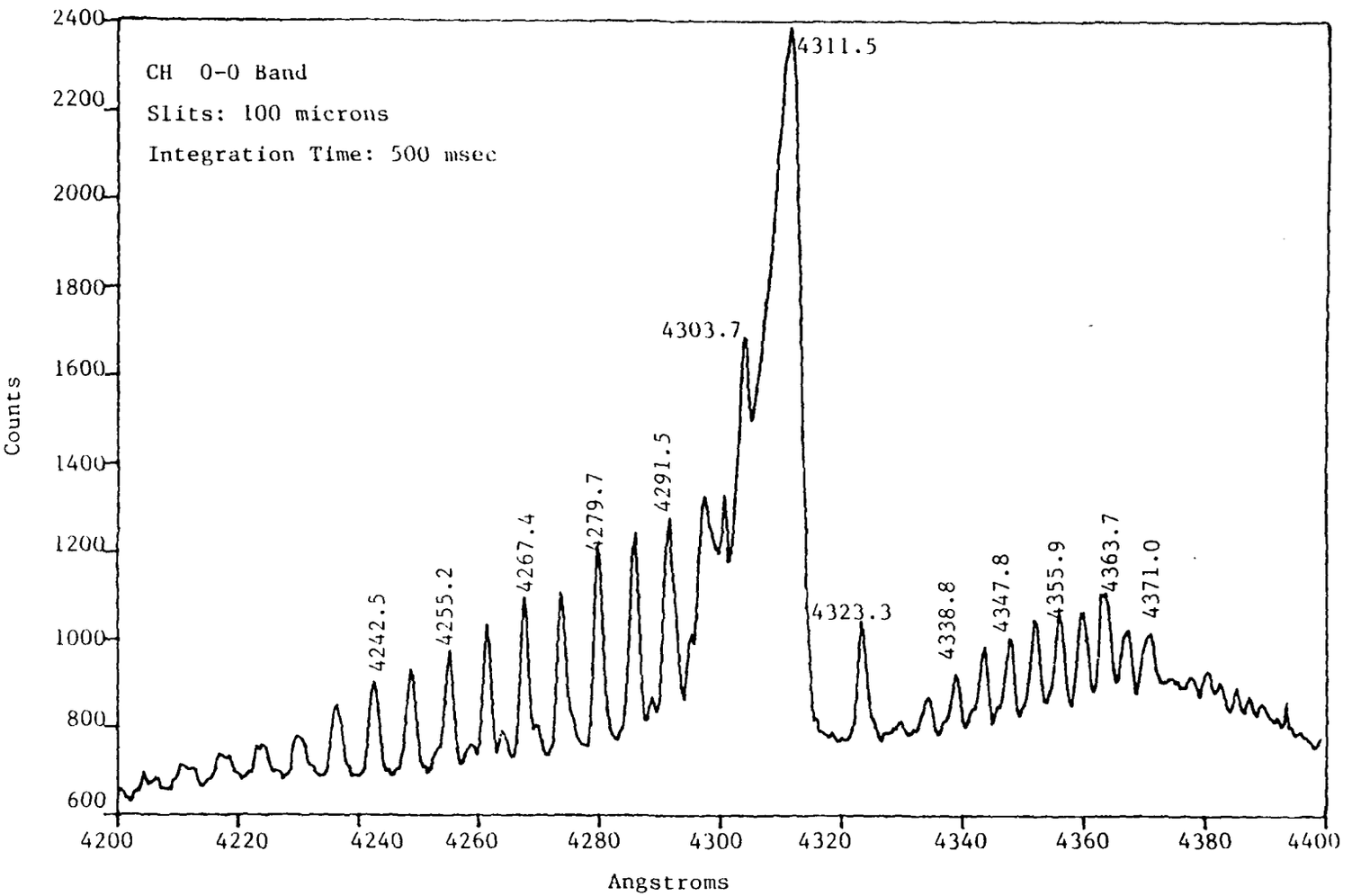


Figure 27. Flame Emission, 4200-4400 Å

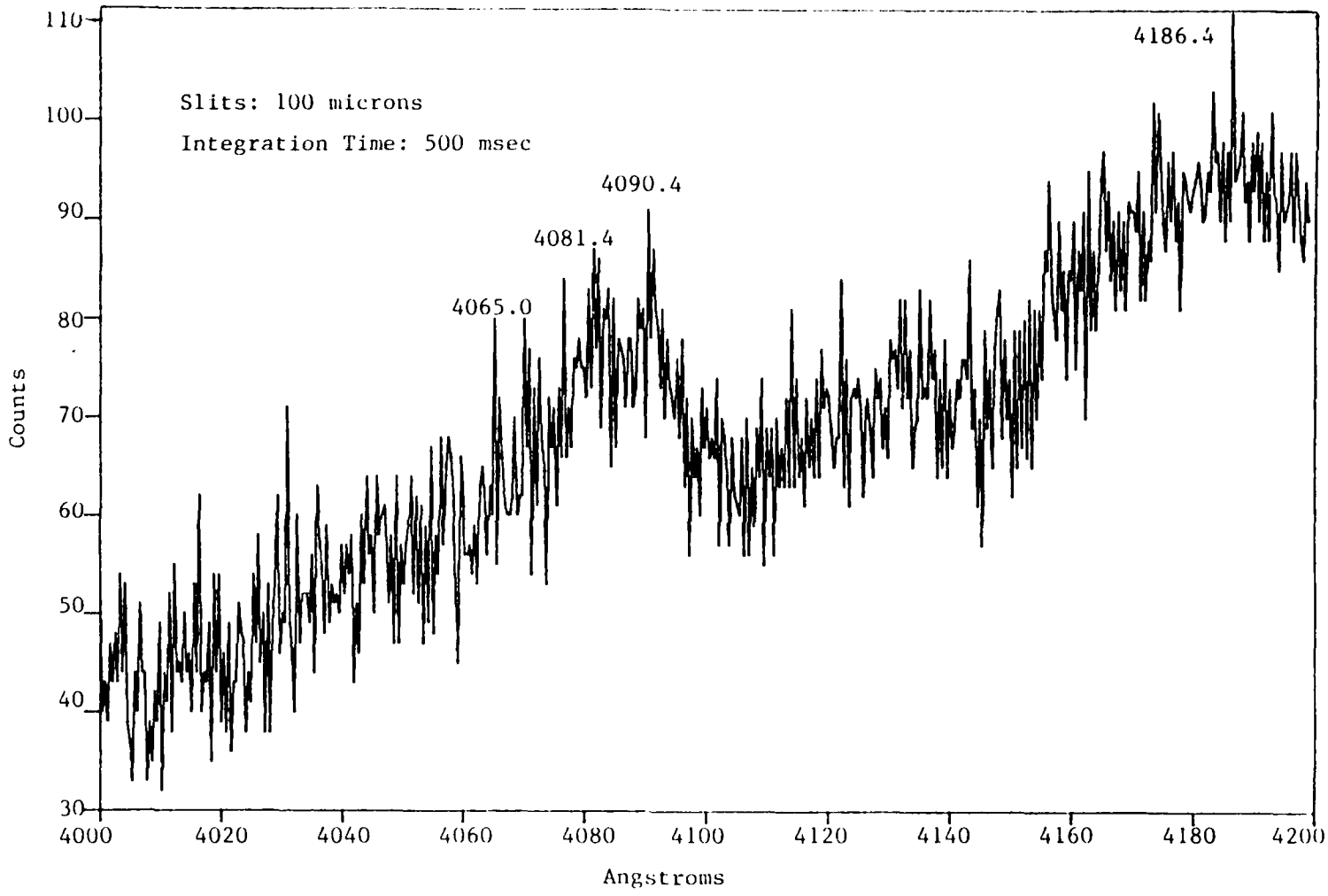


Figure 28 . Flame Emission, 4000-4200 Å

Appendix D: Compiled Band Spectrum of BO_2

Band Heads of the A-X System of BO_2

λ_{air}, Å	Present Work υ_{vac} cm^{-1}	Snowden	Johns	Fried-Mathews	Branch ($*B^{10}$)	Upper Level	Lower Level
6429.4		15549.3	15549.0		R_2*	$00^00^12\Pi$	$00^02^12\Pi$
6408.7		15601.3	15599.0		R_1*	$00^00^12\Pi$	$00^02^12\Pi$
6401.0		15618.3	15618.0				
6396.0		15634.4	15630.0		R_2	$00^00^12\Pi$	$00^02^12\Pi$
6389.9		15645.4	15645.0				
6377.1		15676.1					
6376.6		15678.5	15678.0		R_1	$00^00^12\Pi$	$00^02^12\Pi$
6360.5		15717.9	15717.0				
6352.1		15738.5	15738.0				
6349.2		15745.6	15746.0				
6344.1		15758.1	15758.0				
6341.2		15765.5	15766.0				
6331.5		15792.2	15790.0				
6327.1		15800.7	15801.0				
6320.0		15818.4	15818.0				
6312.0		15838.5	15838.0				
6290.8	15891.9						
6288.8	15896.9						
6280.1	15918.9						
6275.3	15931.1						
6273.6	15935.4						

Band Heads of the A-X System of BO_2 (Cont'd.)

λ_{air}, Å	Present Work $\tilde{\nu}_{vac}$ cm^{-1}	Snowden	Johns	Fried-Mathews	Branch ($*B^{10}$)	Upper Level	Lower Level
6262.3	15964.2						
6249.2	15997.6						
6246.8	16003.8						
6242.5	16014.8	16015.6					
6240.9	16018.9						
6235.3	16033.3						
6230.2	16046.4						
6227.8	16052.6						
6222.3	16066.8	16066.6					
6207.6	16104.8						
6204.0	16114.2						
6202.2		16118.8	16118.8	16118.8	R_2	$00^00^02_\Pi$	$20^00^02_\Pi$
6200.9	16122.2						
6198.1	16129.5						
6194.1	16139.9						
6191.8	16145.9						
6189.4	16152.2	16150.0	16150.8		R_2*	$00^00^02_\Pi$	$20^00^02_\Pi$
6186.2	16160.6						
6179.9	16177.0	16180.1	16719.0		R_2	$01^10^02_\Delta$	$21^10^02_\Delta$
6177.1	16184.4						
6173.9	16192.8						
6170.8	16200.9	16198.8	16198.8	16198.8	R_1	$00^00^02_\Pi$	$20^00^02_\Pi$
6168.4			16207				

Band Heads of the A-X System of BO_2 (Cont'd.)

λ_{air}, Å	Present Work $\tilde{\nu}_{vac}$ cm^{-1}	Snowden	Johns	Fried-Mathews	Branch ($*B^{10}$)	Upper Level	Lower Level
6167.2	16210.3						
6162.4	16223.0						
6160.9	16226.9	16228.8			R_1	$01^10^22_\Delta$	$21^10^22_\Delta$
6159.8		16230.2	16229.9		R_1*	$00^00^22_\Pi$	$20^00^22_\Pi$
6154.9	16242.7						
6153.3	16247.0	16246.8	16246.5		R_2	$00^00^22_\Pi$	$04^00^22_\Pi$
6146.6	16264.7						
6144.6	16270.0						
6137.5	16288.8						
6135.1	16295.2						
6122.4	16328.9						
6114.9	16349.0						
6091.2		16412.6					
6089.9	16416.1						
6073.6	16460.2						
6066.5	16479.4						
6063.3	16488.1						
6060.9	16494.7						
6052.1	16518.6						
6050.6		16522.7					
6045.4	16536.9						
6042.2	16545.7						
6038.2	16556.7						

Band Heads of the A-X System of BO_2 (Cont'd.)

λ_{air}, Å	Present Work $\tilde{\nu}_{vac}$ cm^{-1}	Snowden	Johns	Fried-Mathews	Branch ($*B^{10}$)	Upper Level	Lower Level
6032.7	16571.8						
6031.8		16574.2					
6028.0	16584.7						
6023.5	16597.1		16598.0				
6019.8		16607.2					
6017.7		16613.0	16614.0				
6016.7	16615.8	16617.2					
6015.0	16620.5						
6014.4		16622.6					
6011.2	16631.0						
6005.6	16646.5		16646.0				
6001.2	16658.7	16660.9	16657.0				
5996.8	16671.0						
5990.9	16687.4	16685.4	16685.0				
5981.0	16715.0	16715.5	16716.0				
5978.9	16720.9						
5971.0	16743.0	16736.5	16745.0				
5939.5	16831.8	16833.2					
5926.0	16870.1						
5916.5	16897.2						
5912.5	16908.7						
5909.0	16918.7						
5862.2	17053.7						

Band Heads of the A-X System of BO_2 (Cont'd.)

λ_{air}, Å	Present Work $\tilde{\nu}_{vac}$ cm^{-1}	Snowden	Johns	Fried-Mathews	Branch ($*B^{10}$)	Upper Level	Lower Level
5857.8	17066.5						
5855.4	17073.5	17075.6					
5850.6	17087.5						
5844.3	17106.0						
5839.1	17121.2			17117.7	R_1	$02^0 0^2 \Pi$	$20^0 0^2 \Pi$
5833.5	17137.6						
5831.9		17142.4	17142.3		R_2	$10^0 0^2 \Pi$	$20^0 0^2 \Pi$
5829.1	17150.6			17153.7	R_2	$02^0 0^2 \Pi$	$12^0 0^2 \Pi$
5824.8		17163.2					
5822.3	17170.6						
5818.7	17181.2						
5813.1	17197.8	17197.6	17197.5	17197.6	R_2	$00^0 0^2 \Pi$	$10^0 0^2 \Pi$
5812.6				17199.3	R_1	$00^0 0^2 \Pi$	$02^2 0^2 \Pi$
5809.1	17209.6	17209.4	17209.0		R_2*	$00^0 0^2 \Pi$	$10^0 0^2 \Pi$
5806.7	17216.7	17219.6	17219.4		R_1	$10^0 0^2 \Pi$	$20^0 0^2 \Pi$
5801.6	17231.9	17233.1	17232.0		R_2	$01^1 0^2 \Delta$	$11^1 0^2 \Delta$
5797.2	17244.9		17245.0				
5795.0	17251.5	17249.9			R_1	$10^0 0^2 \Pi$	$12^0 0^2 \Pi$
5793.0	17257.4			17261.8	R^1	$02^2 0^2 \Pi$	$20^0 0^2 \Pi$
5790.4	17265.2	17264.3	17264.2	17264.2	R_1	$00^0 0^2 \Pi$	$10^0 0^2 \Pi$
5785.2	17280.7	17280.1	17280.1		R_1*	$00^0 0^2 \Pi$	$10^0 0^2 \Pi$
5782.4	17289.1	17289.4	17289.3		R_1	$01^1 0^2 \Delta$	$11^1 0^2 \Delta$
5779.6	17297.5						

Band Heads of the A-X System of BO_2 (Cont'd.)

λ_{air}, Å	Present Work $\tilde{\nu}_{vac}$ cm^{-1}	Snowden	Johns	Fried-Mathews	Branch ($*B^{10}$)	Upper Level	Lower Level
5777.6	17303.4	17302.8					
5776.0	17308.2	17307.3					
5773.6	17315.4	17315.9					
5768.8	17329.8						
5767.4		17334.3	17334.1	17334.1	R_2	$00^00^22\Pi$	$02^00^22\Pi$
5766.4	17337.1	17336.9	17336.8	17336.9	R_1	$02^00^22\Pi$	$12^00^22\Pi$
5765.4		17339.9		17341.0	R_2	$02^00^22\Pi$	$04^00^22\Pi$
5764.7		17343.9	17342.0	17343.7	R_2	$02^20^22\Pi$	$12^20^22\Pi$
5761.6	17351.5	17348.7					
5759.5		17357.8					
5756.5	17366.9	17367.4					
5754.1		17374.0					
5750.1	17386.2	17385.4					
5746.1	17398.3	17398.6					
5744.1		17404.4					
5742.9	17408.0	17407.0					
5739.7	17417.7	17414.4					
5734.9	17432.3	17431.2					
5732.0	17441.1						
5729.3	17449.3	17452.2					
5724.9		17462.7					
5723.7		17466.4					
5722.5	17470.1						

Band Heads of the A-X System of BO_2 (Cont'd.)

λ_{air},Å	Present Work $\tilde{\nu}_{vac}$ cm^{-1}	Snowden	Johns	Fried-Mathews	Branch ($*B^{10}$)	Upper Level	Lower Level
5720.5	17476.2	17479.1					
5717.1		17486.4					
5715.8	17490.5	17492.9					
5712.6		17500.4					
5710.1		17507.9					
5709.4	17510.1	17510.1		17510.5	R_1	$00^00^02\Pi$	$02^00^02\Pi$
5705.9		17520.8					
5695.1		17553.9					
5688.4	17574.8	17573.2			R_1	$01^10^02\Delta$	$03^10^02\Delta$
5683.2	17590.9						
5681.6	17595.8	17597.5		17597.2	R_2	$00^00^02\Pi$	$02^20^02\Pi$
5672.4		17624.2					
5672.0		17625.6					
5668.7		17635.8					
5663.6	17651.7	17650.3		17650.3	R_1	$02^00^02\Pi$	$04^00^02\Pi$
5660.2				17662.5	R_2	$02^20^02\Pi$	$04^20^02\Pi$
5658.7		17666.9					
5653.4		17683.4					
5648.8	17698.0	17698.5					
5645.0		17709.9					
5633.6	17745.7			17742.7	R_2	$02^00^02\Pi$	$04^20^02\Pi$
5620.4	17787.4	17786.4					
5604.0	17839.5						

Band Heads of the A-X System of BO_2 (Cont'd.)

λ_{air}, Å	Present Work $\tilde{\nu}_{vac}$ cm^{-1}	Snowden	Johns	Fried-Mathews	Branch ($*B^{10}$)	Upper Level	Lower Level
5554.0	18000.1						
5550.8	18010.4			18012.6	R_1	$04^0 0^2 \Pi$	$20^0 0^2 \Pi$
5548.0	18019.5						
5536.8				18056.1	R_2	$04^0 0^2 \Pi$	$12^0 0^2 \Pi$
5529.6	18079.5						
5525.4				18093.4	R_1	$12^0 0^2 \Pi$	$12^2 0^2 \Pi$
5522.9				18101.5	R_1	$04^0 0^2 \Pi$	$04^2 0^2 \Pi$
5517.8				18118.1	R_1	$02^0 0^2 \Pi$	$02^2 0^2 \Pi$
5516.5				18122.3	R_2	$02^0 0^2 \Pi$	$10^0 0^2 \Pi$
5514.0	18130.6						
5508.4	18149.1			18146.9	R_2	$04^2 0^2 \Pi$	$04^0 0^2 \Pi$
5505.2	18158.6	18158.9		18159.1	R_1	$12^0 0^2 \Pi$	$20^0 0^2 \Pi$
5503.6	18164.9	18166.4	18166.4				
5500.2		18176.1			R_2	$12^0 0^2 \Pi$	$20^0 0^2 \Pi$
5499.0				18180.2	R_2	$02^2 0^2 \Pi$	$02^0 0^2 \Pi$
5497.5	18185.1			18183.5	R_1	$02^0 0^2 \Pi$	$10^0 0^2 \Pi$
5491.1	18206.2	18209.2			R_2	$03^1 0^2 \Sigma$	$03^1 0^2 \Sigma$
5489.1	18212.9	18211.9			R_1	$03^1 0^2 \Sigma$	$03^1 0^2 \Sigma$
5486.7		18220.8			R_2	$10^0 0^2 \Pi$	$10^0 0^2 \Pi$
5485.9	18223.5	18226.1					
5484.3		18232.1		18229.0	R_2	$04^2 0^2 \Pi$	$12^2 0^2 \Pi$
5483.8				18230.6	R_1	$04^0 0^2 \Pi$	$12^0 0^2 \Pi$
5482.1				18236.0	R_1	$04^2 0^2 \Pi$	$04^2 0^2 \Pi$

Band Heads of the A-X System of BO_2 (Cont'd.)

λ_{air}, Å	Present Work $\tilde{\nu}_{vac}$ cm^{-1}	Snowden	Johns	Fried-Mathews	Branch ($*B^{10}$)	Upper Level	Lower Level
5479.5	18244.8			18242.6	R_2	$04^00^22\Pi$	$04^00^22\Pi$
5478.1				18249.6	R_1	$12^00^2\,\Pi$	$04^20^2\,\Pi$
5477.7		18250.8		18251.8	R_1	$20^00^2\,\Pi$	$20^00^2\,\Pi$
5476.7	18254.1	18255.4	18255.0				
5474.7	18260.8	18259.8		18259.9	R_2	$02^00^2\,\Pi$	$02^00^2\,\Pi$
5474.4				18261.8	R_1	$02^20^2\,\Pi$	$02^20^2\,\Pi$
5472.7	18267.5	18265.8	18268.0				
5471.5	18271.5	18273.5	18273.5	18273.5	R_2	$00^00^2\,\Pi$	$00^00^2\,\Pi$
5469.1	18279.5	18282.5	18282.0				
5467.5	18284.8	18284.8			R_1	$10^00^2\,\Pi$	$10^00^2\,\Pi$
5464.7	18294.2	18294.9	18294.9		R_2*	$00^00^2\,\Pi$	$00^00^2\,\Pi$
5460.3	18308.9	18309.5	18309.5		R_2	$01^10^2\,\Delta$	$01^10^2\,\Delta$
5457.0	18320.0	18320.6	18320.6	18320.6	R_1	$00^00^2\,\Pi$	$00^00^2\,\Pi$
5453.8	18330.8	18332.0	18332.0		R_2	$03^10^2\,\Delta$	$03^10^2\,\Delta$
5450.6	18341.5	18342.0	18342.2		R_1*	$00^00^2\,\Pi$	$00^00^2\,\Pi$
5450.4				18342.3	R_1	$20^00^2\,\Pi$	$04^20^2\,\Pi$
5447.4	18352.3	18353.4	18353.4		R_1	$01^10^2\,\Delta$	$01^10^2\,\Delta$
5445.9		18357.3					
5443.4	18365.8			18365.3	R_1	$04^20^2\,\Pi$	$12^00^2\,\Pi$
5441.0	18373.9	18375.8	18375.8		R_1*	$01^10^2\,\Delta$	$01^10^2\,\Delta$
5439.8				18378.1	R_1	$12^20^2\,\Pi$	$12^00^2\,\Pi$
5437.5		18385.7	18385.6		R_2	$01^10^2\,\Pi$	$01^10^2\,\Pi$
5436.6	18388.8	18390.8	18390.8		R_1	$01^10^2\,\Pi$	$01^10^2\,\Pi$

Band Heads of the A-X System of BO_2 (Cont'd.)

λ_{air}, Å	Present Work ν_{vac} cm^{-1}	Snowden	Johns	Fried-Mathews	Branch ($*B^{10}$)	Upper Level	Lower Level
5429.8	18411.8	18410.1	18410.2		R_2*	$01^10^22\Sigma$	$01^10^22\Sigma$
5428.2	18417.2	18415.5	18415.4		R_1*	$01^10^22\Sigma$	$01^10^2?$
5425.0	18428.1	18430.1	18430.2	18430.0	R_1	$02^00^22\Pi$	$02^20^22\Pi$
5421.0	18441.7	18442.7	18442.6	18442.6	R_2	$02^20^22\Pi$	$02^20^22\Pi$
5418.5	18450.2						
5417.8		18452.5					
5416.1	18458.4						
5412.9	18469.3	18469.3	18469.4		R_2*	$02^20^22\Pi$	$02^20^22\Pi$
5412.6				18470.2	R_1	$20^00^22\Pi$	$12^00^22\Pi$
5411.3	18474.7						
5408.9	18482.9	18483.6					
5407.2		18488.7	18488.6		$^QR_{12}$	$01^10^22\Sigma$	$01^10^2?$
5406.5	18491.1	18491.8	18491.7		R_2	$03^30^22\Delta$	$03^30^2?$
5404.1	18499.3	18500.4	18500.4		$^SR_{21}$	$01^10^22\Sigma$	$01^10^2?$
5400.1	18513.0	18513.4	18513.4		R_1	$03^10^22\Delta$	$03^10^2?$
5398.5	18518.5						
5397.3				18522.8	R_2	$02^00^2?$	$02^20^2?$
5394.5	18532.3	18530.9					
5391.0				18544.4	R_1	$04^00^22\Pi$	$04^00^2?$
5390.0				18547.8	R_2	$04^20^2?$	$04^20^2?$
5384.2		18567.7	18567.8				
5382.6				18573.1	R_1	$02^20^2?$	$02^00^2?$
5372.0	18609.9						

Band Heads of the A-X System of BO_2 (Cont'd.)

λ_{air}, Å	Present Work $\tilde{\nu}_{vac}$ cm^{-1}	Snowden	Johns	Fried-Mathews	Branch (*B^{10})	Upper Level	Lower Level
5365.4		18632.8					
5362.1				18644.4	R_2	$04^0 0^2 \Pi$	$04^2 0^2 \Pi$
5353.2	18675.2			18678.8	R_1	$04^2 0^2 \Pi$	$04^0 0^2 \Pi$
5348.5				18691.8	R_1	$12^0 0^2 \Pi$	$04^0 0^2 \Pi$
5322.2				18784.0	R_1	$20^0 0^2 \Pi$	$04^0 0^2 \Pi$
5259.2	19009.0			19011.8	R_1	$04^0 0^2 \Pi$	$02^2 0^2 \Pi$
5245.9	19057.2						
5244.0				19064.2	R_2	$04^2 0^2 \Pi$	$02^0 0^2 \Pi$
5239.9	19079.0	19075.4		19076.9	R_1	$04^0 0^2 \Pi$	$10^0 0^2 \Pi$
5231.0		19111.5					
5229.0		19118.8	19118.9	19118.9	R_2	$02^2 0^2 \Pi$	$00^0 0^2 \Pi$
5222.2	19143.7	19145.9		19146.3	R_1	$04^2 0^2 \Pi$	$02^2 0^2 \Pi$
5221.5		19157.3		19157.3	R_1	$12^0 0^2 \Pi$	$02^2 0^2 \Pi$
5217.4	19161.3			19161.1	R_2	$04^0 0^2 \Pi$	$02^0 0^2 \Pi$
5213.8	19174.6	19173.1	19173.0				
5207.3	19198.5	19198.8	19198.8	19198.9	R_2	$02^0 0^2 \Pi$	$00^0 0^2 \Pi$
5204.9	19207.3	19205.8				$03^1 0^2 \Sigma$	$01^1 0^2 \Sigma$
5203.6				19212.2	R_1	$04^2 0^2 \Pi$	$10^0 0^2 \Pi$
5201.7	19219.2	19218.9	19219.9				
5200.1	19225.1			19224.4	R_1	$12^0 0^2 \Pi$	$10^0 0^2 \Pi$
5198.3		19231.7	19237.2		R_2*	$02^0 0^2 \Pi$	$00^0 0^2 \Pi$
5196.1	19239.9	19239.8	19239.8	19239.8	R_1	$02^0 0^2 \Pi$	$00^0 0^2 \Pi$
5194.2		19246.9					

Band Heads of the A-X System of BO_2 (Cont'd.)

λ_{air}, Å	Present Work $\tilde{\nu}_{vac}$ cm^{-1}	Snowden	Johns	Fried-Mathews	Branch ($*B^{10}$)	Upper Level	Lower Level
5192.9	19251.7	19251.0		19252.5	R_1	$20^0 0^2 \Pi$	$02^2 0^2 \Pi$
5192.1		19254.7	19254.5				
5188.9	19266.6						
5185.6	19278.8	19279.2	19279.1		R_1	$12^2 0^2 \Pi$	$02^2 0^2 \Pi$
5184.9		19281.3			R_2	$00^0 1^2 \Pi$	$00^0 1^2 \Pi$
5183.5		19286.6	19286.6		R_2	$11^1 0^2 \Sigma$	$11^1 0^2 \Sigma$
5182.4	19290.7	19290.3	19290.2		R_1	$11^1 0^2 \Pi$	$11^1 0^2 \Pi$
5180.8	19296.7	19297.0	19296.9		R_2	$10^0 0^2 \Pi$	$00^0 0^2 \Pi$
5177.3		19309.7					
5176.0	19314.6	19316.4		19316.9	R_1	$20^0 0^2 \Pi$	$10^0 0^2 \Pi$
5173.4				19324.2	R_1	$04^0 0^2 \Pi$	$02^0 0^2 \Pi$
5172.8	19326.5	19328.0		19328.4	R_2	$04^2 0^2 \Pi$	$02^2 1^2 \Pi$
5170.3		19335.8	19335.8		R_2*	$10^0 0^2 \Pi$	$00^0 0^2 \Pi$
5168.8	19341.5	19341.4	19341.3		R_1	$10^0 0^2 \Pi$	$00^0 0^2 \Pi$
5166.3	19350.8	19351.6	19351.6		R_2	$11^1 0^2 \Delta$	$01^1 0^2 \Delta$
5163.9	19359.8						
5162.3	19365.8	19365.8			R_2	$12^0 0^2 \Pi$	$02^0 0^2 \Pi$
5159.9	19374.8	19377.8	19377.8		R_1*	$10^0 0^2 \Pi$	$00^0 0^2 \Pi$
5157.5	19383.9	19383.1	19383.2	19383.2	R_1	$02^2 0^2 \Pi$	$00^0 0^2 \Pi$
5155.9	19389.9	19388.4	19388.4				
5154.9		19393.5			R_1	$11^1 0^2 \Delta$	$01^1 0^2 \Delta$
5151.1	19407.9	19409.8					
5149.4			19414.4				

Band Heads of the A-X System of BO_2 (Cont'd.)

λ_{air},Å	Present Work $\tilde{\nu}_{vac}$ cm^{-1}	Snowden	Johns	Fried-Mathews	Branch (*B^{10})	Upper Level	Lower Level
5147.6			19421.0	19424.7	R_2	$04^0 0^2 2\Pi$	$02^2 0^2 2\Pi$
5145.4	19429.4	19427.5	19427.6		R_2	$11^1 0^2 2\Sigma$	$01^1 0^2 2\Sigma$
5144.6		19432.4	19432.4		R_1	$11^1 0^2 2\Sigma$	$01^1 0^2 2\Sigma$
5142.2	19441.5						
5139.8	19450.6	19449.1					
5137.4	19459.7	19457.0	19456.9	19458.1	R_1	$04^2 0^2 2\Pi$	$02^0 0^2 2\Pi$
5136.7		19462.3	19463.0				
5134.4				19471.1	R_1	$12^0 0^2 2\Pi$	$02^0 0^2 2\Pi$
5134.2	19471.8	19471.4	19471.3		R_2*	$11^1 0^2 2\Sigma$	$01^1 0^2 2\Sigma$
5133.1		19475.9	19475.9		R_1*	$11^1 0^2 2\Sigma$	$01^1 0^2 2\Sigma$
5132.6		19477.9					
5129.4	19490.0	19485.8					
5127.8	19496.1	19496.4	19496.4		R_2	$12^2 0^2 2\Sigma$	$02^2 0^2 2\Sigma$
5124.5	19508.7	19507.5	19506.0				
5118.7		19530.9	19530.9		$^QR_{12}$	$11^1 0^2 2\Sigma$	$01^1 0^2 2\Sigma$
5116.3		19539.9					
5115.6		19543.0	19543.0		*	$12^2 0^2 2\Sigma$	$02^2 0^2 2\Sigma$
5114.9	19545.3	19546.4					
5112.5	19554.5	19556.7	19554.0				
5110.1	19563.7	19563.7	19563.7	19563.7	R_1	$20^0 0^2 2\Pi$	$02^0 0^2 2\Pi$
5102.0	19594.7						
5095.6		19619.3					
5087.8		19649.4					

Band Heads of the A-X System of BO_2 (Cont'd.)

λ_{air}, Å	Present Work $\tilde{\nu}_{vac}$ cm^{-1}	Snowden	Johns	Fried-Mathews	Branch ($*B^{10}$)	Upper Level	Lower Level
5085.0	19660.2	19657.1					
5068.7		19723.4					
5063.5		19743.7					
4997.9	20002.8		20004.5	20004.5	R_2	$04^20^22\Pi$	$00^00^22\Pi$
4993.1	20022.1		20024.5				
4987.0	20046.6						
4976.5	20088.9						
4974.4	20097.3		20100.6	20100.6	R_2	$04^00^22\Pi$	$00^00^22\Pi$
4970.8	20111.9						
4965.5	20133.4		20133.8	20133.8	R_1	$04^00^22\Pi$	$00^00^22\Pi$
4963.1	20143.1		20137.3				
4961.9	20148.0						
4959.4			20158.2		R_2*	$04^00^22\Pi$	$00^00^22\Pi$
4957.4	20166.3						
4955.9			20172.5		R_2	$12^20^22\Pi$	$00^00^22\Pi$
4951.8	20189.1		20192.1		R_1*	$04^00^22\Pi$	$00^00^22\Pi$
4948.9	20200.9						
4945.3	20215.6						
4942.9	20225.4						
4941.3			20232.1		R_2	$20^00^22\Pi$	$00^00^22\Pi$
4939.6	20238.9						
4933.9			20262.2		R_2*	$20^00^22\Pi$	$00^00^22\Pi$
4932.3	20268.9		20268.2	20268.2	R_1	$04^20^22\Pi$	$00^00^22\Pi$

Band Heads of the A-X System of BO_2 (Cont'd.)

λ_{air}, Å	Present Work $\tilde{\nu}_{vac}$ cm^{-1}	Snowden	Johns	Fried-Mathews	Branch ($*B^{10}$)	Upper Level	Lower Level
4929.9	20278.7		20281.0	20281.0	R_1	$12^0 0^2 \Pi$	$00^0 0^2 \Pi$
4925.5	20296.9						
4922.6	20308.8		20313.0		R_1*	$20^0 0^2 \Pi$	$00^0 0^2 \Pi$
4918.2	20327.0		20332.1		R_2	$12^0 0^2 \Pi$	$00^0 0^2 \Pi$
4913.7	20345.6		20344.5				
4909.3	20363.8						
4906.9			20373.8	20373.8	R_1	$20^0 0^2 \Pi$	$00^0 0^2 \Pi$
4903.2	20389.2		20390.5		R_2*	$12^0 0^2 \Pi$	$00^0 0^2 \Pi$
4901.0			20398.1				
4898.7	20407.9		20402.6		R_2	$21^1 0^2 \Delta$	$01^1 0^2 \Delta$
4893.5	20429.6		20435.3		R_1*	$12^0 0^2 \Pi$	$00^0 0^2 \Pi$
4891.8			20436.7		R_1	$12^2 0^2 \Pi$	$00^0 0^2 \Pi$
4891.6			20437.5		R_1	$21^1 0^2 \Delta$	$01^1 0^2 \Delta$
4887.4	20455.1						
4883.0	20473.5		20477.4		R_2	$21^1 0^2 \Pi$	$01^1 0^2 \Pi$
4881.0			20481.7		R_1	$21^1 0^2 \Pi$	$01^1 0^2 \Pi$
4791.8	20863.2						
4786.5	20886.3						
4781.3	20909.0						
4775.6	20933.9						
4766.6	20973.5						
4761.8	20994.6						
4758.5	21009.2						

Band Heads of the A-X System of BO_2 (Cont'd.)

λ_{air}, Å	Present Work $\tilde{\nu}_{vac}$ cm^{-1}	Snowden	Johns	Fried-Mathews	Branch ($*B^{10}$)	Upper Level	Lower Level
4745.1	21068.5						
4736.6	21106.3						
4734.8			21114.4				
4733.3	21121.0						
4728.4	21142.9		21147.8		R_2	$14^0 0^2 \Pi$	$00^0 0^2 \Pi$
4722.4	21169.8						
4719.5			21182.8		R_1	$14^0 0^2 \Pi$	$00^0 0^2 \Pi$
4717.5	21191.8						
4715.4	21201.2						
4714.2	21206.6						
4712.6	21213.8						
4708.9	21230.5						
4706.1	21243.1						
4703.3	21255.7		21251.7				
4698.8	21276.1		21267.4		R_1*	$14^0 0^2 \Pi$	$00^0 0^2 \Pi$
4695.9	21289.2		21294.0		R_2	$22^0 0^2 \Pi$	$00^0 0^2 \Pi$
4694.1			21297.5				
4692.7	21303.8						
4686.6	21331.5		21335.0		R_1	$22^0 0^2 \Pi$	$00^0 0^2 \Pi$
4678.9	21366.6						
4676.0	21379.8						
4671.2	21401.8						
4666.7	21422.4		21421.7				

Band Heads of the A-X System of BO_2 (Cont'd.)

λ_{air}, Å	Present Work $\tilde{\nu}_{vac}$ cm^{-1}	Snowden	Johns	Fried-Mathews	Branch ($*B^{10}$)	Upper Level	Lower Level
4666.3			21424.4				
4661.4	21446.8						
4655.7	21473.1						
4592.7	21767.6						
4589.5	21782.8						
4574.4	21854.7						
4567.1	21889.6						
4563.0	21909.3						
4554.9	21948.3						
4550.8	21968.0						
4548.4	21979.6						
4541.1	22014.9						
4528.5	22076.2						
4523.6	22100.1						
4520.7	22114.3						
4514.2	22146.1						
4509.4	22169.7						
4504.1	22195.8		22186.1		R_2	$16^0 0^2 \Sigma$	$00^0 0^2 \Sigma$
4503.0			22201.2		R_1	$16^0 0^2 \Sigma$	$00^0 0^2 \Sigma$
4502.0	22206.2		22203.6		R_2	$24^0 0^2 \Sigma$	$00^0 0^2 \Sigma$
4497.2	22229.8		22231.8		R_1	$24^0 0^2 \Sigma$	$00^0 0^2 \Sigma$
4485.0	22290.3		22284.2				
4481.7	22306.7						

Band Heads of the A-X System of BO_2 (Cont'd.)

λ_{air}, Å	Present Work $\tilde{\nu}_{vac}$ cm^{-1}	Snowden	Johns	Fried-Mathews	Branch ($*B^{10}$)	Upper Level	Lower Level
4478.5	22322.7		22328.6		R_1*	$24^0 0^2 \Pi$	$00^0 0^2 \Pi$
4474.4	22343.1						
4459.8	22416.3						
4451.6	22457.6						
4442.3	22504.6						
4436.2	22535.5						
4411.8	22660.1						
4349.0			22987.1		R_2	$00^0 2^2 \Pi$	$00^0 0^2 \Pi$
4348.1			22992.3		R_2	$01^1 2^2 \Delta$	$01^1 0^2 \Delta$
4340.5			23032.5		R_1	$00^0 2^2 \Pi$	$00^0 0^2 \Pi$
4340.0			23034.9		R_1	$01^1 2^2 \Delta$	$01^1 0^2 \Delta$
4335.4			23059.5		R_2	$01^1 2^2 \Sigma$	$01^1 0^2 \Sigma$
4335.0			23061.5		R_1	$01^1 2^2 \Sigma$	$01^1 0^2 \Sigma$
4314.2			23172.6		R_2*	$00^0 2^2 \Pi$	$00^0 0^2 \Pi$
4305.9			23217.5		R_1*	$00^0 2^2 \Pi$	$00^0 0^2 \Pi$
4305.1			23221.5		R_2	$26^0 0^2 \Pi$	$00^0 0^2 \Pi$
4302.6			23235.0		R_1	$26^0 0^2 \Pi$	$00^0 0^2 \Pi$
4173.0	23956.9						
4168.9			23980.5		R_2	$02^0 2^2 \Pi$	$00^0 0^2 \Pi$
4165.0	24002.9						
4162.9			24015.0		R_1	$02^0 2^2 \Pi$	$00^0 0^2 \Pi$
4156.0	24054.8						
4143.0	24130.3						

Band Heads of the A-X System of BO_2 (Cont'd.)

λ_{air}, Å	Present Work $\tilde{\nu}_{vac}$ cm^{-1}	Snowden	Johns	Fried-Mathews	Branch ($*B^{10}$)	Upper Level	Lower Level
4135.1			24176.4		R_2*	$02^02^2\Pi$	$00^00^2\Pi$
4132.0	24194.6						
4129.3			24211.4		R_1*	$02^02^2\Pi$	$00^00^2\Pi$
4122.0	24253.3						
4003.0	24974.2		24979.4		R_2	$04^02^2\Pi$	$00^00^2\Pi$
3997.4			25009.1		R_1	$04^02^2\Pi$	$00^00^2\Pi$
3964.8			25214.7		R_1*	$04^02^2\Pi$	$00^00^2\Pi$

Band Heads of the B-X System of BO_2

λ_{air}, Å	Present Work $\tilde{\nu}_{vac}$ cm^{-1}	Snowden	Johns	Fried-Mathews	Branch ($^*B^{10}$)	Upper Level	Lower Level
4090.4	24440.6		24438.8		Q_2	$00^00^2\Sigma$	$00^00^2\Pi$
			24439.4		$^QR_{12}$	$00^00^2\Sigma$	$00^00^2\Pi$
			24442.6		Q_2^*	$00^00^2\Sigma$	$00^00^2\Pi$
			24443.5		$^QR_{12}^*$	$00^00^2\Sigma$	$00^00^2\Pi$
4081.4	24494.5		24493.7		Q_2	$01^10^2\Pi$	$01^10^2\Delta$
			24494.0		$^QR_{12}$	$01^10^2\Pi$	$01^10^2\Delta$
4080.1			24502.4				
4070.0	24563.1						
4065.0	24593.3		24590.1		R_1	$00^00^2\Sigma$	$00^00^2\Pi$
			24590.9		$^RQ_{21}$	$00^00^2\Sigma$	$00^00^2\Pi$
			24592.9		R_1^*	$00^00^2\Sigma$	$00^00^2\Pi$
			24593.6		$^RQ_{21}^*$	$00^00^2\Sigma$	$00^00^2\Pi$
4057.0	24641.8		24640.8		$R+^RQ_{21}$	$01^10^2\Pi$	$01^10^2\Delta$
4051.9			24673.1		Q_1	$01^10^2\Pi$	$01^10^2\Sigma$

Appendix E: Laser-Induced Fluorescence Survey Spectra

The following figures illustrate the background-corrected laser-induced fluorescence produced in the BCl_3-seeded flame under the following conditions:

Mix: CH_4/Air/O_2/BCl_3 .21/.65/.12/.017

Pump: 5470.8 A, 7.4 mJ per pulse

Spectrometer Slits: 200 microns

Scans: 500

The laser beam was positioned 3 cm above the burner, i.e., approximately 1 cm above the inner cone, and centered in the flame along the detection axis. The detection volume was 4 mm off-center toward the laser along the laser beam axis.

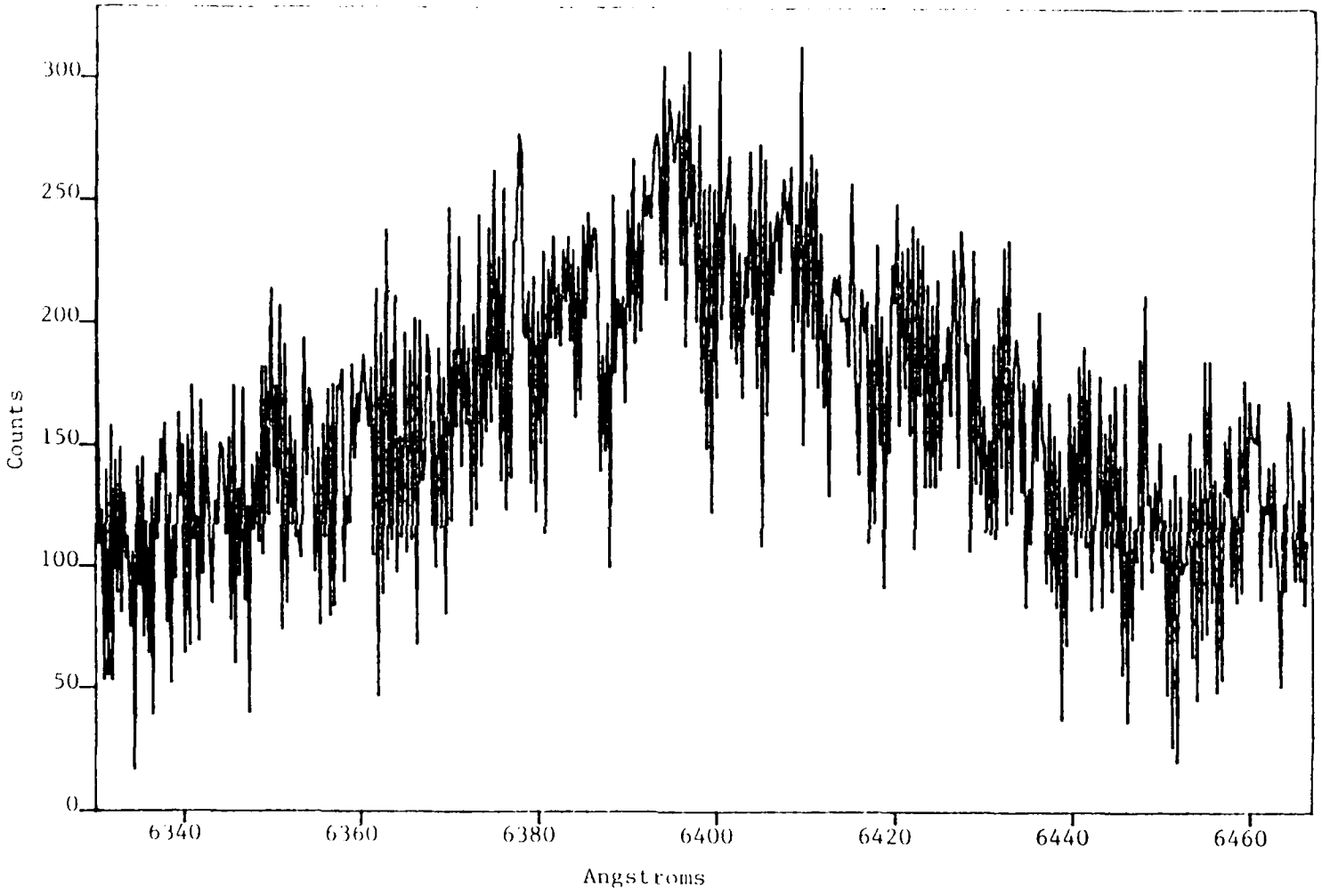


Figure 29. Induced Fluorescence, 6330-6470 Å

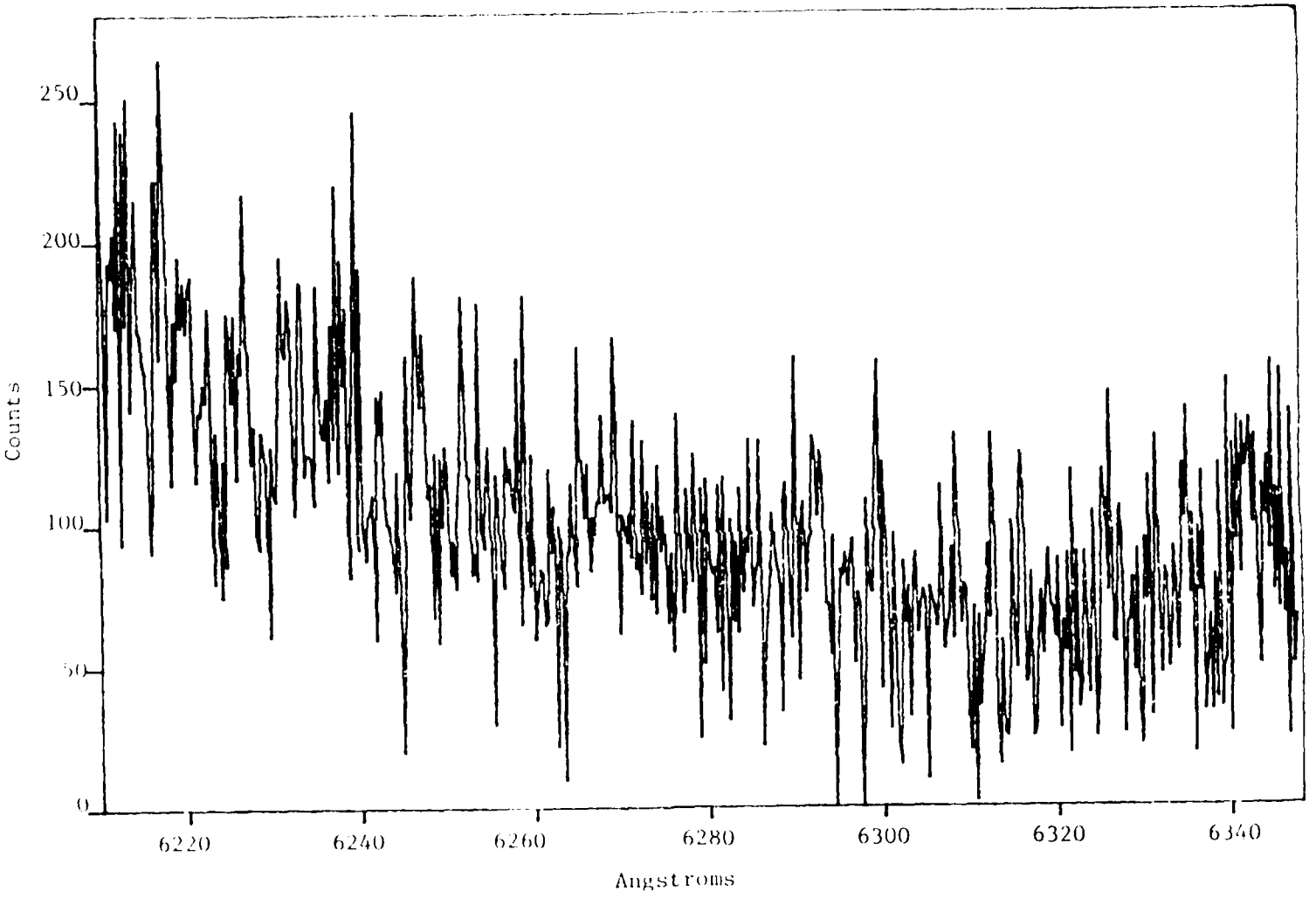


Figure 30. Induced Fluorescence, 6210-6350 Å

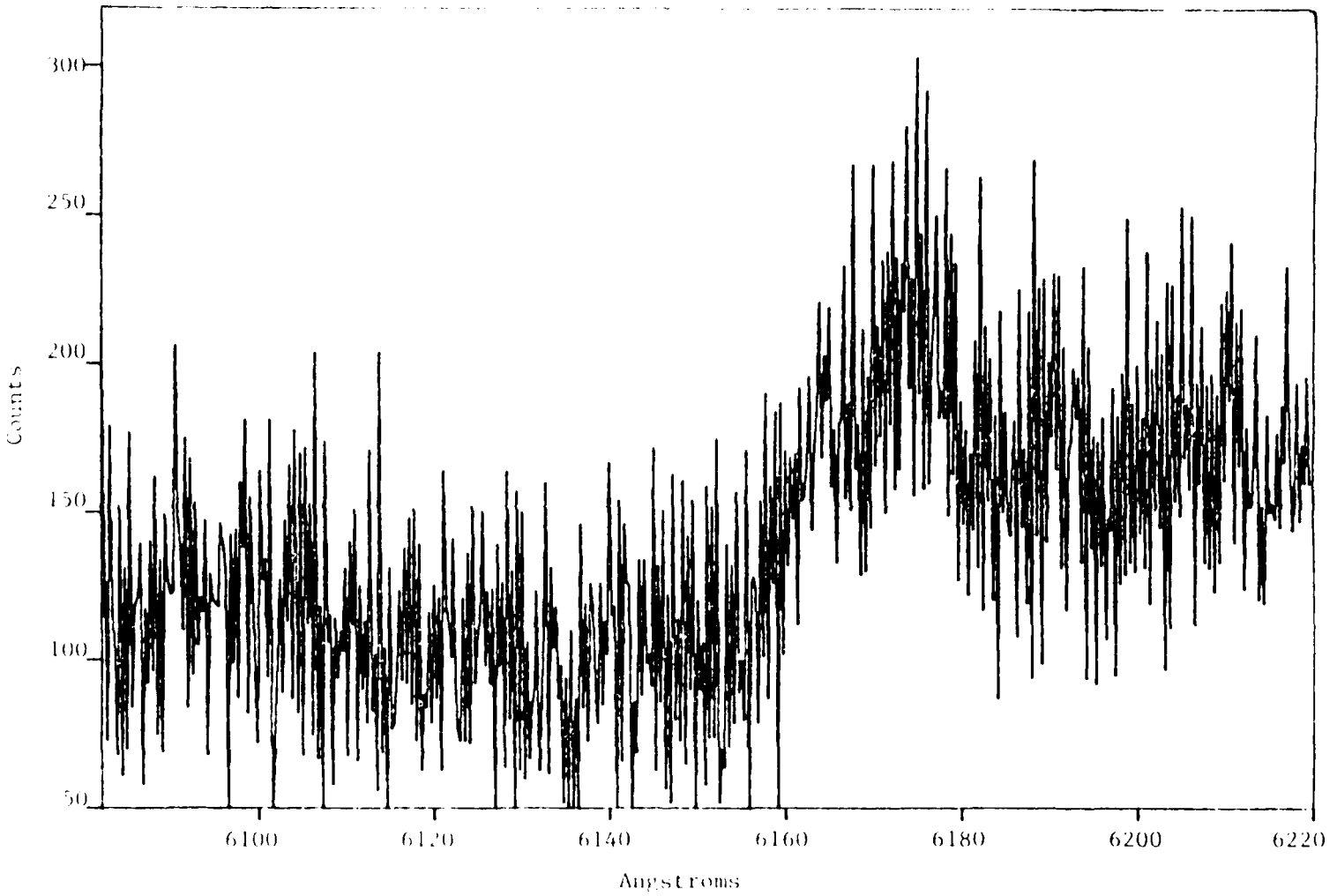


Figure 31. Induced Fluorescence, 6080-6220 Å

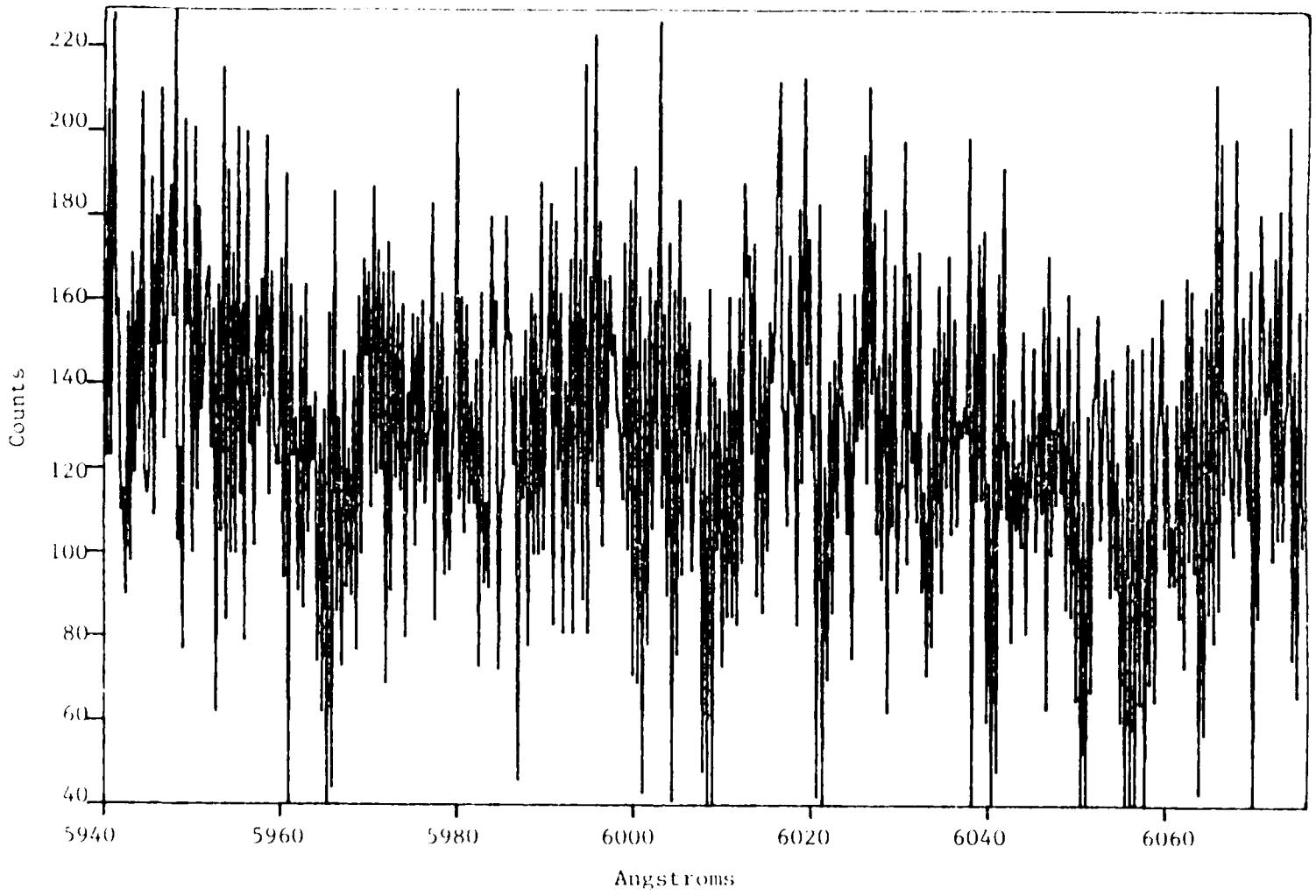


Figure 32. Induced Fluorescence, 5940-6080 Å

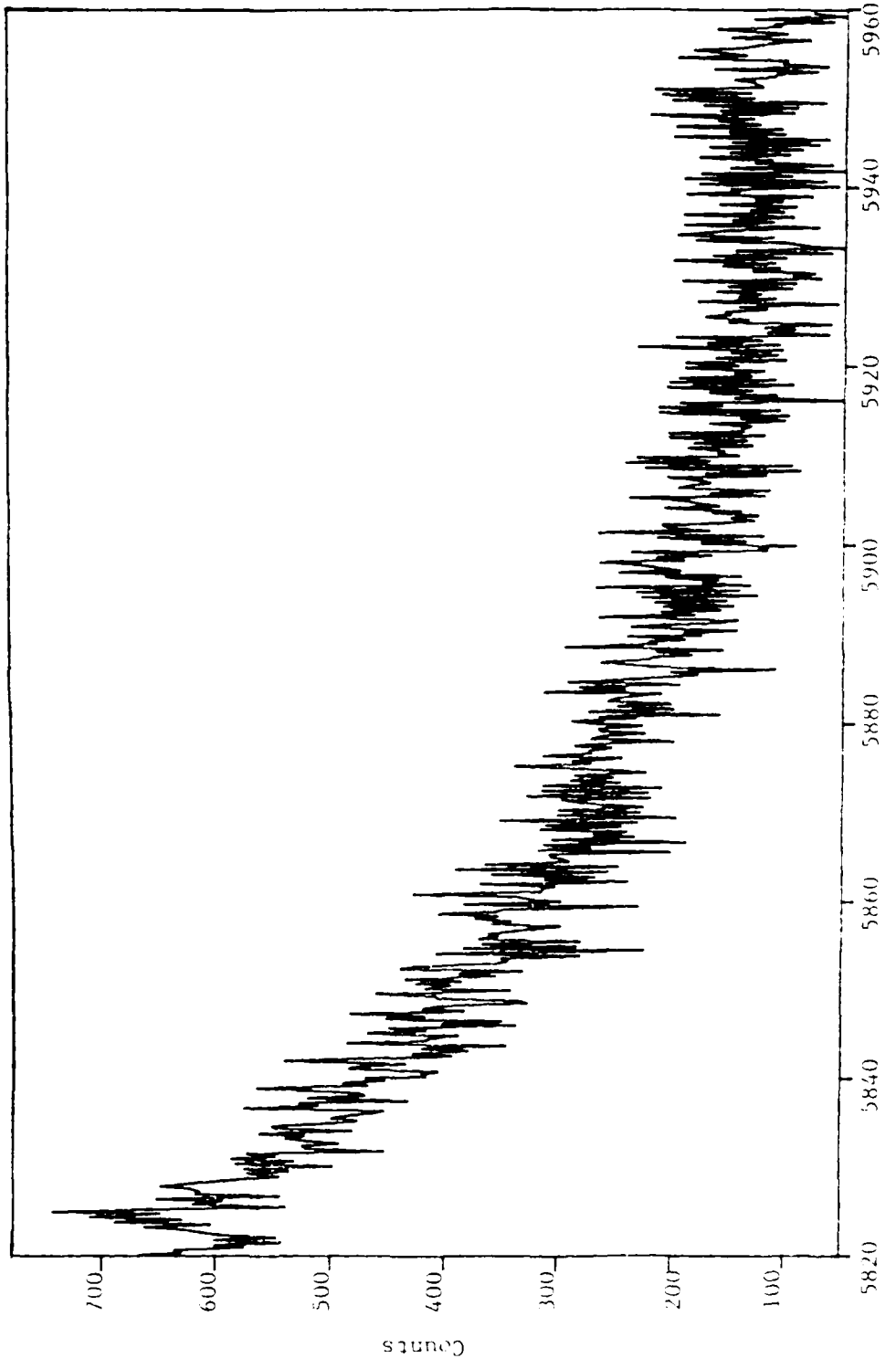


Figure 33. Induced Fluorescence, 5820-5960 Å

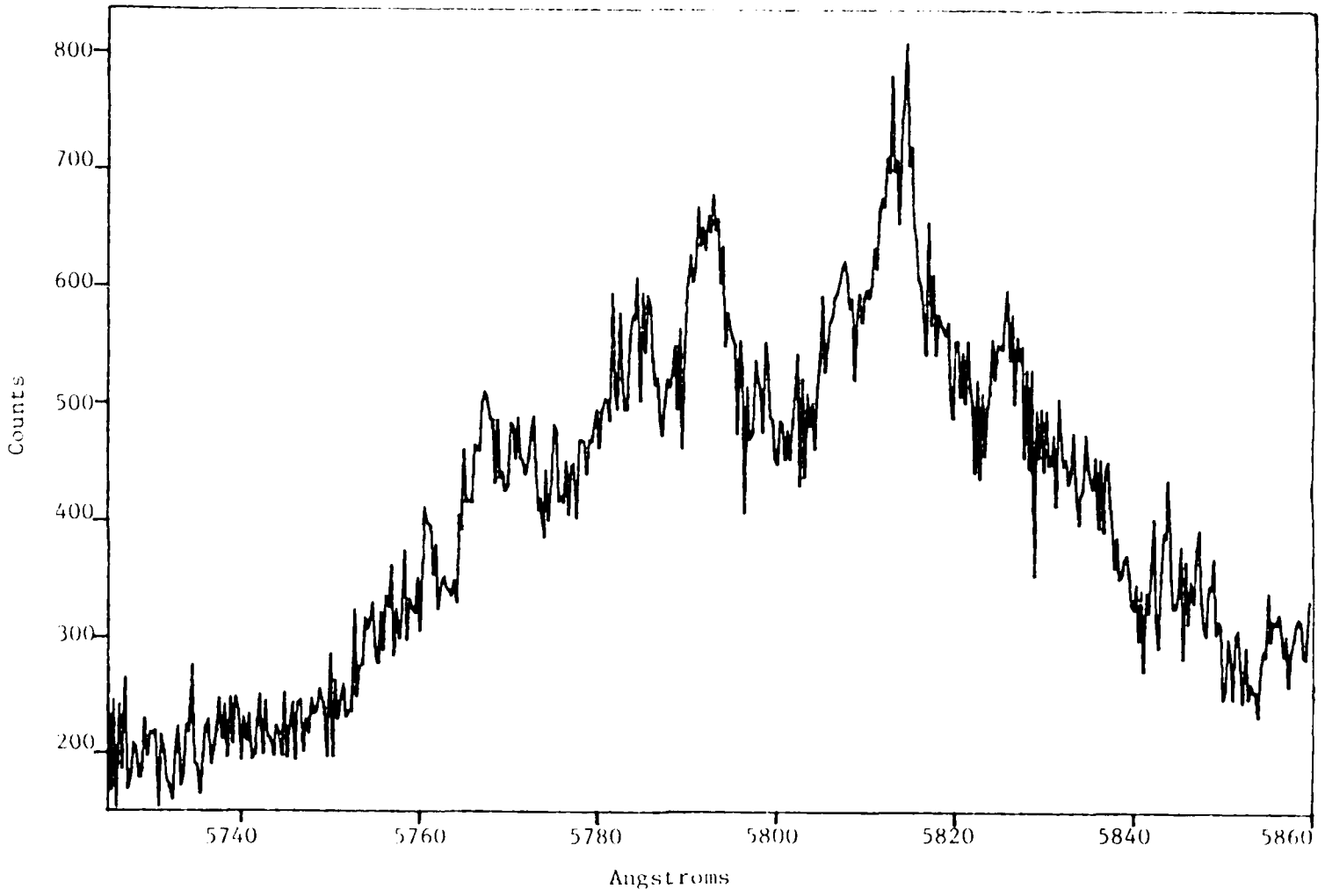


Figure 34. Induced Fluorescence, 5720-5860 Å

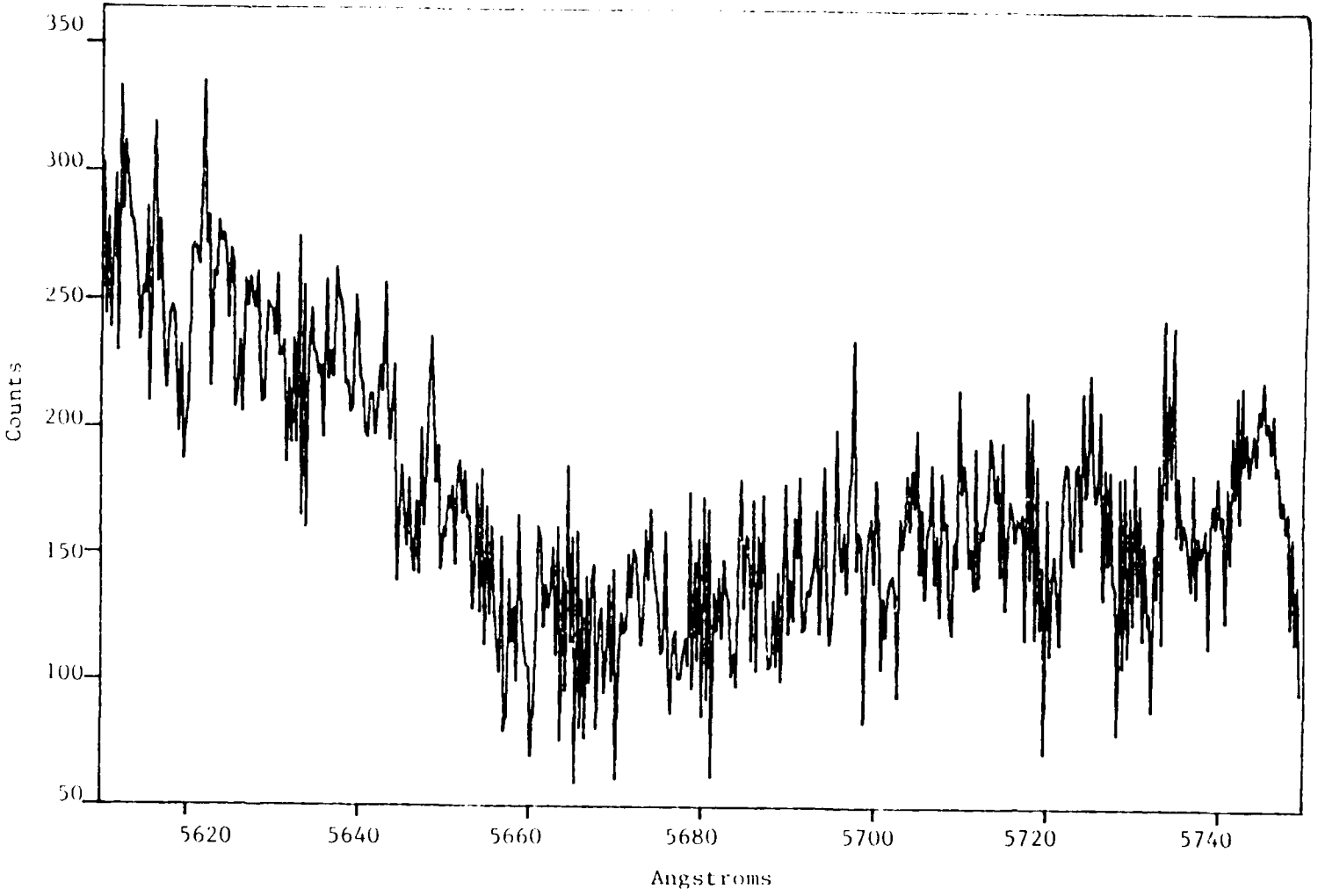


Figure 35. Induced Fluorescence, 5610-5750 Å

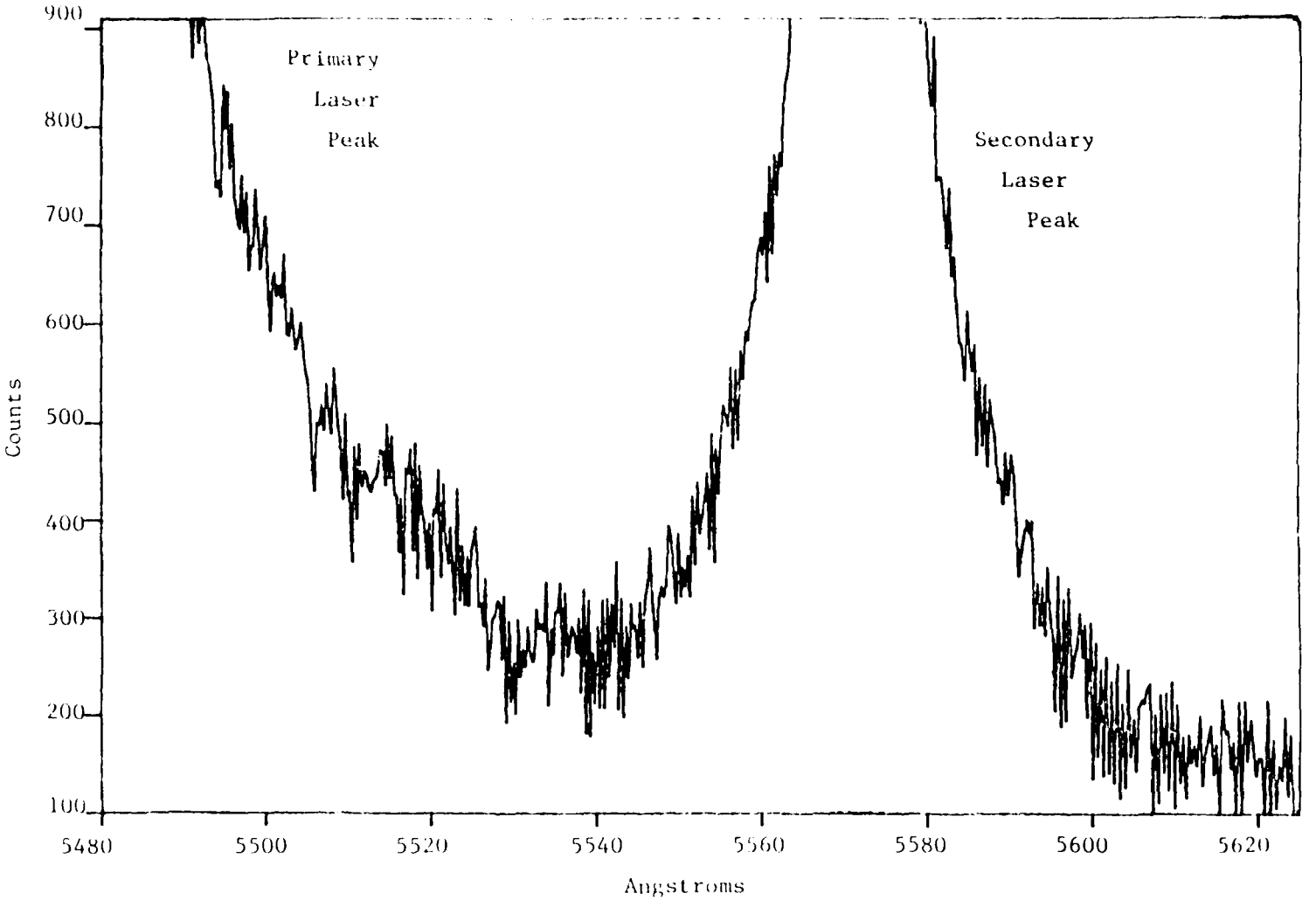


Figure 36. Induced Fluorescence, 5480-5620 Å

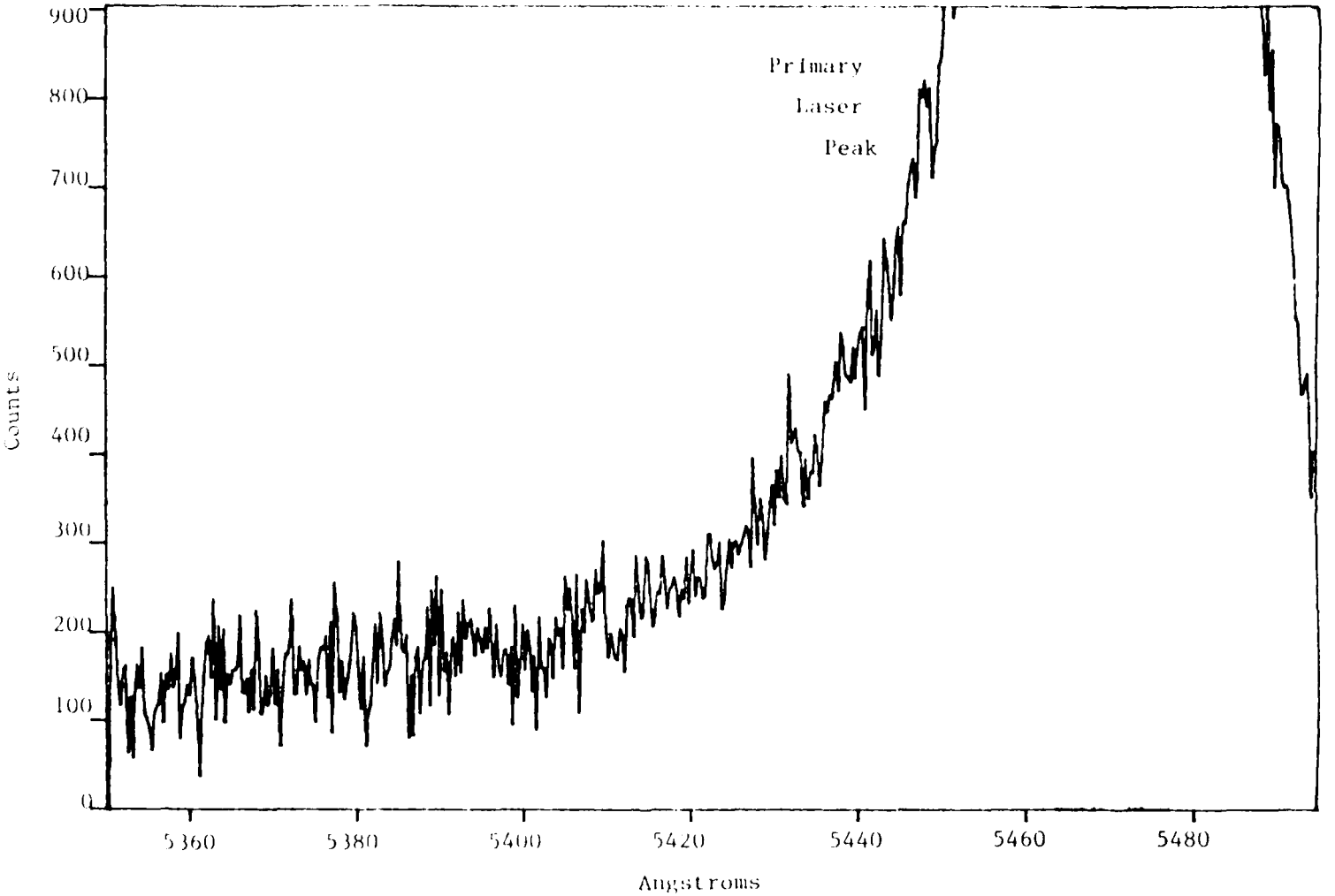


Figure 37. Induced Fluorescence, 5350-5490 Å

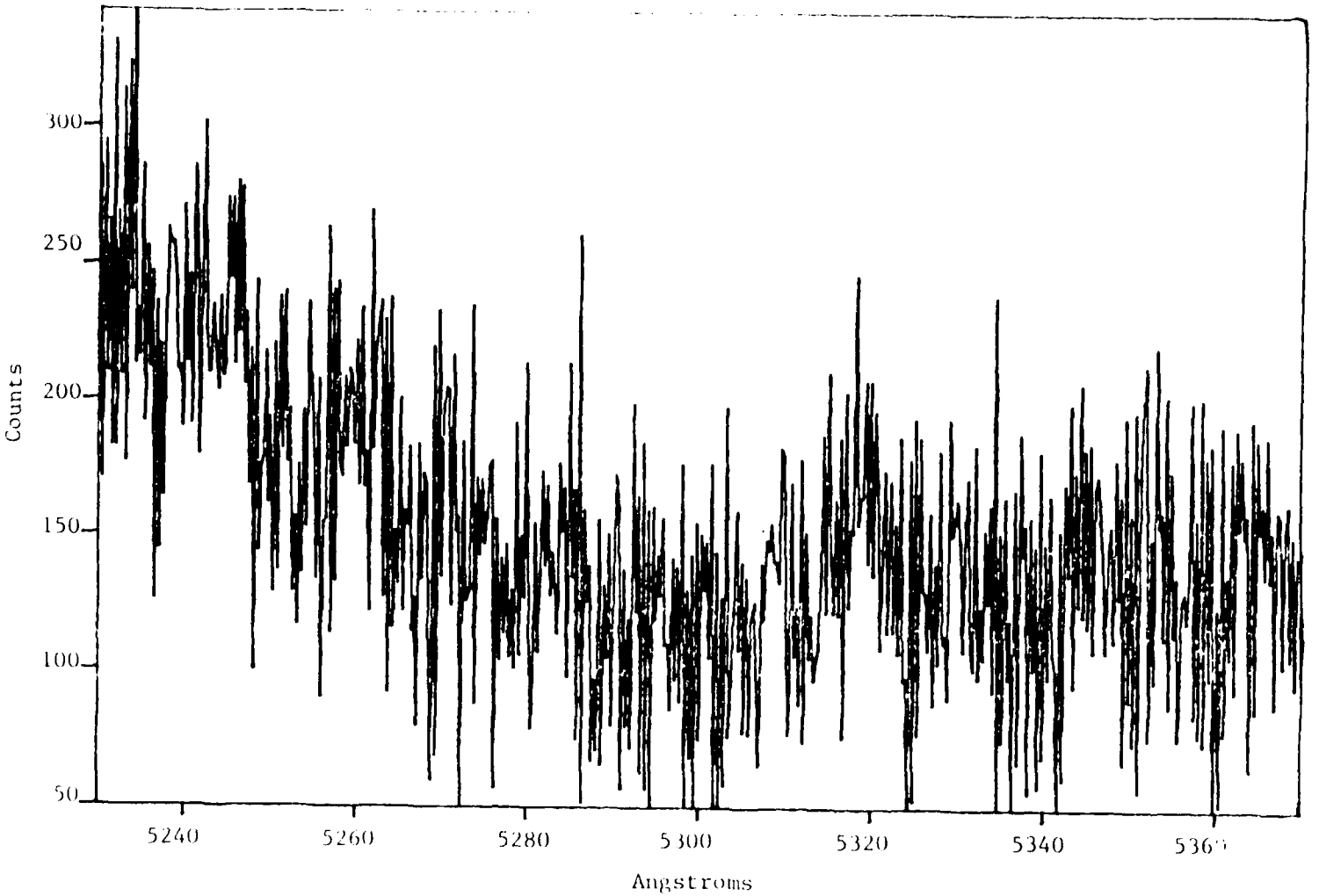


Figure 38. Induced Fluorescence, 5230-5370 Å

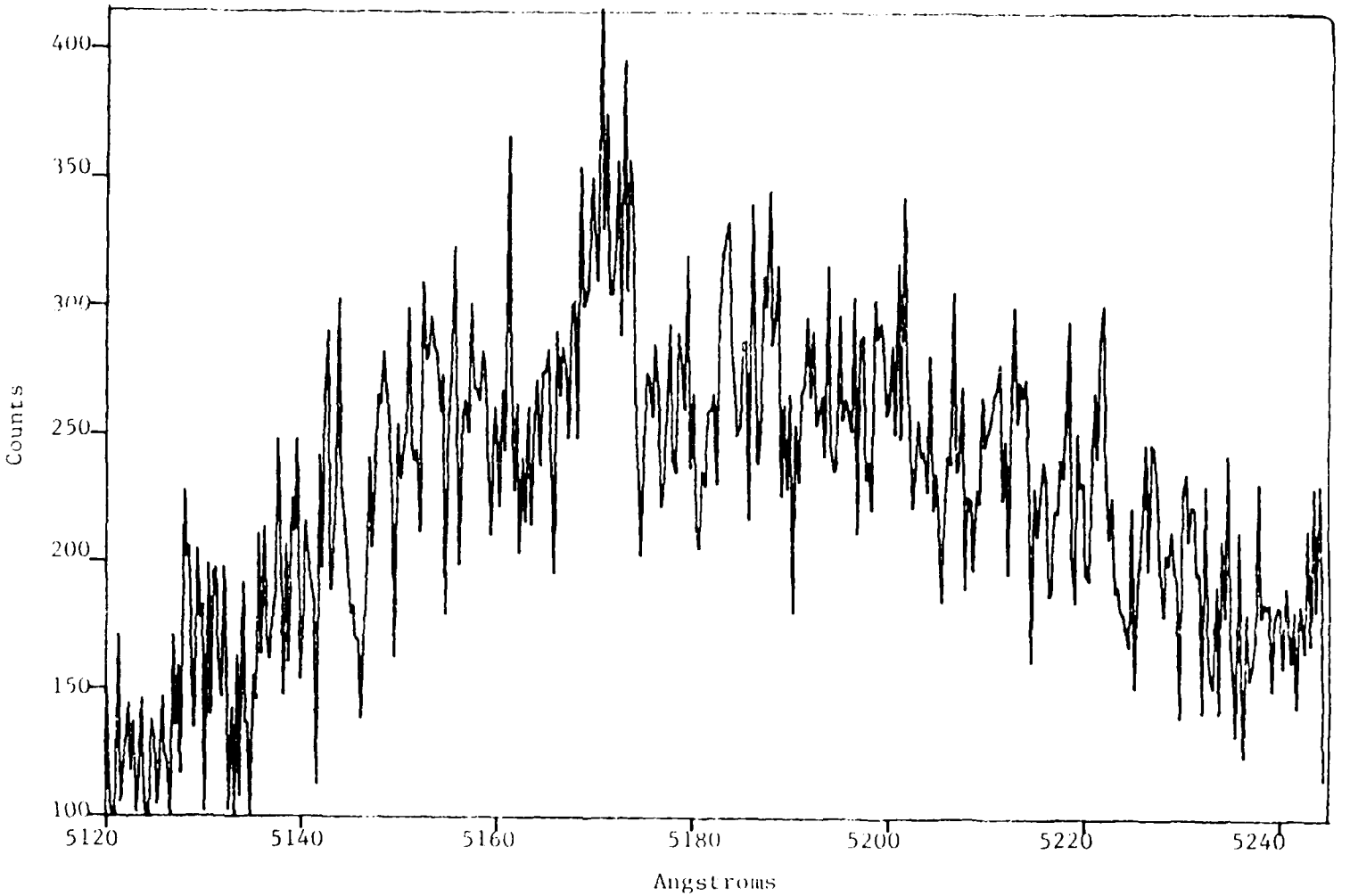


Figure 39. Induced Fluorescence, 5120-5240 Å

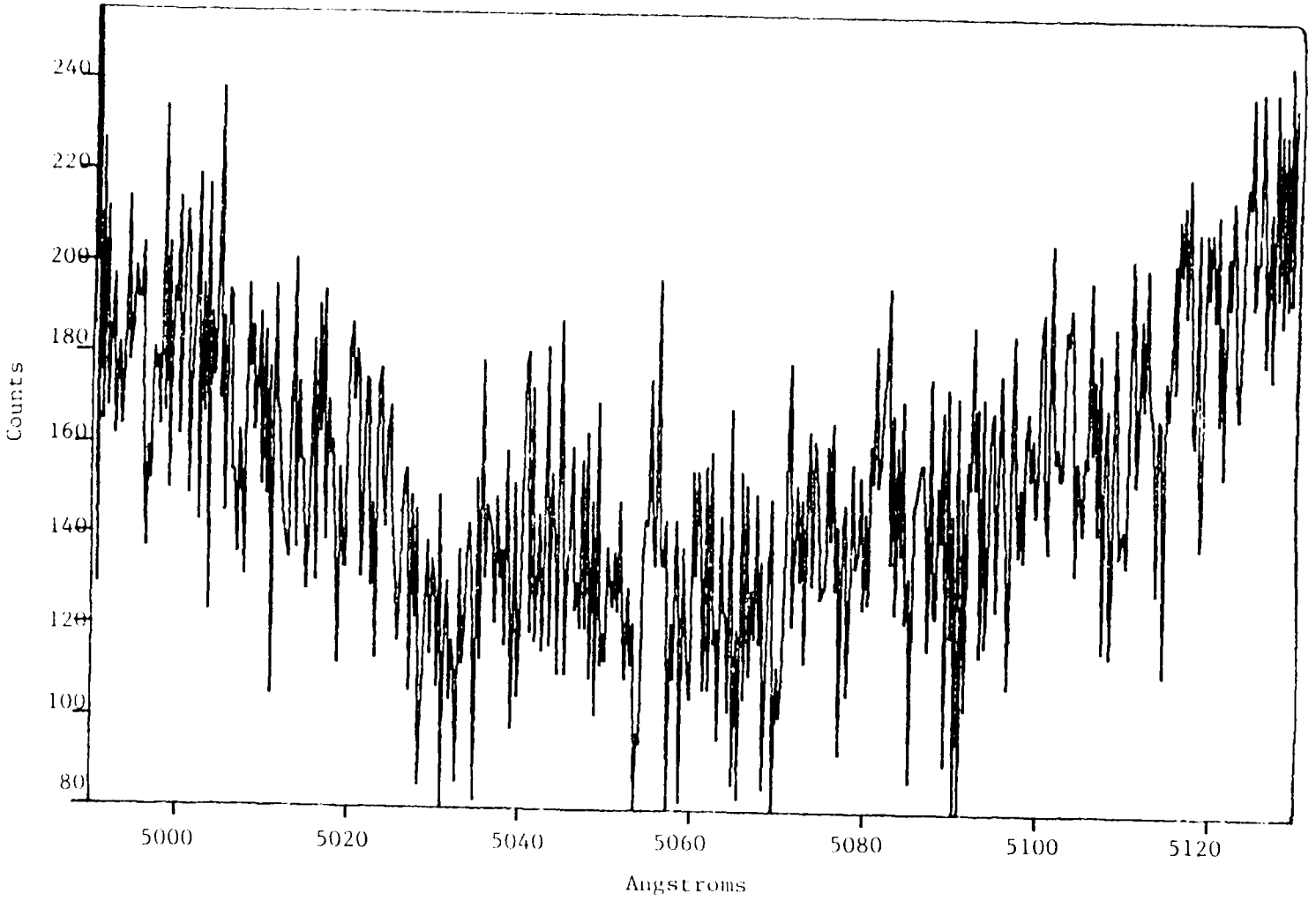


Figure 40. Induced Fluorescence, 4990-5130 Å

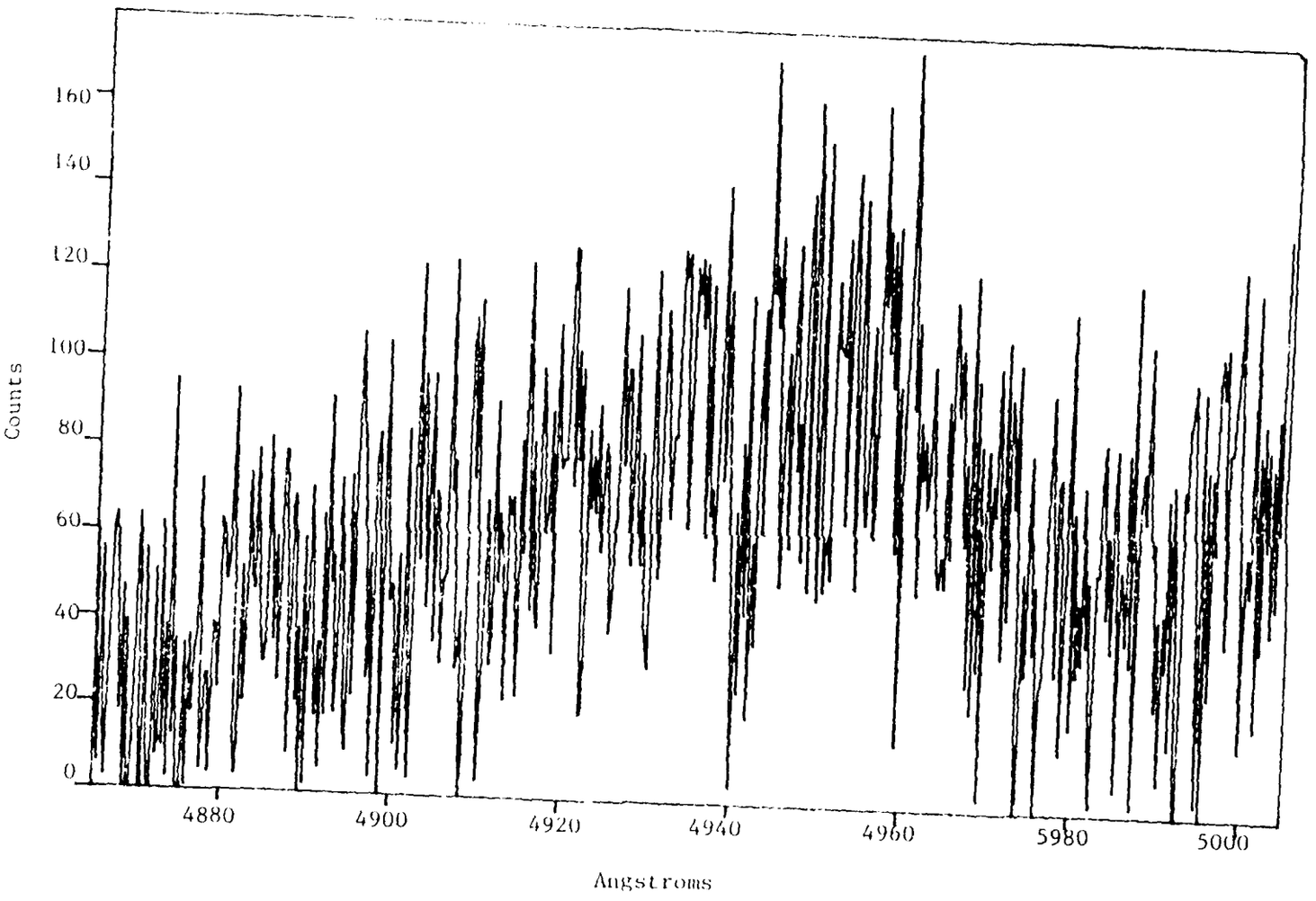


Figure 41. Induced Fluorescence, 4860-5000 Å

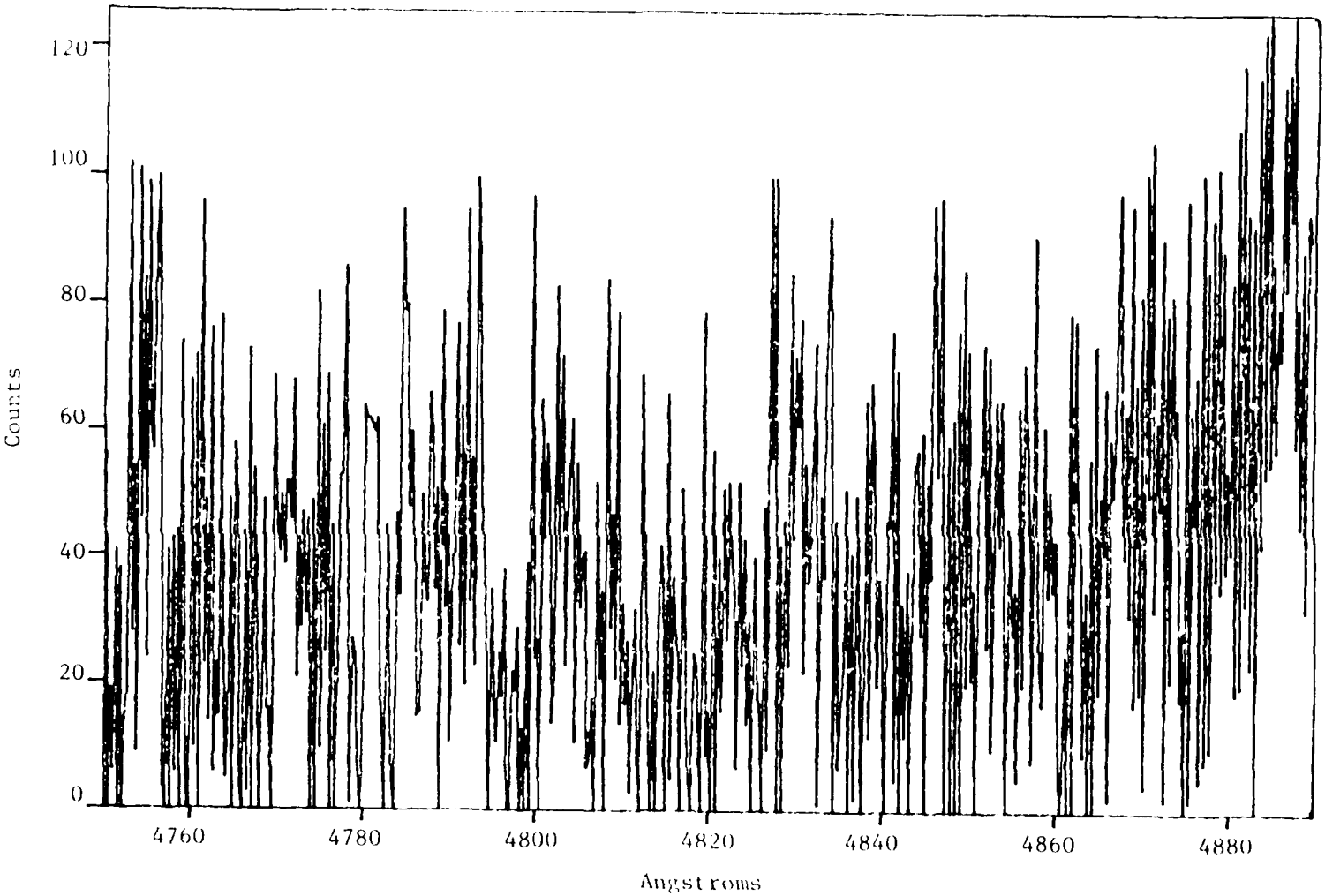


Figure 42. Induced Fluorescence, 4750-4890 Å

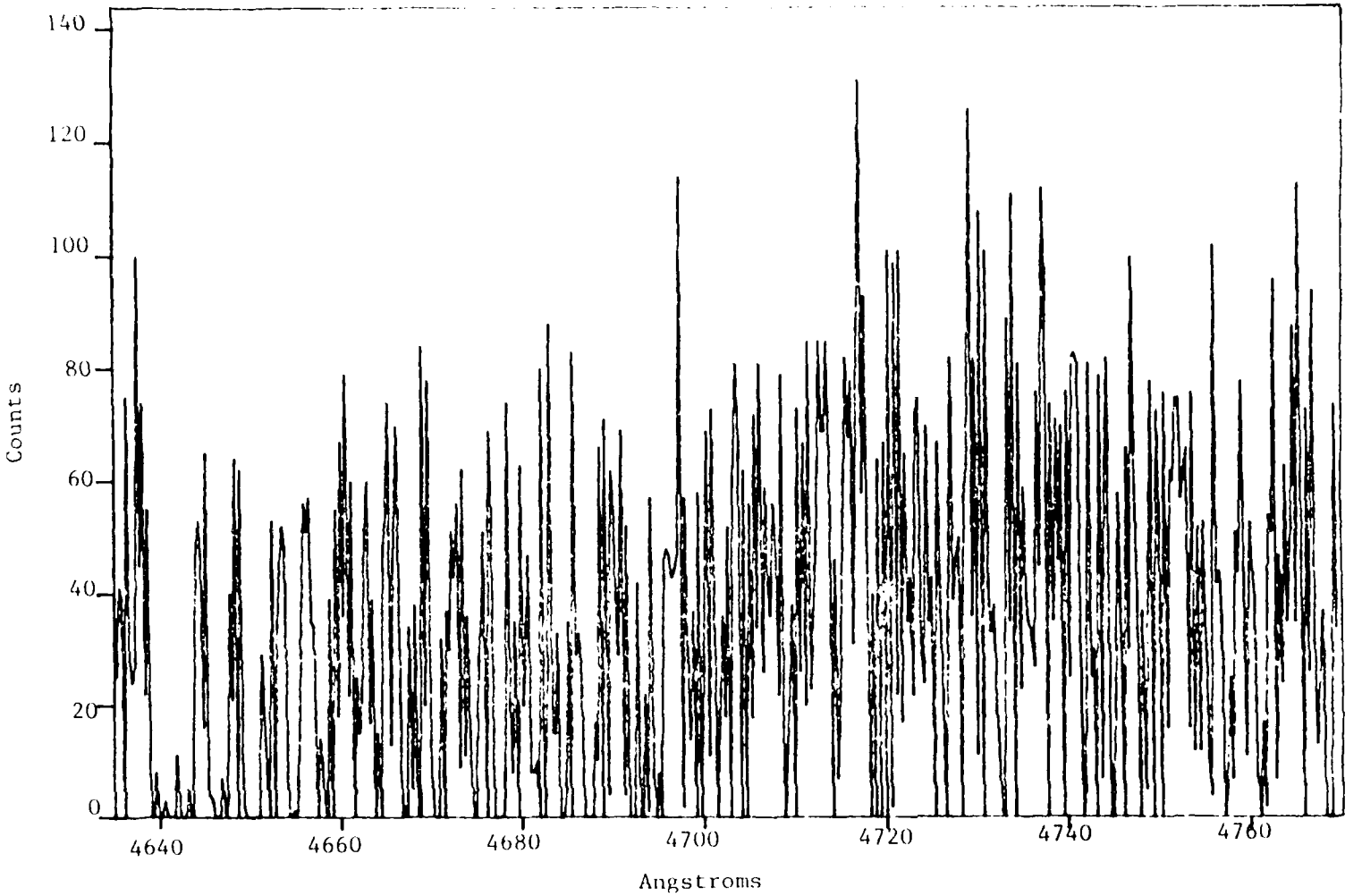


Figure 43. Induced Fluorescence, 4635-4765 Å

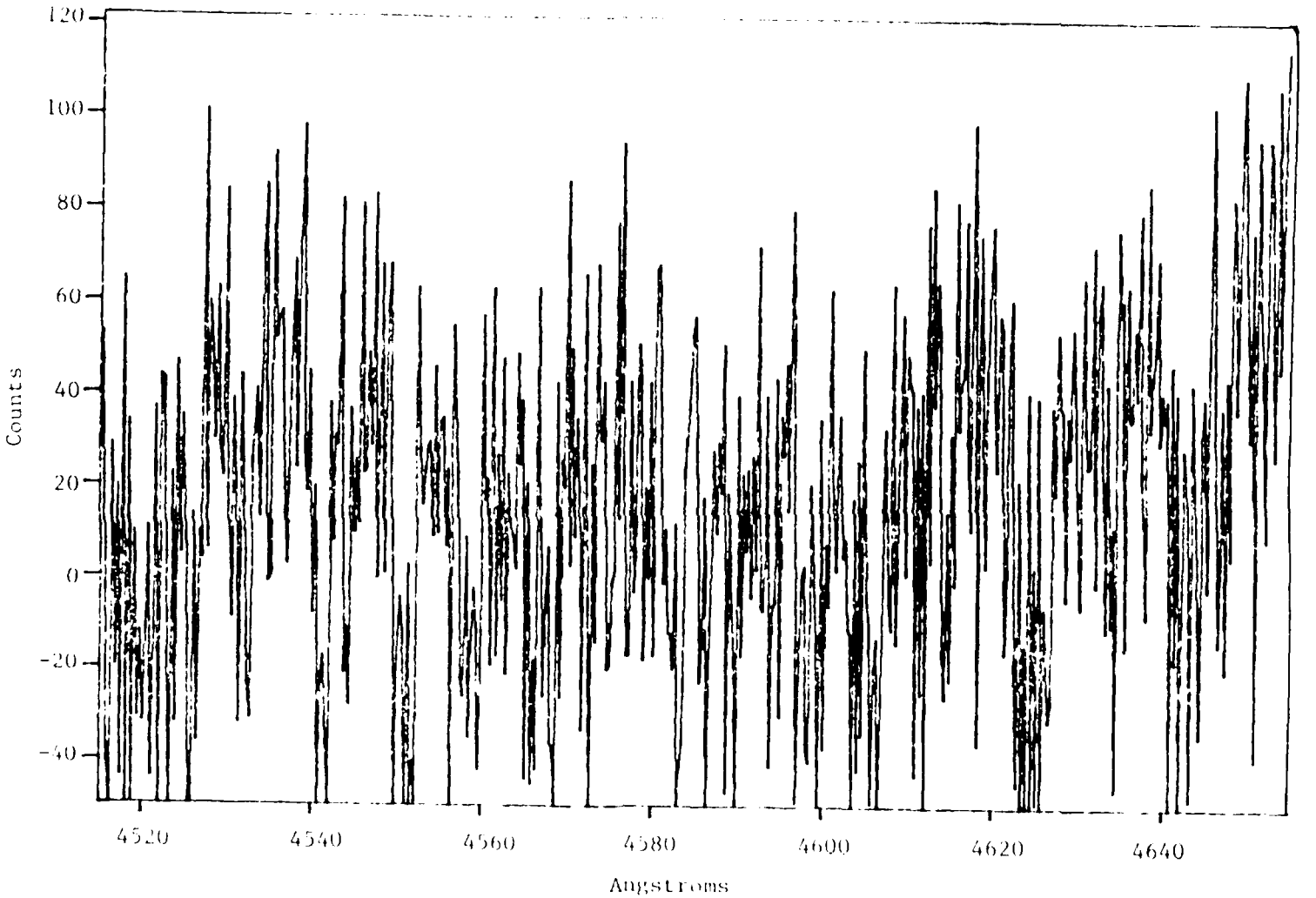


Figure 44. Induced Fluorescence, 4515-4655 Å

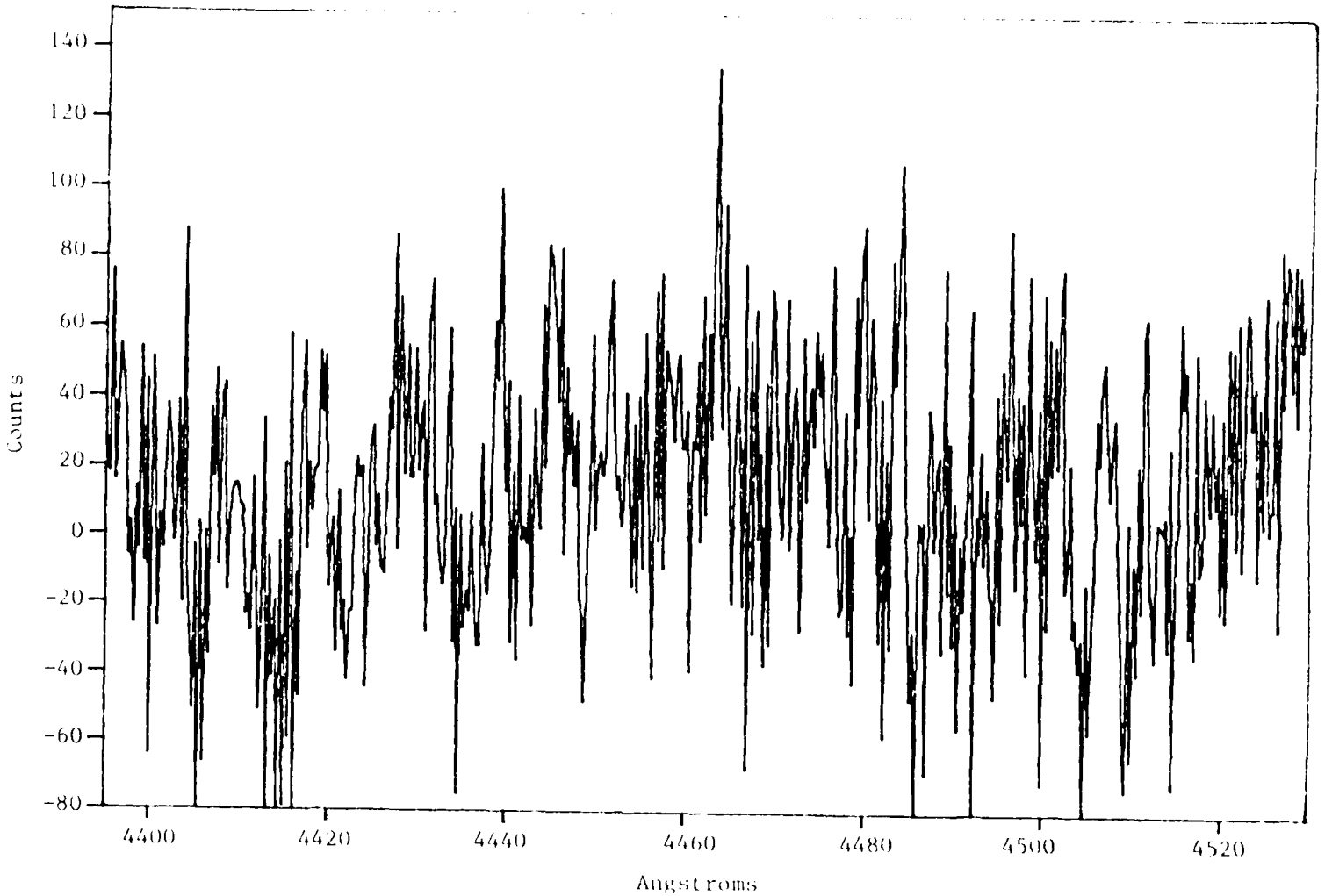


Figure 45. Induced Fluorescence, 4395-4525 Å

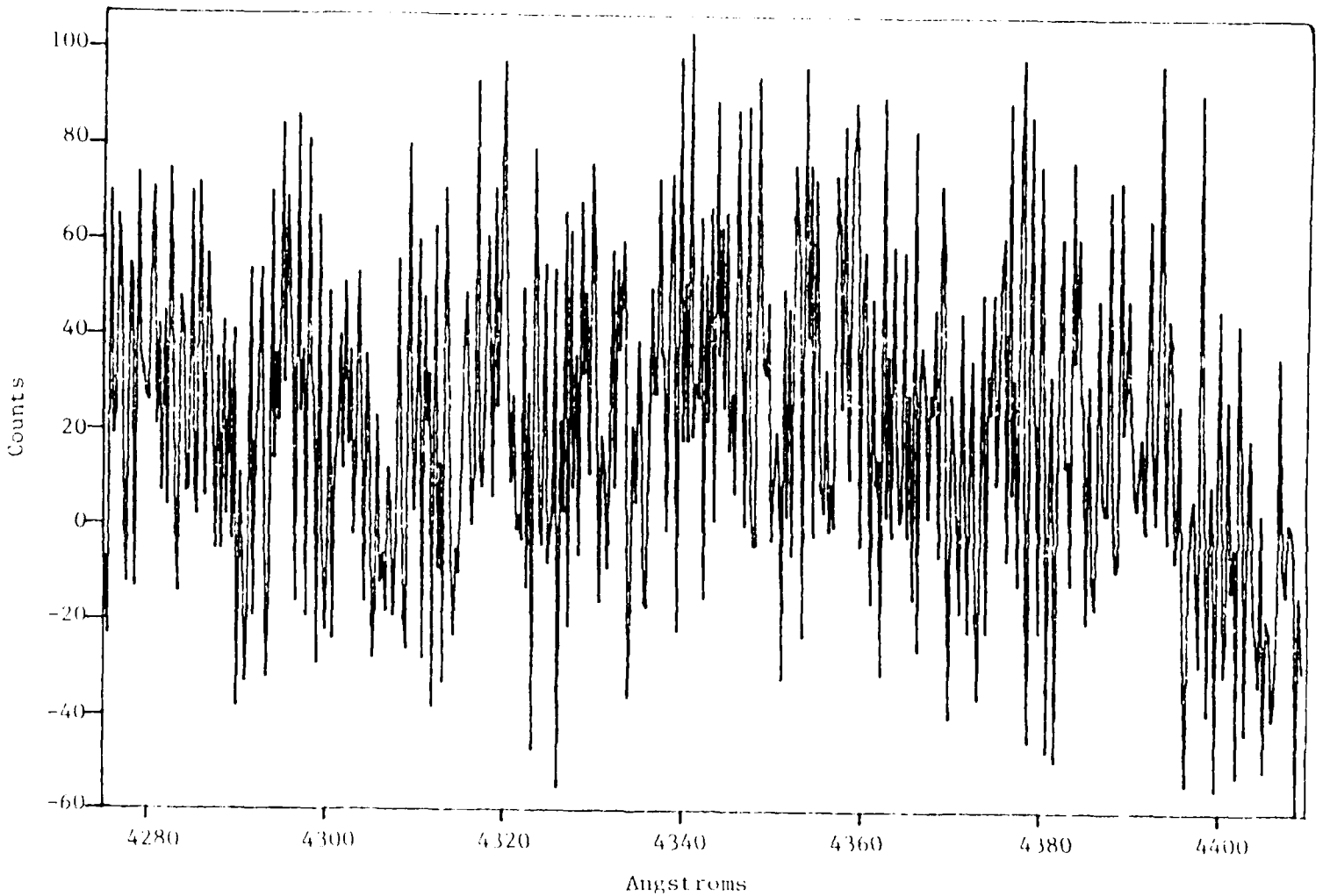


Figure 46. Induced Fluorescence, 4275-4405 Å

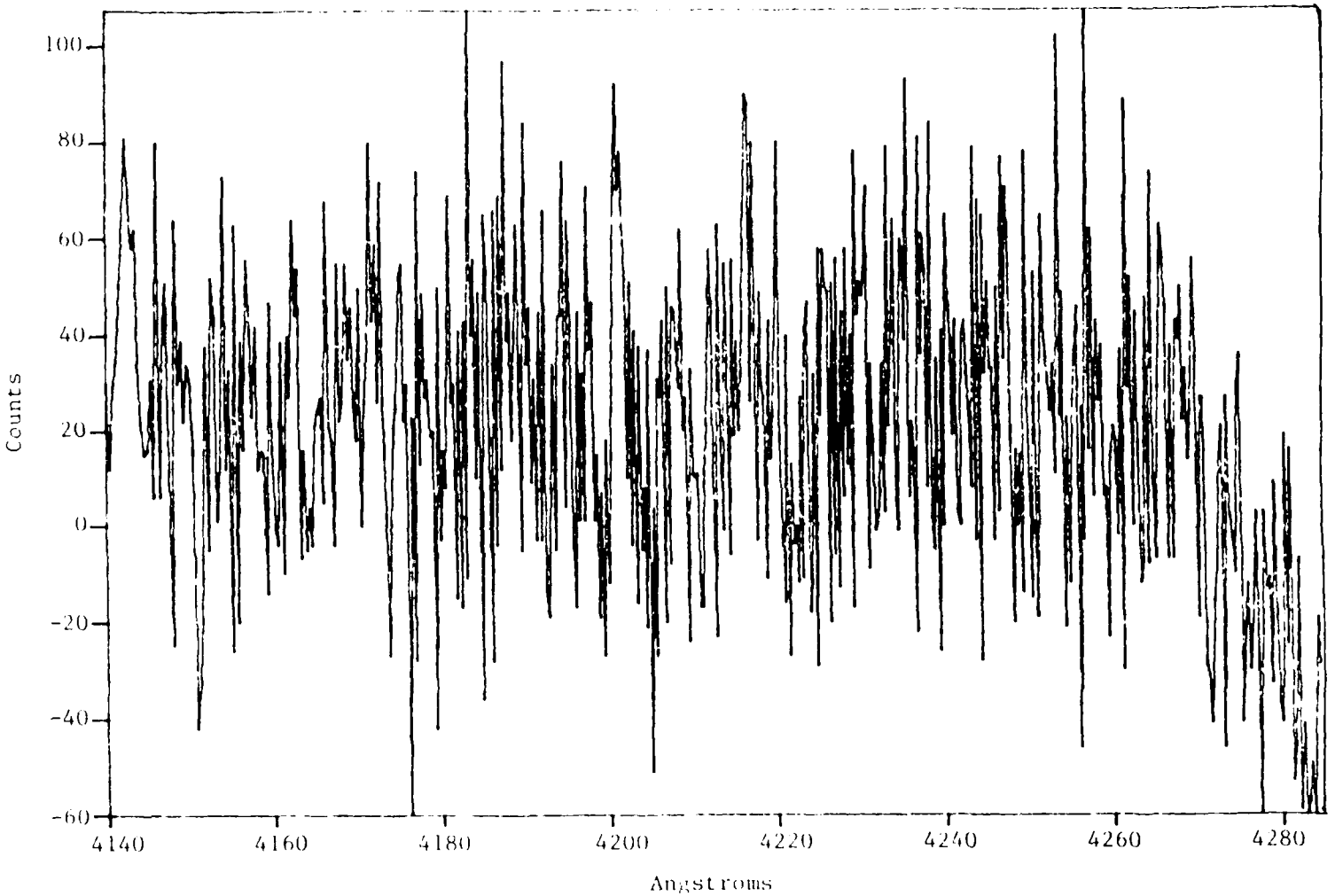


Figure 47. Induced Fluorescence, 4140-4280 Å

BIBLIOGRAPHY

1. King, Merrill K. "Ignition and Combustion of Boron Particles and Clouds," Journal of Spacecraft, 19: 294-306 (July-August 1982).

2. Stull, D.R. and H. Prophet, Ed. JANAF Thermochemical Tables, Third Edition. Washington, D.C.: Natioanl Bureau of Standards, 1985.

3. Talley, Claude P. Combustion of Elemental Boron: Quarterly Report. February-April 1959. Contract NOnr-1883(00). Experiment Incorporated, Richmond 2 VA, 1 May 1959 (AD 225A04).

4. Kaskan, W.E. and R.C. Millikan. "Source of Green Bands from Boron-Containing Flames," Journal of Chemical Physics, 32: 1273-1274 (1960).

5. Macek, Andrej and J. McKenzie Semple. "Combustion of Boron Particles at Atmospheric Pressure," Combustion Science and Technology, 1: 181-191 (1969).

6. Macek, Andrej and J. McKenzie Semple. "Combustion of Boron Particles at Elevated Pressures," 13th Symposium (International) on Combustion. 859-868. The Combustion Institute, Pittsburgh PA, 1970.

7. Macek, Andrej. "Combustion of Boron Particles: Experiment and Theory," 14th Symposium (International) on Combustion. 1401-1411. The Combustion Institute, Pittsburgh PA, 1972.

8. Mohan, G. and F.A. Williams. "Ignition and Combustion of Boron in O_2/Inert Atmospheres," AIAA Journal, 10: 776-783 (June 1972).

9. McLain, William H. and Robert W. Evans. Spectrometric Evaluation of Metal Containing Fuels: Final Report, June 1965-June 1966. Contract AF 04(611)-10782. University of Denver, Denver CO, July 1967 (AD 816133).

10. Morrison, M.E. and K. Scheller. "Spectral Characteristics of Hydrocarbon-Air Flames Containing Aluminium, Magnesium, and Boron," Combustion and Flame, 13: 93-97 (February 1969).

11. Gaydon, A.G. The Spectroscopy of Flames, Second Edition. New York: John Wiley & Sons, 1974.

12. Schadow, K. "Boron Combustion Characteristics in Ducted Rockets," Combustion Science and Technology, 5: 107-117 (1972).

13. Ormand, LtCol L.W. The Characteristics of Self-Sustained Particulate Boron Combustion in Air at Ambient Pressure. PhD Dissertation, DS/ME/74-2. School of Engineering, Air Force Institute of Technology (AU), Wright-Patterson AFB OH, September 1974.

14. King, M.K. and A. Macek. Studies of the Ignition and Combustion of Boron Particles for Air-Augmented Rocket Applications, 1 July 1971-31 December 1973. Contract F44620-71-C-0124. Atlantic Research Corporation, Alexandria VA, 21 October 1974 (AD A003731).

15. Komar, J.J. and others. "Experimental Determination of Boron Oxide-Water Vapor Reaction Kinetics," AIAA 21st Aerospace Sciences Meeting. AIAA Paper AIAA-83-0070. American Institute of Aeronautics and Astronautics, New York, 1983.

16. Miller, William J. Boron Combustion Product Chemistry: Final Report 1 March 1974-31 August 1976. Contract N00014-74-C-0326. AeroChem Research Laboratories, Inc., Princeton NJ, October 1976 (AD A032577).

17. Glassman, I. and others. "A Physical and Chemical Interpretation of Boron Particle Combustion," 19th JANNAF Combustion Meeting. 63-72. CPIA Publication 366, Vol 1, Chemical Propulsion Information Agency, October 1982.

18. Oldenborg, Richard C. and S.L. Baughman. "Gas-Phase Oxidation of Boron Compounds," Abstract for AFOSR Contractor's Meeting on Air-breathing Combustion, June, 1986.

19. Faeth, G.M. "Status of Boron Combustion Research," 21st JANNAF Combustion Meeting. CPIA Publication 412, Chemical Propulsion Information Agency, October 1984.

20. Llewellyn, Ian P. and others. "Kinetics of the Reaction BO + $O_2 \rightarrow BO_2$ + O," Chemical Physics Letters, 84: 504-508 (15 December 1981).

21. Brzychcy, A. and others. "Chemiluminescent Studies of Boron Atom Reactions with O_2 and N_2O," Chemical Physics Letters, 60: 102-103 (15 December 1978).

22. Green, G.J. and James L. Gole. "Contrasting Chemiliuminescent Metal Oxide Formation in the Single Collision Reactions of Boron with O_2, NO_2, N_2, O, O_3, and ClO_2," Chemical Physics Letters, 69: 45-49 (1 January 1980).

23. Gole, J.L. and S.A. Pace. "Chemiluminescence from the Interaction of Boron Atoms and Water Vapor," Journal of Physical Chemistry, 85: 2651-2655 (1981).

24. DeHaven, James and others. "Studies of Chemiluminescence in Boron Atom Reactions with O_2, SO_2, N_2O, NO_2, and H_2O_2," Journal of Chemical Physics, 75: 1746-1751 (15 August 1981).

25. Schreiber, Paul W. and others. "Application of Lasers to Combustion Diagnostics," Proceedings of SPIE, Vol 158 Laser Spectroscopy. 42-58. The International Society for Optical Engineering, Bellingham WA, 1978.

26. Crosley, D.R., Ed. Laser Probes for Combustion Chemistry. ACS Symposium Series No 134. Washington DC: American Chemical Society, 1980.

27. Harvey, Albert B., Ed. Applications of Laser Chemistry and Diagnostics, Proceedings of SPIE, Vol 482. Bellingham WA: The International Society for Optical Engineering, 1984.

28. Crosley, David R. and G.P. Smith. "Laser-Induced Fluorescence Spectroscopy for Combustion Diagnostics," Optical Engineering, 22: 545-553 (Sep-Oct 1983).

29. Daily, John W. "Laser-Induced Fluorescence Spectroscopy in Flames," Laser Probes for Combustion Chemistry. David R. Crosley, Ed. ACS Symposium Series 134. Washington DC: American Chemical Society, 1980. 61-83.

30. Bonczyk, P.A. "Laser Detection of Combustion Species," Analytical Laser Spectroscopy. S. Martellucci and A.N. Chester, Eds. NATO ASI Series B: Physics Vol 119. New York: Plenum Press, 1985. 107-130.

31. Mulliken, R.S. "The Isotope Effect in Band Spectra, II: The Spectrum of Boron Monoxide," The Physical Review, 25: 259-294 (March 1925).

32. Jenkins, F.A. and Andrew McKellar. "Mass Ratio of the Boron Isotopes from the Spectrum of BO," The Physical Review, 42: 464-486 (15 November 1932).

33. Dunn, T.M. and Louise Hanson. "Rotational Analysis of the 0,2 Band of the ^{11}BO System," Canadian Journal of Physics, 47: 1657-1659 (1969).

34. Coxon, J.A. and others. "Rotational Analysis of the $A^2\Pi - X^2\Sigma^+$ Visible Band System of Boron Monoxide, BO," Journal of Molecular Spectroscopy, 105: 465-479 (1984).

35. Melen, F. and others. "The A-X and B-X Transitions of BO," Journal of Physics B: Atomic and Molecular Physics, 18: 2423-2432 (1985).

36. Nicholls, R. W. and others. "Transition Probability Parameters of Molecular Spectra Arising from Combustion Processes," Combustion and Flame, 3: 13-23 (1959).

37. Liszt, H.S. and William Hayden Smith. "RKR Franck-Condon Factors for Blue and Ultraviolet Transitions of Some Metal Oxides," Journal of Quantitative Spectroscopy and Radiative Transfer, 11: 1043-1062 (1971).

38. Dean, John A. and Clarice Thompson. "Flame Photometric Study of Boron," Analytical Chemistry, 27: 42-46 (January 1955).

39. Johns, J.W.C. "The Absorption Spectrum of BO_2," Canadian Journal of Physics, 39: 1738-1768 (1961).

40. Snowden, B.S., Jr. The Emission Spectrum of the BO_2 Molecule. PhD Dissertation. Vanderbilt University, Nashville TN, 1963.

41. Russell, D.K. and others."Analysis of the Laser-Excited Fluorescence Spectra of BO_2," Journal of Chemical Physics, 66: 1999-2008 (1 March 1977).

42. Fried, Alan and C. Weldon Mathews. "The Resonance Fluorescence of BO_2 Excited by a Pulsed Dye Laser," Chemical Physics Letters, 52: 363-367 (1 December 1977).

43. Huie, R.E. and others. "The Radiative Lifetimes of the First Excited States of BO and BO_2," Chemical Physics Letters, 55: 404-406 (1 May 1978).

44. Clyne, Michael A.A. and Michael C. Heaven. "Laser-Induced Fluorescence of the BO and BO_2 Free Radicals," Chemical Physics, 51: 299-309 (1980).

45. Hodgson, Andrew. "The $A\tilde{1}^2{}_u$ State of BO_2," Journal Chemical Society, Faraday Transactions 2, 81: 1445-1461 (1985).

46. Moore, C.E. and H.P. Broida. "CH in the Solar Spectrum," Journal of Research of the National Bureau of Standards, A, 63A: 19-53 (July-August 1959).

47. Garland, Nancy L. and David R. Crosley. "Energy Transfer Processes in the CH A^2 and B^2 in an Atmospheric Pressure Flame," Applied Optics, 24: 4229-4237 (1 December 1985).

48. Crosley, David R. "Collisional Effects on Laser-Induced Fluorescence Flame Measurements," Optical Engineering, 20: 511-521 (July-August 1981).

49. Gordon, Sanford and Bonnie J. McBride. Computer Program for Calculation of Complex Chemical Equilibrium Compositions, Rocket Performance, Incident and Reflected Shocks, and Chapman-Jouguet Detonations. NASA SP-73. Washington DC: National Aeronautics and Space Administration, 1971.

50. Samsonov, G.V. and others. Boron: Its Compounds and Alloys. Kiev, USSR: Academy of Sciences Ukrainian SSR, 1960.

51. Garscadden, A., Personal Correspondence, Air Force Wright Aeronautical Laboratories, Wright-Patterson AFB, OH, 9 SEP 1987.

52. Bell, R.P., J.O. Edwards, and R.B. Jones. "The Structure and Acidity of Boric Acids and Their Relation to Reaction Mechanisms," The Chemistry of Boron and Its Compounds. Earl L. Muetterties, Ed. New York: John Wiley and Sons, Inc., 1967. 209 -221.

53. Kizirnis, S.W. and others. "Hydroxyl (OH) Distributions and Temperature Profiles in a Premixed Propane Flame Obtained by Laser Deflection Techniques," Applied Optics, 23: 3873-3881 (1 November 1984)

54. Yariv, Amnon, and David M. Pepper. "Amplified Reflection, Phase Conjugation, and Oscillation in Degenerate Four-Wave Mixing," Optics Letters, 1: 16-18 (July 1977).

55. Bloom, D.M. and others. "Observation of Amplified Reflection by Degenerate Four-Wave Mixing in Atomic Sodium Vapor," Optics Letters, 2: 58-60 (March 1978).

56. Pender, John and Lambertus Hesselink. "Phase Conjugation in a Flame," Optics Letters, 10: 264-266 (June 1985).

57. Ewart, P. and S.V. O'Leary. "Detection of OH in a Flame by Degenerate Four-Wave Mixing," Optics Letters, 11: 279-281 (May 1986).

VITA

Major Greg R. Schneider was born on 13 December 1953 in Davenport, Iowa. He graduated from Alleman High School in Rock Island, Illinois, in 1972, and attended the United States Air Force Academy, from which he was a distinguished graduate receiving a Bachelor of Science degree in Physics and a regular commission in the United States Air Force in 1976. His first assignment was to the Electric Laser Branch of the Air Force Weapons Laboratory, Kirtland AFB, New Mexico. In June, 1979, he entered the School of Engineering, Air Force Institute of Technology, graduating with a Master of Science degree in Engineering Physics in December, 1981. He was then assigned to the Plasma Physics Group of the Aero Propulsion Laboratory, Wright-Patterson AFB, Ohio, serving first as a research physicist and later as the Technical Area Manager until entering the School of Engineering, Air Force Institute of Technology, in June, 1984.

Permanent address: 2432 - 19 Avenue

Rock Island, Illinois, 61201

REPORT DOCUMENTATION PAGE

Form Approved
OMB No. 0704-0188

1a. REPORT SECURITY CLASSIFICATION UNCLASSIFIED	1b. RESTRICTIVE MARKINGS
2a. SECURITY CLASSIFICATION AUTHORITY	3. DISTRIBUTION / AVAILABILITY OF REPORT Approved for public release; distribution unlimited
2b. DECLASSIFICATION / DOWNGRADING SCHEDULE	
4. PERFORMING ORGANIZATION REPORT NUMBER(S) AFIT/DS/PH/87-4	5. MONITORING ORGANIZATION REPORT NUMBER(S)
6a. NAME OF PERFORMING ORGANIZATION School of Engineering 6b. OFFICE SYMBOL (If applicable) AFIT/ENP	7a. NAME OF MONITORING ORGANIZATION
6c. ADDRESS (City, State, and ZIP Code) Air Force Institute of Technology (AU) Wright-Patterson AFB, Ohio 45433-6583	7b. ADDRESS (City, State, and ZIP Code)
8a. NAME OF FUNDING / SPONSORING ORGANIZATION 8b. OFFICE SYMBOL (If applicable)	9. PROCUREMENT INSTRUMENT IDENTIFICATION NUMBER
8c. ADDRESS (City, State, and ZIP Code)	10. SOURCE OF FUNDING NUMBERS PROGRAM ELEMENT NO. / PROJECT NO. / TASK NO. / WORK UNIT ACCESSION NO.

11. TITLE (Include Security Classification)

APPLICATION OF LASER-INDUCED FLUORESCENCE IN AN ATMOSPHERIC-PRESSURE BORON-SEEDED FLAME

12. PERSONAL AUTHOR(S)
Greg R. Schneider, Major, USAF

13a. TYPE OF REPORT	13b. TIME COVERED	14. DATE OF REPORT (Year, Month, Day)	15. PAGE COUNT
PhD Dissertation	FROM _____ TO _____	1987, December	149

16. SUPPLEMENTARY NOTATION

17. COSATI CODES			18. SUBJECT TERMS (Continue on reverse if necessary and identify by block number)
FIELD	GROUP	SUB-GROUP	
20	10		laser-induced fluorescence, flame spectroscopy, boron, combustion, BO_2, BO

19. ABSTRACT (Continue on reverse if necessary and identify by block number)

Advisory Committee Chairman: Won B. Roh
Professor of Engineering Physics

Approved for public release: IAW AFR 190-1
Lynn Wolaver 31 Dec 87
Dean for Research and Development

20. DISTRIBUTION / AVAILABILITY OF ABSTRACT ☐ UNCLASSIFIED/UNLIMITED ☒ SAME AS RPT ☐ DTIC USERS	21. ABSTRACT SECURITY CLASSIFICATION UNCLASSIFIED
22a. NAME OF RESPONSIBLE INDIVIDUAL Won B. Roh, Professor	22b. TELEPHONE (Include Area Code) (513) 255-2012 22c. OFFICE SYMBOL AFIT/ENP

DD Form 1473, JUN 86 — Previous editions are obsolete

The purpose of this research was to demonstrate the feasibility of using laser-induced fluorescence (LIF) of boron oxide radicals in atmospheric-pressure flames. Such a demonstration would provide a useful tool with which to probe the detailed combustion chemistry of boron fuels. The radical species sought were BO_2 and BO, both having spectra in the visible region of the spectrum. These two species are believed to play critical roles in the boron combustion process.

A $CH_4/air/O_2$ flame was seeded with BCl_3 producing the green emission characteristic of boron flames. Unfortunately, it also created significant quantities of aerosols of solid boric acid from the reaction of the BCl_3 with water vapor in the air supply. The burner was 1 cm in diameter and composed of approximately 60 capillary tubes. The burner could be remotely translated in two directions permitting investigation of different regions of the flame.

The flame was first probed using standard emission spectroscopy and exhibited only spectra from BO_2 and CH. The CH spectra dominated everything in its 0-0 band region, which also is the 0-0 band region of BO.

Next a pulsed dye laser pumped by a Nd:YAG laser was tuned to absorption bands of either BO_2 or BO. A strong LIF signal was generated from the pumping of both the R_1 and R_2 branches of the $00^00\text{-}00^00$ transitions of the A-X system of BO_2. The effect was monitored by observing the $00^00\text{-}10^00$ transition. This is the first known demonstration of LIF of BO_2 at atmospheric pressure. No LIF signal was observed from BO.

Certain regions of the flame exhibited strong Mie scattering due to the aerosols. These regions also showed preliminary evidence of resonant Raman scattering although a thorough examination of this effect was not made due to time limitations.

END

DATE

FILMED

APRIL

1988

DTIC